Technical Report Documentation Page

1. Report No. FHWA/TX-07/0-4096-2	2. Government Accession No.	3. Recipient's Catalog No.
4. Title and Subtitle **Methodology for the Quantitative Evaluation of the Remaining Fatigue Life of Fracture Critical Bridges**		5. Report Date October 2007 6. Performing Organization Code
7. Author(s) Sharon L. Wood and Peter K. Dean		8. Performing Organization Report No. 4096-2
9. Performing Organization Name and Address Center for Transportation Research The University of Texas at Austin 3208 Red River, Suite 200 Austin, TX 78705-2650		10. Work Unit No. (TRAIS) 11. Contract or Grant No. Research Project 0-4096
12. Sponsoring Agency Name and Address Texas Department of Transportation Research and Technology Implementation Office P.O. Box 5080 Austin, TX 78763-5080		13. Type of Report and Period Covered Research Report (9/2003 - 8/2005) 14. Sponsoring Agency Code

15. Supplementary Notes

Project performed in cooperation with the Texas Department of Transportation and the Federal Highway Administration.

16. Abstract

Two fracture critical bridges were instrumented using miniature, battery-powered data acquisition systems as part of this investigation. The measured rainflow response was then used to estimate the remaining fatigue life of each bridge. The primary advantages of the monitoring system are that the units were designed to be installed easily in the field and interpretation of the rainflow data is straightforward. However, to utilize the full potential of the monitoring system, analytical models of each bridge must be developed prior to instrumentation and careful evaluation of the rainflow data is required.

Incorporating the data acquisition units into regular inspections of fracture critical bridges will represent a significant change in TxDOT procedures. However, the rainflow data provide a quantitative metric for identifying the bridges that are most vulnerable to fatigue damage and will assist TxDOT in setting priorities for inspection and replacement of these bridges as they approach the end of their service life.

17. Key Words bridge monitoring systems, fracture critical bridges, fatigue life, rainflow histogram		18. Distribution Statement No restrictions. This document is available to the public through the National Technical Information Service, Springfield, Virginia 22161; www.ntis.gov.	
19. Security Classif. (of report) Unclassified	20. Security Classif. (of this page) Unclassified	21. No. of pages 150	22. Price

Form DOT F 1700.7 (8-72) Reproduction of completed page authorized

Methodology for the Quantitative Evaluation of the Remaining Fatigue Life of Fracture Critical Bridges

Sharon L. Wood
Peter K. Dean

CTR Research Report:	4096-2
Report Date:	October 2007
Research Project:	0-4096
Research Project Title:	Evaluation and Monitoring of Texas' Major and Unique Bridges
Sponsoring Agency:	Texas Department of Transportation
Performing Agency:	Center for Transportation Research at the University of Texas at Austin

Project performed in cooperation with the Texas Department of Transportation and the Federal Highway Administration.

Center for Transportation Research
The University of Texas at Austin
3208 Red River
Austin, TX 78705

www.utexas.edu/research/ctr

Disclaimers

Author's Disclaimer: The contents of this report reflect the views of the authors, who are responsible for the facts and the accuracy of the data presented herein. The contents do not necessarily reflect the official view or policies of the Federal Highway Administration or the Texas Department of Transportation (TxDOT). This report does not constitute a standard, specification, or regulation.

Patent Disclaimer: There was no invention or discovery conceived or first actually reduced to practice in the course of or under this contract, including any art, method, process, machine manufacture, design or composition of matter, or any new useful improvement thereof, or any variety of plant, which is or may be patentable under the patent laws of the United States of America or any foreign country.

Notice: The United States Government and the State of Texas do not endorse products or manufacturers. If trade or manufacturers' names appear herein, it is solely because they are considered essential to the object of this report.

Engineering Disclaimer

THIS REPORT IS NOT INTENDED FOR CONSTRUCTION, BIDDING,
OR PERMIT PURPOSES.

Sharon L. Wood, Texas P.E. #83804
Research Supervisor

Acknowledgments

This research project was funded by the Texas Department of Transportation (TxDOT) under Project No. 0-4096. The support of the project director, Alan Kowalik (BRG) is greatly appreciated.

Products

Research Product P1, specifications and plans for installation of monitoring system, is included in Chapter 7 of this research report. Research Product P2, manual for operation of monitoring system, is included in Appendix A of this research report.

TABLE OF CONTENTS

LIST OF FIGURES

FIGURE **PAGE**

FIGURE **PAGE**

FIGURE **PAGE**

FIGURE **PAGE**

LIST OF TABLES

SUMMARY

Two fracture critical bridges were instrumented using miniature, battery-powered data acquisition systems as part of this investigation. The measured rainflow response was then used to estimate the remaining fatigue life of each bridge. The primary advantages of the monitoring system are that the units were designed to be installed easily in the field and interpretation of the rainflow data is straightforward. However, to utilize the full potential of the monitoring system, analytical models of each bridge must be developed prior to instrumentation and careful evaluation of the rainflow data is required.

Incorporating the data acquisition units into regular inspections of fracture critical bridges will represent a significant change in TxDOT procedures. However, the rainflow data provide a quantitative metric for identifying the bridges that are most vulnerable to fatigue damage and will assist TxDOT in setting priorities for inspection and replacement of these bridges as they approach the end of their service life.

CHAPTER 1: INTRODUCTION

Within the State of Texas, several important bridges utilize relatively uncommon structural systems. Because of their unique designs, the Texas Department of Transportation (TxDOT) expressed concerned that standard inspection techniques may not be sufficient to detect the onset of structural damage. TxDOT project 0-4096, Structural Health Evaluation and Monitoring of Major and Unique Bridges in Texas, was funded to identify and evaluate monitoring technologies that could provide information about the behavior of these unique bridges that is not available during routine inspections.

During the first phase of the project, two monitoring technologies were evaluated in the laboratory (Bilich and Wood, 2004). TxDOT selected one of these technologies for evaluation in the field. Two fracture critical bridges in central Texas were selected as demonstration structures, and the results of those field tests are documented in this report.

Since the recent collapse of the I-35W bridge across the Mississippi River in Minneapolis, public interest in the inspection of fracture critical bridges has increased dramatically. Because these bridges lack redundancy, the consequences of failure of one member are high. Procedures are presented in this report for measuring the live-load response of a fracture critical steel bridge and determining the remaining fatigue life. The procedures are more extensive than currently used within the State of Texas for inspection of fracture critical bridges; however, the results provide quantitative information that can be used to identify the bridges that are most susceptible to fatigue damage and set priorities for bridge inspections and possible replacement.

1.1 OVERVIEW OF REPORT

Two fracture critical bridges were instrumented as part of this investigation and the measured response of those two bridges is used to demonstrate the potential benefits of using the proposed monitoring system. The primary advantages of the monitoring system are that it is designed to be installed easily in the field and the acquired data can be used directly to evaluate the fatigue life of a steel bridge.

Background information regarding the fatigue life of steel bridges, measured traffic loads, and the miniature data acquisition systems is presented in this Chapter 2. The two bridges monitored as part of this investigation are described in Chapter 3. Information about the geometry and the results of simple analytical models are presented. The measured response of the Medina River Bridge is discussed in Chapter 4. This is the older of the two bridges and carries heavier traffic loads. The measured response of the 12th Street Exit Ramp is presented in Chapter 5. The fatigue life of the two bridges is calculated

using the measured data in Chapter 6. Recommended procedures for installing the miniature data acquisition systems and interpreting the data are presented in Chapter 7. Conclusions are discussed in Chapter 8.

Appendix A describes the software used to program the miniature data acquisition systems, and includes a summary of the operation manual. Appendix B provides information about interpreting data from weigh-in-motion stations.

1.2 POTENTIAL IMPACT OF MONITORING SYSTEM

Current federal requirements mandate a thorough inspection of all fracture critical bridges at least once every two years without distinguishing among bridges based on the level of traffic or the number of years that the bridge has been in service. The proposed monitoring system provides quantitative data about the service-load response of the bridge, which can be used to evaluate the remaining fatigue life. Although a structural model of the bridge is needed to select the locations of instruments and estimate maximum stress ranges, interpretation of the measured response does not depend on the assumptions made in the structural model. Therefore, the data provide an unbiased assessment of the bridge. In the event that the trends in the measured data do not match those from the structural model, detailed inspection of those areas of the bridge may be warranted. This information may be particularly useful in evaluating the efficacy of pinned connections and expansion joints.

CHAPTER 2: FATIGUE LIFE OF STEEL BRIDGES

The primary application of the miniature data acquisition systems evaluated in this project is to determine the remaining fatigue life of fracture critical bridges. This information will assist TxDOT in identifying the steel bridges that are most susceptible to fatigue damage and in setting priorities for detailed bridge inspections and possible replacement of existing bridges. Background information needed to calculate the fatigue life of an existing bridge is summarized in this chapter.

The AASHTO fatigue models used for design are summarized in Section 2.1. These models are used to determine the fatigue life of an existing bridge from the effective stress range induced by the spectrum of vehicles crossing the bridge. The effective stress range is calculated from the measured response of the bridge. As a first step, rainflow counting is used to simplify a variable-amplitude strain history – such as that induced in a steel girder by traffic loads – into a series of strain cycles. The rainflow counting algorithm is discussed in Section 2.2 and the results are used in Section 2.3 to calculate the effective stress range. The resulting fatigue life of the steel bridge is calculated in Section 2.4.

For most bridges, the traffic loads are not known. However, the Medina River Bridge is located seven miles north of a weigh-in-motion station on I-35. The characteristics of the spectrum of trucks recorded at this station are discussed in Section 2.5. A commercial data acquisition system was used to capture the strain response of two fracture critical bridges. The basic attributes of the data acquisition system are described in Section 2.6.

2.1 AASHTO DESIGN MODEL

When designing a steel bridge, the S-N curves in the AASHTO LRFD Bridge Design Specifications (2004) are used to relate the calculated stress range, S_r, to the fatigue life, N. Eight detail categories are defined and the two constants are used to characterize the S-N curves for each detail category. The idealized S-N curves for representative detail categories are shown in Figure 2.1.

The threshold stress defines the region of infinite fatigue life for each detail category (Table 2.1). For higher stress ranges, the finite fatigue life is defined as:

$$N = AS_r^{-3} \tag{2.1}$$

where the value of A is given in Table 2.1, and the stress range, S_r, is reported in units of ksi.

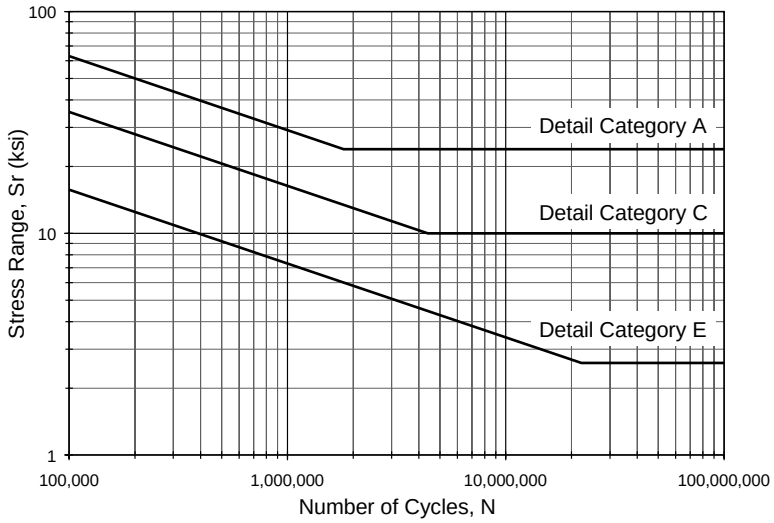

Figure 2.1 Selected Design Stress Range Curves (AASHTO, 2004)

The AASHTO design model was developed from fatigue tests conducted using a constant-amplitude stress history. However, vehicular traffic induces variable-amplitude stress histories in a bridge. The strain history shown in Figure 2.2 corresponds to a single truck crossing a continuous, steel girder bridge with a composite concrete deck (Bilich and Wood, 2004). The procedure used to convert a variable-amplitude stress history into an equivalent constant stress range, which is called the effective stress range, S_{re}, is discussed in Section 2.3.

Table 2.1 Constants Used to Define Fatigue Life of Steel Bridges (AASHTO, 2004)

Detail Category	Threshold Stress (ksi)	Constant A (ksi^3)
A	24	250×10^8
B	16	120×10^8
B′	12	61×10^8
C	10	44×10^8
C′	12	44×10^8
D	7.0	22×10^8
E	4.5	11×10^8
E′	2.6	3.9×10^8

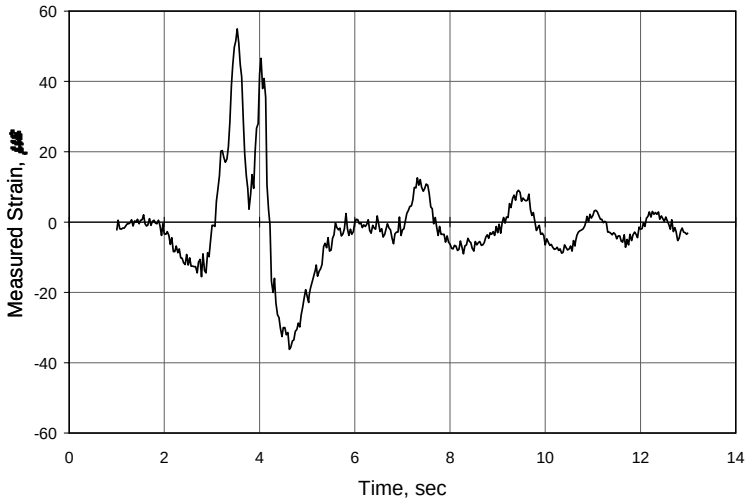

Figure 2.2 Representative Strain History for Truck Crossing a Continuous, Steel Girder Bridge

2.2 RAINFLOW COUNTING

Rainflow counting is a method of simplifying a complex strain history into a series of strain ranges from which the effective stress range can be calculated. The ASTM E 1049 (1997) algorithm for rainflow counting was used in all calculations described in this report and is integrated into the miniature data acquisition systems described in Section 2.6.

The easiest way to visualize the rainflow counting algorithm is to rearrange the order of the strain history and visualize the modified strain history as a reservoir (Tilly and Page, 1980). The strain history shown in Figure 2.2 is replotted in Figure 2.3, with the maximum strain plotted as the first data point. All strains that were recorded before the maximum strain are shown at the end of the record. The final strain reading in the rearranged history has the same amplitude as the first reading – the maximum value in the original strain history.

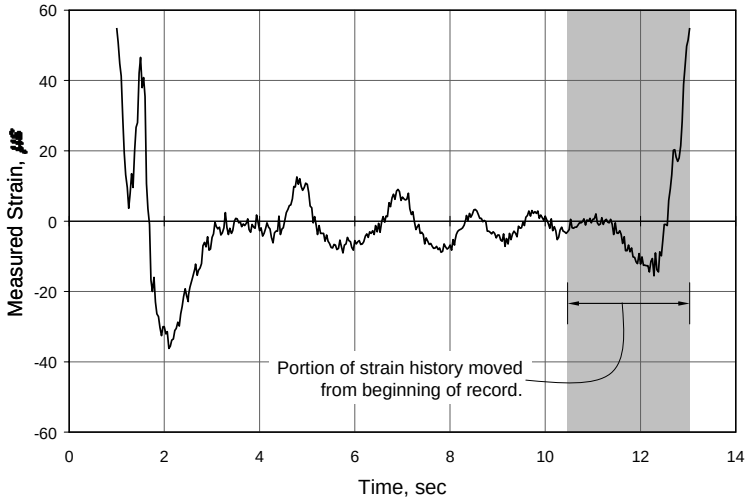

Figure 2.3 Modified Strain History

The reservoir corresponding to the modified strain history is plotted in Figure 2.4. The water level shown corresponds to the maximum strain. The difference between the water level and the minimum measured strain represents the largest amplitude strain cycle in the strain history (91.2 $\mu\varepsilon$). The reservoir is then drained from the lowest point in the strain history. Water is trapped in various locations, as shown in Figure 2.5, and the next two largest strain cycles are identified as 42.9 $\mu\varepsilon$ and 28.1 $\mu\varepsilon$. Each of these sections is then drained from their lowest points, and the remaining cycles are counted. The process is repeated until the entire reservoir is emptied.

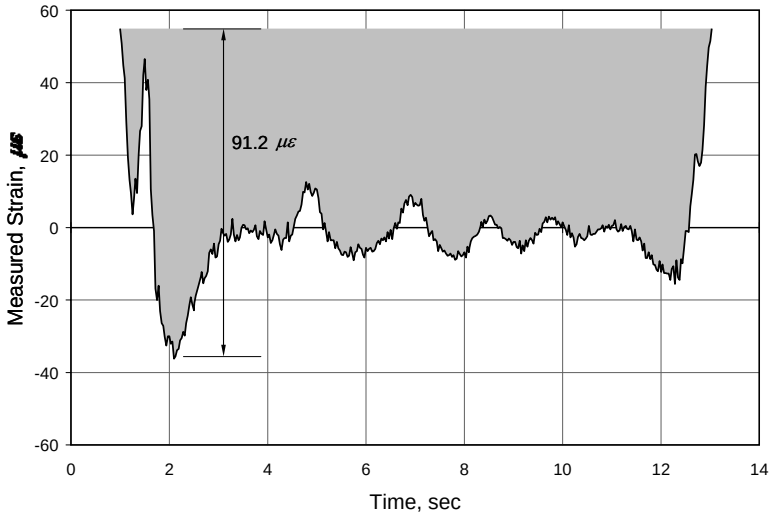

Figure 2.4 Idealized Reservoir for Modified Strain History

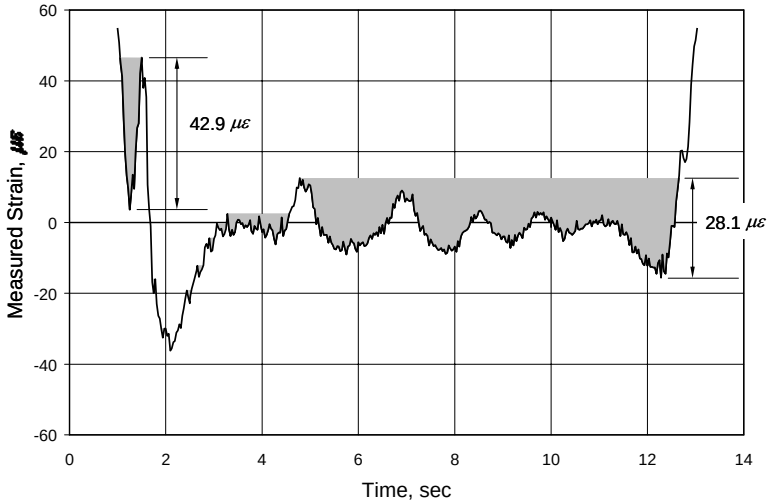

Figure 2.5 Idealized Reservoir for Modified Strain History after Counting the Largest Strain Cycle

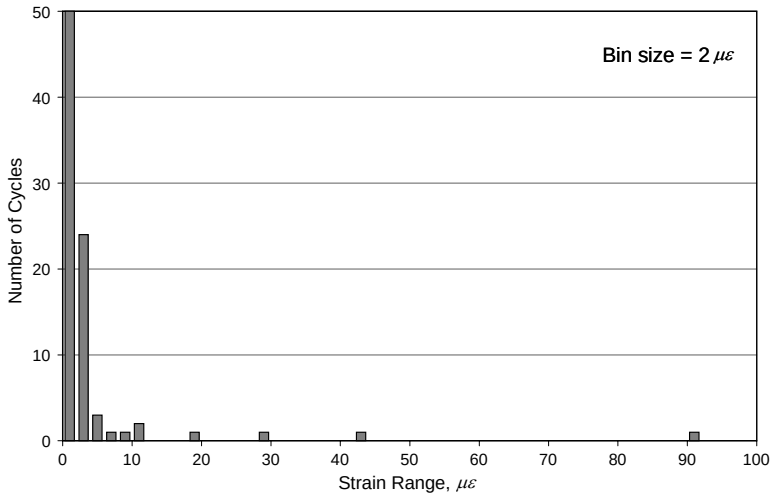

Figure 2.6 Strain Histograms for Representative Strain History

The resulting distribution of strain cycles is shown in Figure 2.6, where the cycle amplitudes were grouped into 2-$\mu\varepsilon$ bins. The selection of an appropriate bin size proved to be extremely important when collecting rainflow data in the field. This topic is addressed in more detail in Chapters 6 and 7.

The original strain history (Figure 2.2) exhibited a large number of low-amplitude strain cycles. These cycles dominate the histogram shown in Figure 2.6. The likely cause of many of these low-amplitude cycles is electrical noise in the data acquisition system and instrumentation used to monitor the response of the bridge, rather than vehicular traffic. As discussed in Chapter 6, these low-amplitude cycles do not influence the fatigue life of the bridge and make it more difficult to identify the strain cycles of interest in the strain histograms. Therefore, the cycles corresponding to strain ranges below the noise threshold are often deleted before using the strain histories to calculate the effective stress range. The choice of noise threshold depends on the unique combination of bridge, instrumentation, and data acquisition system; however, in this project, the noise threshold was typically in the range of 3 to 5 $\mu\varepsilon$. In this example, the noise threshold was taken as 4 $\mu\varepsilon$, and cycles below this level have been deleted from the strain histogram shown in Figure 2.7. This histogram includes eleven strain cycles ranging in amplitude from 5.2 to 91.2 $\mu\varepsilon$. The largest strain cycle corresponds to a stress range of 2.7 ksi, which is below the threshold stress for all AASHTO detail categories except E′.

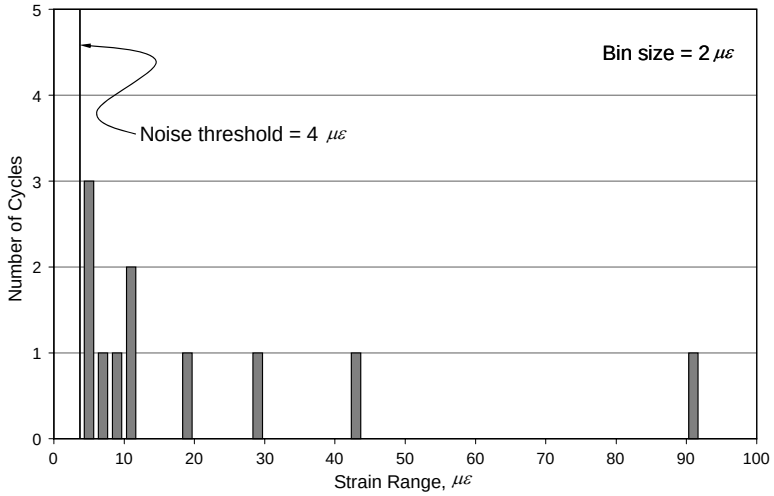

Figure 2.7 Strain Histogram after Removal of Cycles below the Noise Threshold

2.3 EFFECTIVE STRESS RANGE

As discussed in Section 2.1, the S-N curves defined by AASHTO are based on the results of constant-amplitude fatigue tests. However, vehicular traffic induces variable-amplitude stress cycles in bridges. The fatigue life for a given distribution of variable-amplitude stress cycles is the same as the fatigue life for constant-amplitude stress cycles at the effective stress range, S_{re}. The procedure used to calculate S_{re} is discussed in this section and is summarized from a more thorough presentation in Hoadley et al. (1983).

The concept of an effective stress range is based on work by Miner (1945), which demonstrated that fatigue damage accumulates linearly:

$$\sum \frac{n_i}{N_i} = 1.0 \tag{2.2}$$

where n_i is the number of cycles at stress range S_{ri} in a variable-amplitude loading spectrum and N_i is the fatigue life at stress range S_{ri}. Using Eq. 2.1, N_i may be expressed as:

$$N_i = AS_{ri}^{-3} \tag{2.3}$$

Additionally, n_i may be expressed in terms of the fatigue life, N:

$$n_i = \gamma_i N \tag{2.4}$$

where γ_i is the fraction of the total number of cycles at stress range S_{ri}.

Substituting Eq. 2.3 and Eq. 2.4 into Eq. 2.2 and rearranging the terms, yields

$$\frac{N}{A}\sum \gamma_i S_{ri}^3 = 1.0 \tag{2.5}$$

The summation on the left side of Eq. 2.5 is defined as:

$$\sum \gamma_i S_{ri}^3 = S_{re}^3 \tag{2.6}$$

where S_{re} is the effective stress range. Substituting Eq. 2.6 into Eq. 2.5 yields the familiar form:

$$N = AS_{re}^{-3} \tag{2.7}$$

where *N* represents the total number of variable-amplitude stress cycles (fatigue life).

Rather than estimating the fatigue life of the bridge from the measured response of a single truck (Figure 2.2), the strain data should be collected over a longer period of time and be representative of the entire traffic spectrum. The example strain histogram shown in Figure 2.8 represents the traffic-induced strain cycles during a 28-day reporting period and will be used to calculate the effective stress range. A bin size of 25 $\mu\varepsilon$ and a noise threshold of 4 $\mu\varepsilon$ are used in Figure 2.8. Therefore, strain cycles with ranges between 0 and 4 $\mu\varepsilon$ are not included in the histogram.

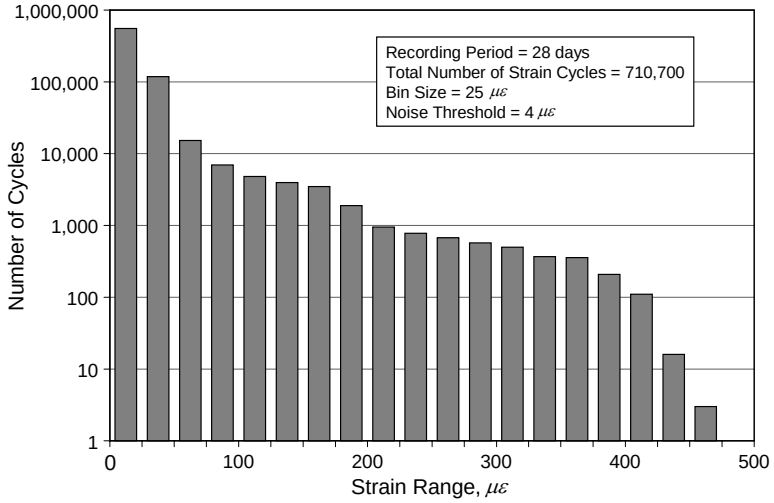

Figure 2.8 Example Strain Histogram

The limiting strains for each bin and the corresponding number of cycles within each bin are reported in Table 2.2. The median stress range for each bin, S_{ri}, was calculated as:

$$S_{ri} = E \times \varepsilon_{ri} / 1{,}000{,}000 \qquad (2.8)$$

where E is Young's modulus for steel (30,000 ksi), ε_{ri} is the median strain for each bin, and the factor of 1,000,000 is used to convert from microstrain to strain. The three largest strain cycles in the sample histogram had ranges between 450 and 475 $\mu\varepsilon$, which corresponds to a maximum stress range of 14.3 ksi.

Table 2.2 Calculation of Effective Stress Range from Example Strain Histogram

Strain Bins			Number of Strain Cycles	Median Stress Range S_{ri} (ksi)	Fraction of Population γ_i	$\gamma_i S_{ri}^3$ (ksi^3)
Minimum Strain ($\mu\varepsilon$)	Maximum Strain ($\mu\varepsilon$)	Median Strain ($\mu\varepsilon$)				
4	14.5	25	551,394	0.44	7.76×10^{-1}	0.0639
25	37.5	50	118,447	1.13	1.67×10^{-1}	0.2373
50	62.5	75	15,241	1.88	2.14×10^{-2}	0.1414
75	87.5	100	6,949	2.63	9.78×10^{-3}	0.1769
100	112.5	125	4,799	3.38	6.75×10^{-3}	0.2596
125	137.5	150	3,952	4.13	5.56×10^{-3}	0.3903
150	162.5	175	3,492	4.88	4.91×10^{-3}	0.5693
175	187.5	200	1,893	5.63	2.66×10^{-3}	0.4740
200	212.5	225	953	6.38	1.34×10^{-3}	0.3475
225	237.5	250	777	7.13	1.09×10^{-3}	0.3953
250	262.5	275	673	7.88	9.47×10^{-4}	0.4626
275	287.5	300	572	8.63	8.04×10^{-4}	0.5159
300	312.5	325	499	9.38	7.02×10^{-4}	0.5781
325	337.5	350	368	10.13	5.18×10^{-4}	0.5376
350	362.5	375	356	10.88	5.01×10^{-4}	0.6450
375	387.5	400	208	11.63	2.93×10^{-4}	0.4596
400	412.5	425	110	12.38	1.54×10^{-4}	0.2928
425	437.5	450	16	13.13	2.25×10^{-5}	0.0509
450	462.5	475	3	13.88	4.22×10^{-6}	0.0113
475	487.5	500	0	14.63	0	0.0000
TOTAL			710,700	—	1.0	6.6090
Effective Stress Range, S_{re} (ksi)			—	—	—	1.88

Rearranging Eq. 2.4, γ_i is calculated for each bin:

$$\gamma_i = \frac{n_i}{N_{tot}} \tag{2.9}$$

where n_i is the number of cycles corresponding to bin *i* and N_{tot} is the total number of strain cycles recorded during the 28-day period. The effective stress range, S_{re}, is then calculated as:

$$S_{re} = \left(\sum \gamma_i S_{ri}^3 \right)^{1/3} \tag{2.10}$$

For this example, the effective stress range is 1.9 ksi. This corresponds to an effective strain range of 63 $\mu\varepsilon$, which is within the third bin in Table 2.2.

Because the rainflow data were recorded over a 28-day period, it is reasonable to assume that the effective stress range is representative of the actual traffic spectrum for this bridge. Had the recording period been significantly shorter, this assumption might not be valid. For example, if strain data were recorded over a 4-day period which included a weekend, the actual traffic spectrum would likely induce larger stresses in the bridge than indicated by the strain histogram.

2.4 CALCULATED FATIGUE LIFE

Once the effective stress range is known, the corresponding fatigue life, *N*, may be calculated using Eq. 2.7. Values are reported in Table 2.3 for each detail category. Because the maximum stress range, 14.3 ksi, is less than the threshold stress for detail categories A and B (Table 2.1), the fatigue life is considered to be infinite in these cases. The calculated fatigue life ranges from 59 million cycles for detail category E′ to 923 million cycles for detail category B.

Table 2.3 Calculated Fatigue Life Based on Example Strain Histogram

Detail Category	Fatigue Life *N* (cycles)
A	Infinite
B	Infinite
B′	923×10^6
C / C′	666×10^6
D	333×10^6
E	166×10^6
E′	59×10^6

In most cases, it is more useful to express the fatigue life in terms of years of service, rather than number of fatigue cycles. This conversion requires several more assumptions, as discussed below. Both legal vehicle loads and traffic volume have increased in the past and are expected to continue to increase in the future. In order to determine the fatigue life of the bridge in years, these growth rates must be estimated.

Traffic volume is often assumed to increase geometrically with annual rates of increase between 2 and 6%. The ratio of annual traffic volume to the traffic volume in the first year of service is plotted in Figure 2.9 over the 75-year design life of a typical bridge. The results are very sensitive to the assumed rate of growth. For an assumed annual rate of growth of 2%, the traffic volume in the last year of service is approximately 4.5 times the traffic volume in the first year of service. However, if the assumed annual rate of growth is taken as 6%, the traffic volume in the last year of service is nearly 75 times the traffic volume in the first year of service.

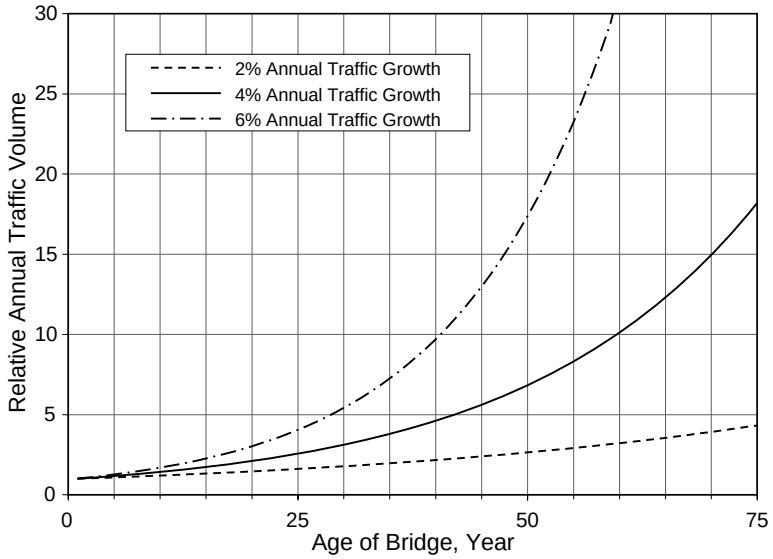

Figure 2.9 Increase in Traffic Volume over 75-Year Design Life of Bridge

Rather than increasing continually over the design life, the legal vehicle loads tend to increase in discrete increments with the legal vehicle loads remaining constant between each increase. Because this type of progression is more difficult to model, and because the changes are more variable, increasing vehicle loads were not considered explicitly in this analysis. However, increases in legal vehicle loads will be reflected in the measured rainflow data, which should be recorded periodically over the life of the bridge.

Based on the assumptions discussed above, the strain histogram shown in Figure 2.8 is considered to be representative of the traffic loads over the service life of the bridge. However, the number of loading cycles is assumed to increase geometrically with time. The fatigue life in cycles, *N*, can therefore be related to the fatigue life in years, *m*, as follows:

$$N = \sum_{i=1}^{m} N_{yi} \tag{2.11}$$

where N_{yi} is the number of loading cycles in year *i*. The traffic volume in year *i* can be calculated from the traffic volume in the first year:

$$N_{yi} = N_{y1}\left(1+r\right)^{(i-1)} \tag{2.12}$$

where N_{y1} is the number of loading cycles during the first year of service and *r* is the annual rate of increase in the traffic volume.

If the current age of the bridge in years is taken as *k*, the number of loading cycles in year *k*, N_{yk}, can be calculated from the rainflow data:

$$N_{yk} = N_{tot} \times \left(\frac{365}{D}\right) \tag{2.13}$$

where N_{tot} is the total number of strain cycles recorded during the reporting period and *D* is the duration of the reporting period in days. For the example strain histogram (Table 2.2), N_{tot} = 710,700 cycles and *D* = 28 days, which leads to N_{yk} = 9,265,000 cycle/yr. The number of cycles during the first year of service life, N_{y1}, can then be calculated as:

$$N_{y1} = \frac{N_{ky}}{\left(1+r\right)^{(k-1)}} \tag{2.14}$$

Substituting Eq. (2.12) into Eq. (2.11) yields:

$$N = N_{y1}\sum_{i=1}^{m}\left(1+r\right)^{(i-1)} \tag{2.15}$$

Rearranging Eq. 2.15:

$$\frac{N}{N_{y1}} = \sum_{i=1}^{m}\left(1+r\right)^{(i-1)} \tag{2.16}$$

The right side of Eq. 2.16 can be expressed as:

$$\sum_{i=1}^{m}(1+r)^{(i-1)} = \frac{(1+r)^m - 1}{r} \tag{2.17}$$

Substituting Eq. 2.17 into Eq. 2.16 yields:

$$\frac{N}{N_{y1}} = \frac{(1+r)^m - 1}{r} \tag{2.18}$$

The fatigue life in years, *m*, can then be calculated as:

$$m = \frac{\log\left(\frac{rN}{N_{y1}} + 1\right)}{\log(1+r)} \tag{2.19}$$

which depends on the current traffic volume, N_{yk}; the current age of the bridge, *k;* the assumed annual rate of increase of traffic volume, *r;* and the detail category for the bridge. The results in Table 2.3 are expressed in terms of years of service in Table 2.4 for two assumed ages of the bridge (10 and 30 years) and two assumed rates of annual traffic growth (2% and 6%). All detail categories with a finite fatigue life are considered, and the current annual traffic volume, N_{yk}, was taken as 9,265,000 cycle/yr in all cases.

Table 2.4 Estimated Fatigue Life in Years

Current Age of Bridge:	10 years		30 years	
Annual Rate of Traffic Growth:	2%	6%	2%	6%
Number of Loading Cycles in First Year of Service:	7.75×10^6	5.48×10^6	5.22×10^6	1.71×10^6
Detail Category	Fatigue Life (years)			
B′	61.5	41.3	76.4	60.2
C / C′	50.5	36.3	64.0	54.8
D	31.3	26.3	41.5	43.6
E	18.0	17.8	24.9	33.0
E′	7.2	8.5	10.3	19.3

Note: Shaded cells represent combinations of parameters for which the calculated fatigue life is less than the current age of the bridge.

As expected the results are extremely sensitive to the annual rate of traffic growth and the detail category. For each combination of age of bridge and annual rate of traffic growth, the longest fatigue lives were calculated for detail category B′. The estimate fatigue lives, which ranged from 41.3 to 76.4 years, exceeded the assumed age of the bridge in all cases. In contrast, the calculated fatigue life of the bridge was less than the current age if the bridge was assigned to detail category E′.

Although the actual increases in traffic volume and vehicle loads is unknown for most bridges, the results reported in Table 2.4 provide a useful tool for planning purposes. If a fracture critical bridge is calculated to have an infinite fatigue life or a finite fatigue life that exceeds the design life, fatigue will not likely limit the service life of the bridge. However, if a fracture critical bridge has a finite fatigue life that is less than the design life of the bridge, fatigue damage is likely and more thorough inspections may be required to monitor for damage. By measuring the strain response of a steel bridge under service loads, the likelihood of fatigue damage can be evaluated and financial resources can be allocated to inspection or replacement of the most vulnerable bridges.

2.5 TRAFFIC LOADS

As part of this project, 50 days of weigh-in-motion data were collected from Station 516 in Lytle, which is on I-35 south of San Antonio (Figure 2.10). The weigh-in-motion data were originally selected to evaluate the response of the Medina River Bridge, because the weigh-in-motion station is seven miles south of the bridge on I-35. Therefore, only the data corresponding to northbound traffic crossing the weigh-in-motion station were considered in this investigation.

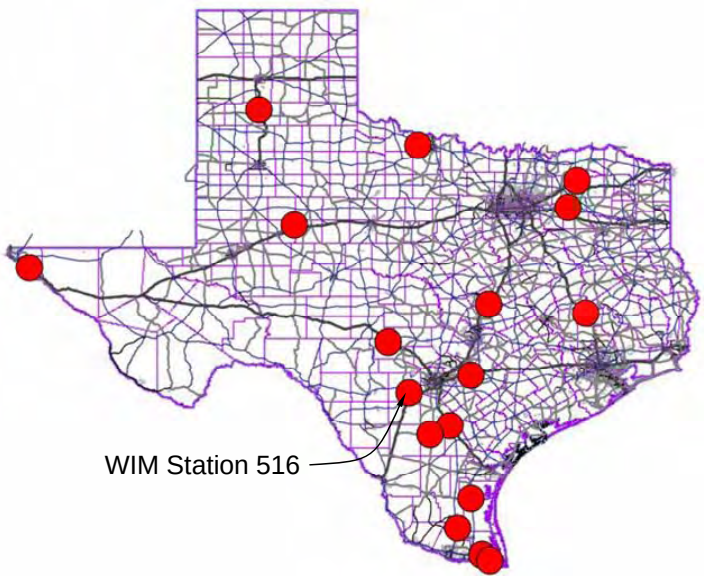

Figure 2.10 Locations of Weigh-in-Motion Stations in Texas (Neidigh and Crawford, 2004)

Nearly 200,000 northbound trucks were recorded by the weigh-in-motion station during the 50-day reporting period (7 days in July 2004, 23 days in August 2004, 7 days in January 2005, and 13 days in February 2005). A total of 60 different types of trucks were detected during this period. The complete list of trucks is presented in Appendix B and the distribution of trucks, based on the number of axles, is shown in Figure 2.11. The maximum number of axles detected was nine, but trucks with seven to nine axles represented less than 1% of the total population, while trucks with five axles represented 56% of the total population.

On average, fifteen types of trucks were detected ten or more times a day (Table 2.5). A five-axle, tractor trailer (T5-1) was the most common and represented 49% of the total truck population, and a two-axle truck (T2-1) represented 33% of the total truck population. The distributions of gross vehicle weights are shown in Figure 2.12 for trucks with two to nine axles, and the distribution of gross vehicle weights for the entire spectrum of trucks is shown in Figure 2.13. A detail of the distribution of the heaviest trucks is shown in Figure 2.14.

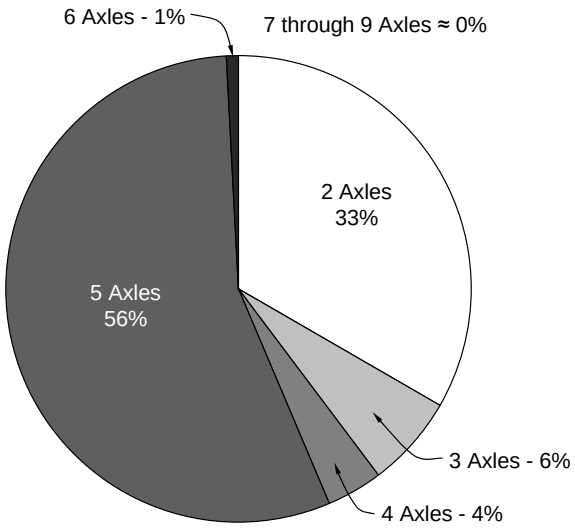

Figure 2.11 Distribution of Trucks Recorded by Weigh-in-Motion Station

Table 2.5 Most Common Types of Trucks Crossing Weigh-in-Motion Station

Truck Designation	Number of Axles	Effective Gross Vehicle Weight (kip)	WIM Truck Designation*	Average Trucks per Day
T5-1	5	56.6	332000	1969
T2-1	2	10.3	220000	1302
T5-2	5	61.7	337000	180
T3-1	3	30.4	230000	143
T4-1	4	24.9	322000	112
T5-3	5	64.5	521200	59
T3-2	3	37.6	190300	54
T3-3	3	19.7	200900	32
T4-2	4	36.1	431000	31
T3-4	3	19.6	421000	21
T4-3	4	32.3	331000	15
T2-2	2	7.5	090000	13
T2-3	2	20.4	190200	12
T6-1	6	57.3	531200	12
T6-2	6	60.4	333000	10

* Six-digit code is discussed in Appendix B.

The ranges of axle weights and axle spacings for trucks T5-1 are reported in Table 2.6. Median axle weights are slightly above 10 kip for each axle, but maximum values exceed 2.5 times the median values. The ranges of axle weights and total length for truck T2-1 are reported in Table 2.7. Median axle weights are in the range of 3 to 4 kip, but the maximum axle weights are more than 8 times the median values. The configurations of the median T5-1 and T2-1 vehicles are compared with the HW-20 design vehicles in Figure 2.15.

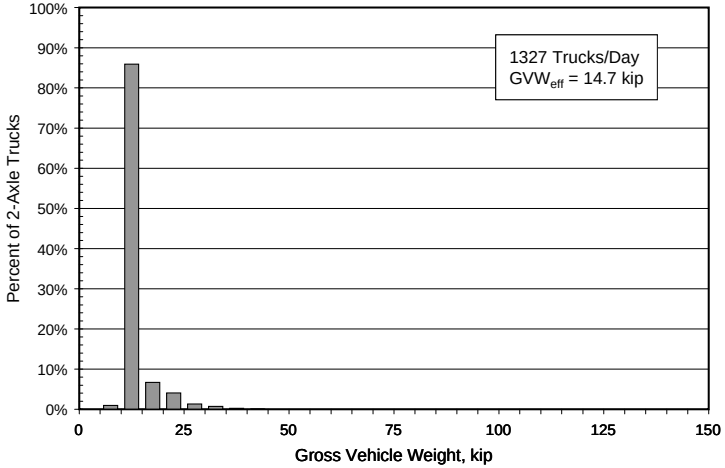

(a) Two-Axle Trucks

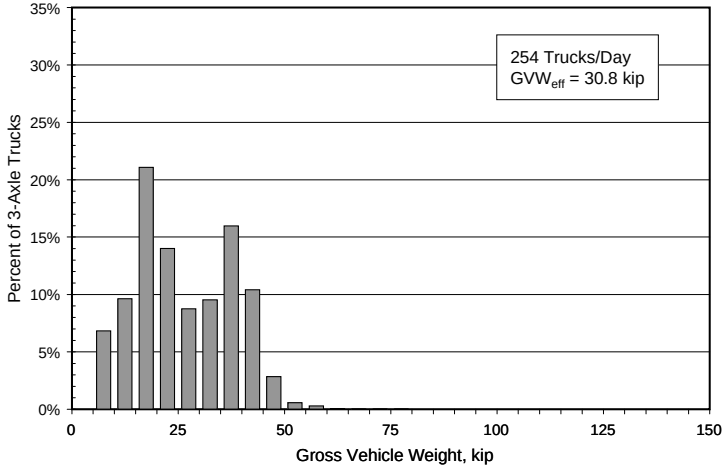

(b) Three-Axle Trucks

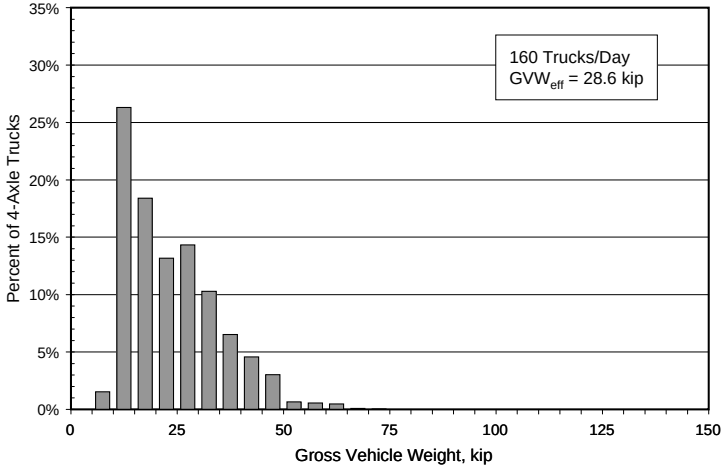

(c) Four-Axle Trucks

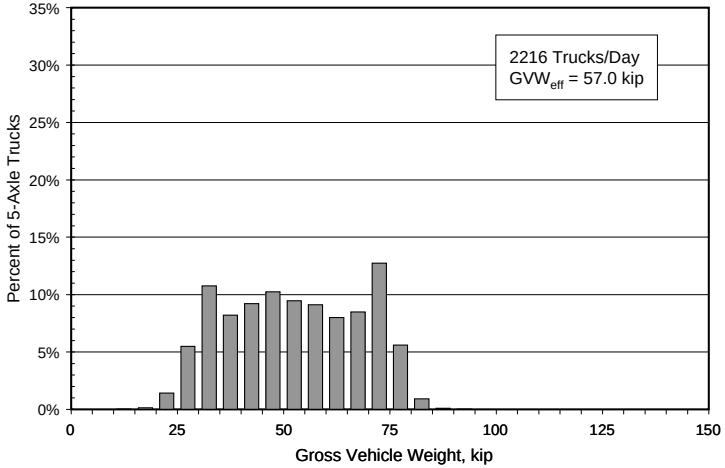

(d) Five-Axle Trucks

Figure 2.12 Distribution of Gross Vehicle Weights for Trucks

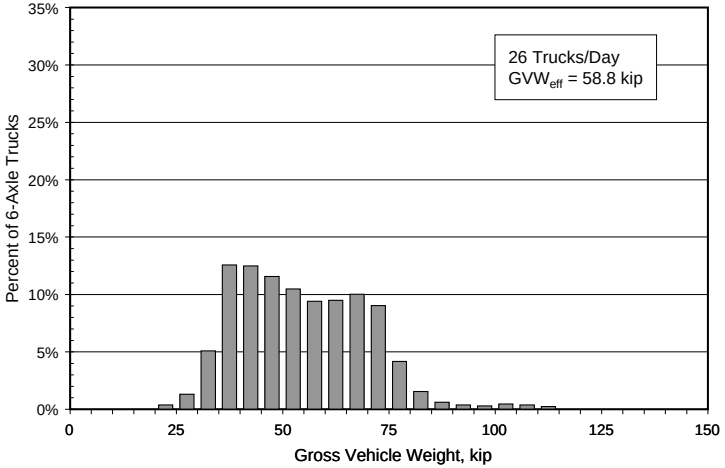

(e) Six-Axle Trucks

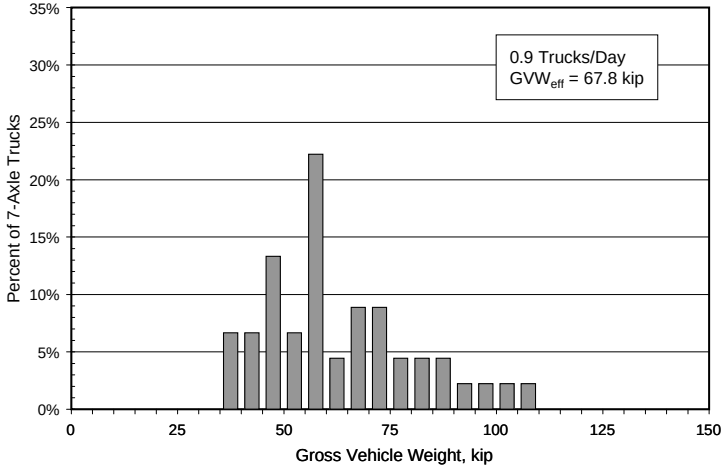

(f) Seven-Axle Trucks

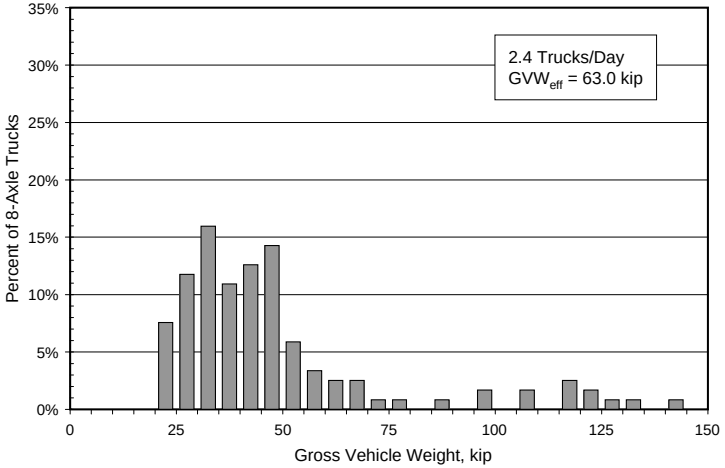

(g) Eight-Axle Trucks

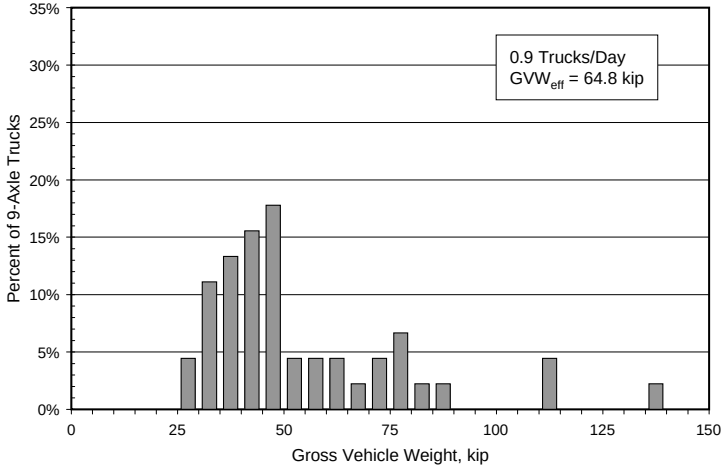

(h) Nine-Axle Trucks

Figure 2.12 (cont). Distribution of Gross Vehicle Weights for Trucks

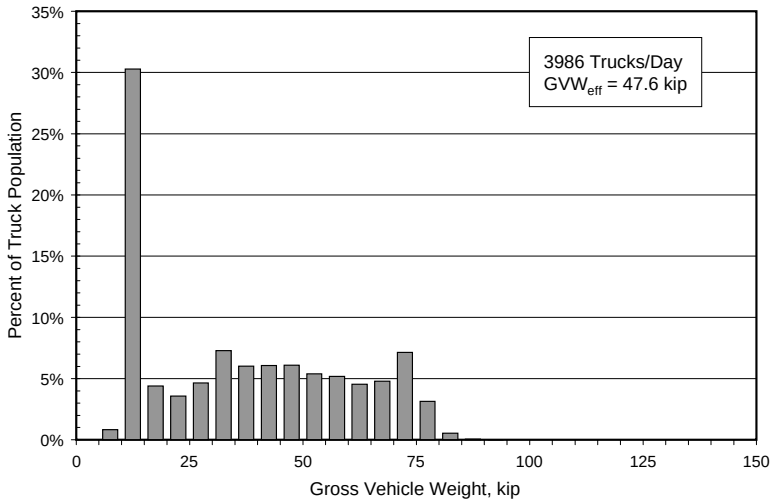

Figure 2.13 Distribution of Gross Vehicle Weights for Complete Truck Population

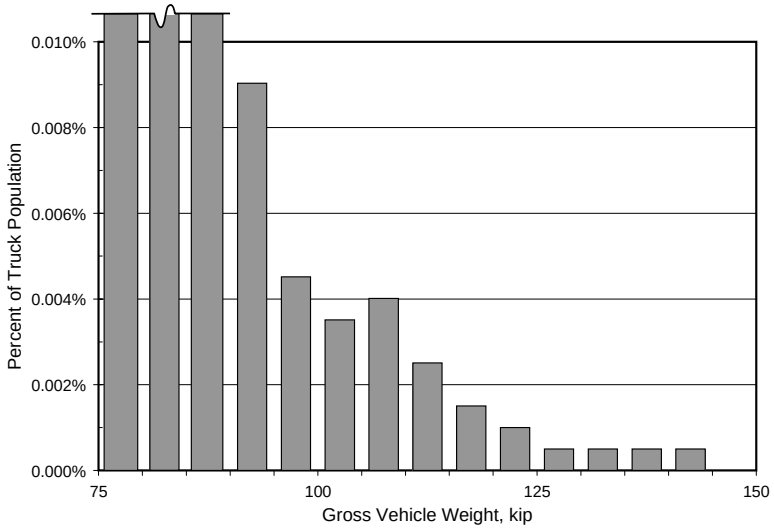

Figure 2.14 Detail of Truck Spectrum

Table 2.6 Summary of Axle Weights and Spacings for T5-1

Parameter	Axle Weight, kip					GVW	Axle Spacing, ft				Total Length
	A	B	C	D	E	(kip)	AB	BC	CD	DE	(ft)
Minimum	3.5	2.1	1.4	1.0	0.7	17.6	8.5	3.4	9.7	2.7	29.1
Mean	10.4	10.9	10.5	10.3	10.2	52.4	17.0	4.3	33.4	4.1	58.9
Median	10.7	10.7	10.3	10.1	10.0	51.7	17.3	4.3	33.7	4.1	59.4
Maximum	28.5	27.2	26.9	25.7	28.5	96.7	24.9	5.4	45.6	9.1	76.8

Note: Statistics developed from population of 98,433 trucks.

Table 2.7 Summary of Axle Weights and Spacings for T2-1

Parameter	Axle Weight, kip		GVW	Total Length
	A	B	(kip)	(ft)
Minimum	3.5	0.9	4.6	2.1
Mean	4.5	4.1	8.6	12.6
Median	4.1	3.4	7.7	12.7
Maximum	32.9	29.7	44.6	23.5

Note: Statistics developed from population of 66,352 trucks.

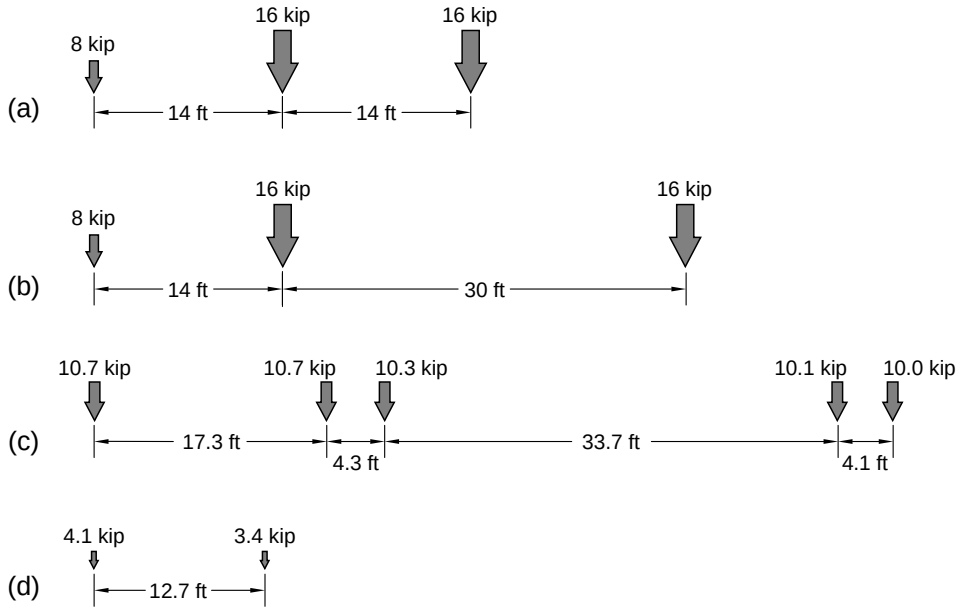

Figure 2.15 Comparison of HS-20 Design Vehicles with Median Weigh-in-Motion Vehicles (a) Short HS-20, (b) Long HS-20, (c) Median T5-1, and (d) Median T2-1

2.6 MINIATURE DATA ACQUISITION SYSTEM

A commercially available data acquisition system, MicroSAFE, was used to collect all field strain data associated with this project. Each unit is a single-channel data acquisition system and has the capability of collecting three types of data: raw strain data, rainflow data, and combined raw strain data and rainflow data. In all cases, the unit is designed to record the response of a 120-Ω strain gage.

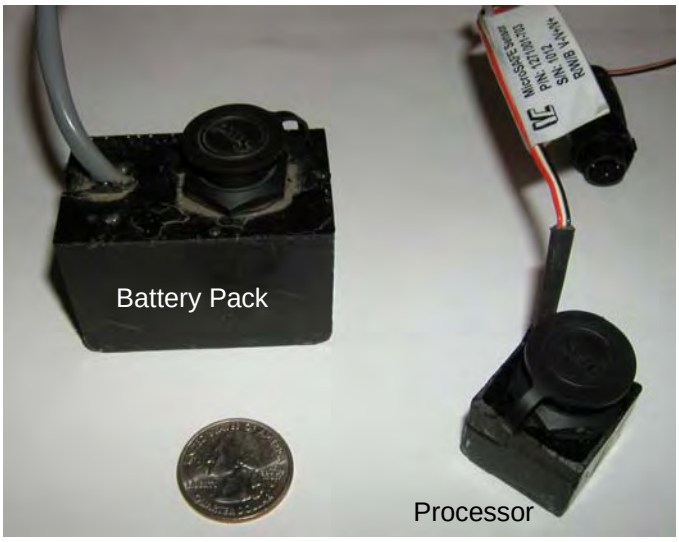

Figure 2.16 MicroSAFE Data Acquisition System

Each MicroSAFE unit comprises two basic components: the processor and a battery pack (Figure 2.16). The electronics within the processor convert the analog signal from the strain gage to a digital signal and then process the data using the rainflow counting algorithm. The unit is programmed using a notebook computer, which is connected to the battery pack using a communications cable. One programmed, the units operate independently in the field; however, each unit must be connected to the notebook computer to download the stored data. The battery packs used in this investigation had an expected life of 45 days when collecting rainflow data; however, it was not possible to determine the remaining life of a battery after a few days of use. Newer models include a remaining charge indicator.

The units are programmed using a graphical user interface (GUI) that was specifically designed to communicate with the MicroSAFE units (Holman, 2003). Details of the GUI and a summary of the input required from the user to program the units are discussed in Appendix A. An overview of each mode of operation is provided in this section.

2.6.1 Acquisition of Raw Strain Data

Strain data are acquired at a rate of 32 Hz in this mode of data acquisition. The collection period may vary from 1 to 33 min. Data may only be acquired during a single collection period and must be downloaded to the notebook computer before beginning the next collection period.

2.6.2 Acquisition of Rainflow Data

Strain data are acquired at a rate of 32 Hz and are converted to rainflow counts in real time. Only the rainflow counts are saved in this mode of data acquisition. A total of 32 bins are available to storing the rainflow counts. The user must specify the bin size and the noise threshold. Cycle counts below the

noise threshold are stored separately from the first bin and cycles with strain ranges larger than the last bin are stored in the last bin. The duration of each collection period may vary from 1 min to 23 hr 59 min. The user may define up to 512 collection periods and a time of at least 1 min must be programmed between each collection period. Data are stored to nonvolatile memory during the time between collection periods. If the battery were to fail during a collection period, data recorded during the current collection period would be lost, but data recorded during previous collection periods are available for download.

In most cases, the data were acquired in this mode during the field tests. A collection period of 23 hr 59 min was typically used with a 1-min gap between the collection periods. In most cases, 28 collection periods were used.

2.6.3 Acquisition of Raw Strain Data and Rainflow Data

Strain data are acquired at a rate of 32 Hz and converted to rainflow counts in real time in this mode of data acquisition. Both the raw data and the rainflow counts are stored. The collection period may vary from 1 to 59 min. Data may only be acquired during a single collection period and must be downloaded to the notebook computer before beginning the next collection period.

This mode of acquisition was used in the field during installation of the MicroSAFE units. Raw and rainflow data would be acquired for short periods of time – on the order of 2 min – in order to determine appropriate values for the bin size and noise threshold.

CHAPTER 3: DESCRIPTION OF TWO BRIDGES MONITORED IN THIS STUDY

The live-load response of two fracture critical bridges was monitored during this investigation. The structural features of the bridges are described in this chapter and the measured rainflow response is discussed in Chapters 4 and 5. Both bridges are considered to be fracture critical because two longitudinal girders and transverse floor beams comprise the superstructure of each bridge. The failure of one longitudinal girder in either bridge is expected to cause collapse of the bridge.

The older of the two bridges, the Medina River Bridge, is discussed in Section 3.1. The two-lane bridge carries the northbound lanes of I-35 over the Medina River, approximately 10 miles south of San Antonio. The traffic volume crossing the bridge is high, and includes a significant number of trucks. In contrast, the 12th Street Exit Ramp from southbound I-35 in downtown Austin experiences moderate traffic volume and very few trucks. The exit ramp is discussed in Section 3.2.

3.1 MEDINA RIVER BRIDGE

The Medina River Bridge (Figure 3.1) was designed in 1935 to carry two lanes of traffic. The bridge comprises eleven spans and has an overall length of 665 ft. The four, 48-ft spans at the south end of the bridge and the four, 50-ft spans at the north end of the bridge are simply-supported, slab-girder systems and are not considered to be fracture critical. Therefore, only the middle three spans were studied in this investigation. As shown in Figure 3.2, the depth of the longitudinal girders varies along the length of the middle three spans and the center portion of the bridge is suspended from cantilevers, which extend beyond the interior supports (Figure 3.3).

In 1971, the bridge was widened to accommodate a third lane of traffic. The extra lane is supported on three longitudinal plate girders, which are continuous over the center supports. Because the structural systems are very different for the older and newer sections of the bridge, the structures were isolated during construction. A longitudinal gap separates the concrete decks in the original structure and the added lane (Figure 3.4). Therefore, the original structure, and the modifications made to it in 1971 to widen the traffic lanes, can be considered to be independent of all other potions of the bridge.

The geometry of the bridge is discussed in Section 3.1.1. The structural model used to evaluate the service-load response is discussed in Section 3.1.2, and the calculated variations in moment and stress corresponding to a standard design vehicle crossing the bridge are presented in Section 3.1.3.

Figure 3.1 Aerial View of Medina River Bridge (www.maps.google.com)

Figure 3.2 Center Three Spans of Medina River Bridge (viewed from North)

Figure 3.3 Center Span of Medina River Bridge (viewed from South)

Figure 3.4 Separation between Original Structure and Lane Added in 1971

3.1.1 Geometry

The center three spans of the Medina River Bridge are symmetrical about the center (Figure 3.5). The end spans are 73′-6″, while the center span is 125′-0″. The longitudinal girders are continuous over the interior supports and extend 30′-7″ into the center span. The center 63′-10″ section of the center span is suspended from these cantilevers.

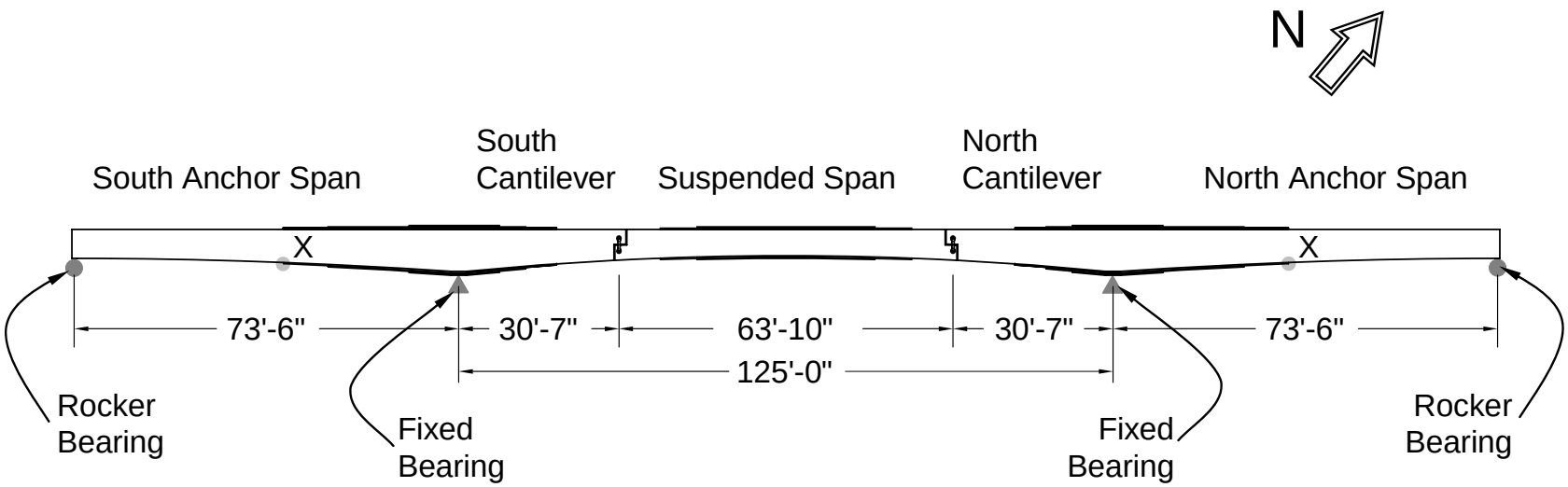

Girder depth (back to back of double angles):
- 5′-6½″ - End supports
- 8′-0″ - Interior supports
- 5′-0″ - Midspan of suspended span

Cover Plates (top and bottom flanges):
- Three, ½″ plates over interior supports
- Two plates ($^{7}/_{16}$″ and ⅜″) along suspended span

Location X:
- Location of highest stress range due to HS-20 design vehicle.

Figure 3.5 Elevation of Medina River Bridge

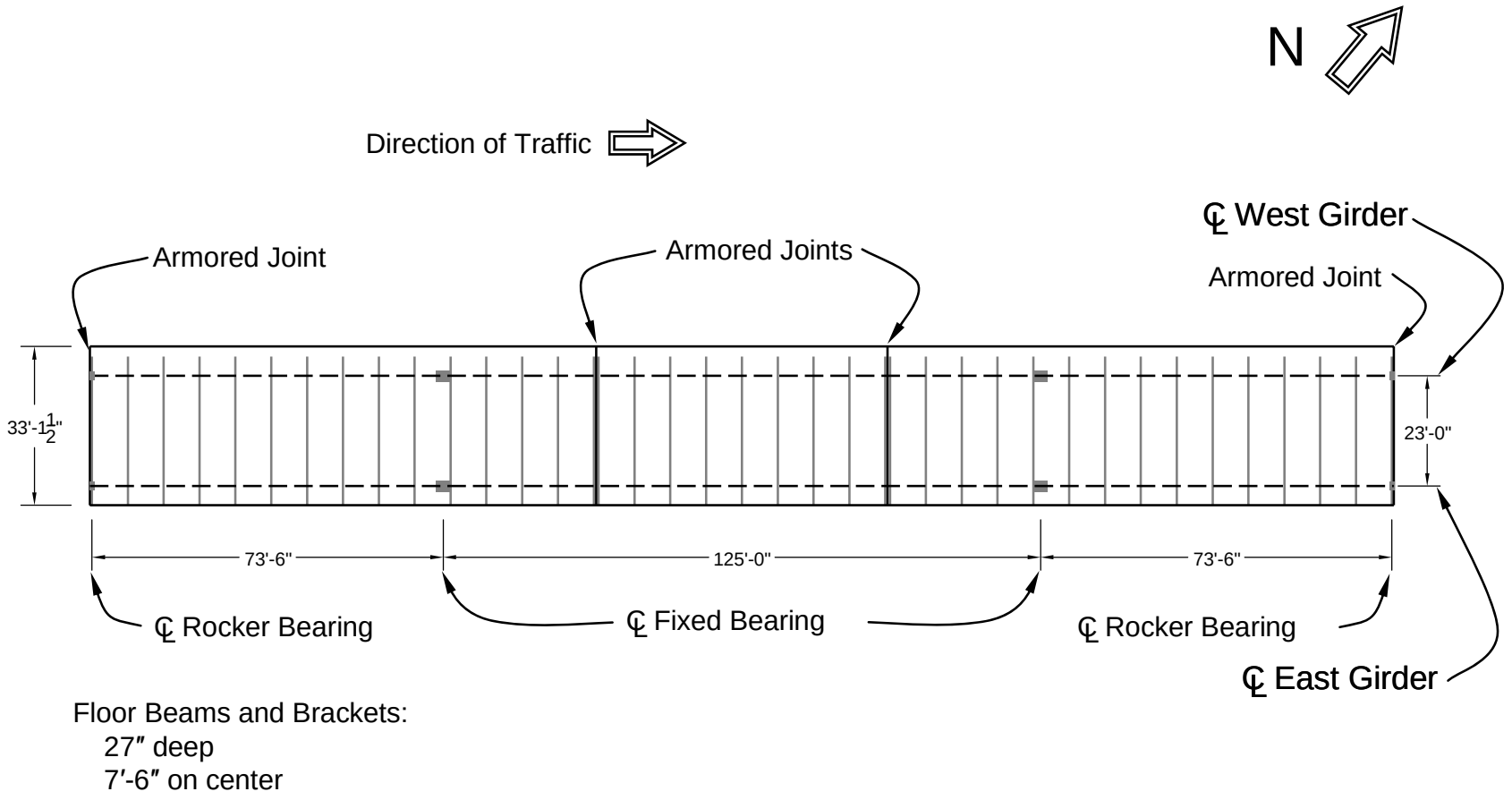

Floor Beams and Brackets:
27″ deep
7′-6″ on center

Figure 3.6 Plan of Medina River Bridge

The longitudinal girders are built-up sections. A ⅜″ plate serves as the web and double 8x8x½ angles form the top and bottom flanges. The depth of the longitudinal girders varies continually along the span of the bridge. At the north and south ends, the girders are 5′-6½″ deep. Over the interior supports, the girders are 8′-0″ deep, and at midspan of the suspended span, the girders are 5′-0″ deep. Cover plates are used over the interior supports and at the center of the suspended span. The maximum thickness of the cover plates is 1½″. All structural connections were made using ¾″ rivets.

The transverse floor beams are 27″ deep and spaced 7′-6″ on center (Figure 3.6) along the length of the bridge. Expansion joints are located at the north and south ends of the bridge and the longitudinal girders are supported on rocker bearings at these locations. The girders are supported on fixed bearings over the center supports. The suspended span is supported by 4½ -in. diameter pins and eye bars.

The centerline distance between the longitudinal girders is 23′-0″. The original bridge accommodated two, 12-ft traffic lanes and two sidewalks (Figure 3.7). After widening, the width of the traffic lanes was increased to 14 ft; however, the lanes were no longer symmetric with respect to the longitudinal girders (Figure 3.8). Transverse, cantilevered brackets were added to the longitudinal girders to support the wider traffic lanes (Figure 3.9). Twelve-in. deep channels run longitudinally at the ends of the brackets, and ¾″-diameter studs were spaced 2′-6″ on center along the channels to engage the 8-in. concrete deck. The original concrete deck was demolished when the bridge was widened.

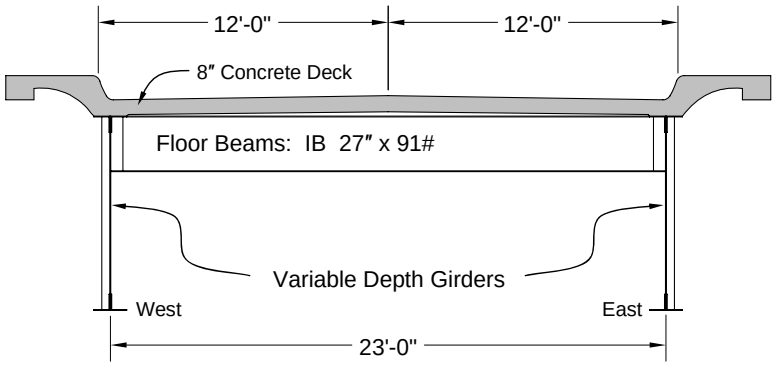

Figure 3.7 Original Cross Section of Bridge

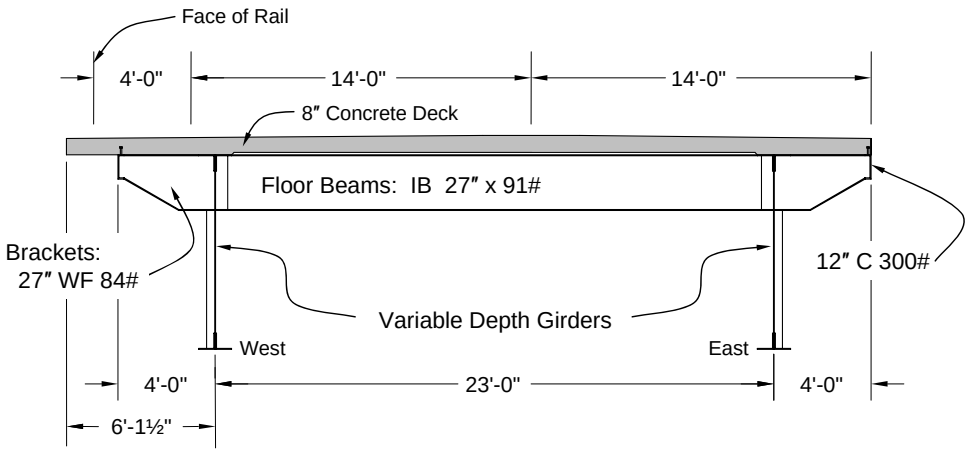

Figure 3.8 Cross Section of Bridge after Widening

Figure 3.9 West Girder of Medina River Bridge

3.1.2 Structural Model

Using the idealized boundary conditions, the Medina River Bridge is considered to be statically determinant. Therefore, a line-girder analysis was used to evaluate the live-load response of the bridge. Calculated moments in the line girder were distributed to the longitudinal girders using the live load distribution factors defined in the AASHTO LRFD Design Specifications (2004):

$$M_g = LLDF \cdot M_b \tag{3.1}$$

where M_g is the moment in a longitudinal girder, M_b is the moment calculated from the line-girder analysis, and *LLDF* is the live load distribution factor. Because only two longitudinal girders support the

deck, the lever rule was used to calculate the live load distribution factors. Vehicles were assumed to be centered in the actual traffic lanes (Figure 3.10).

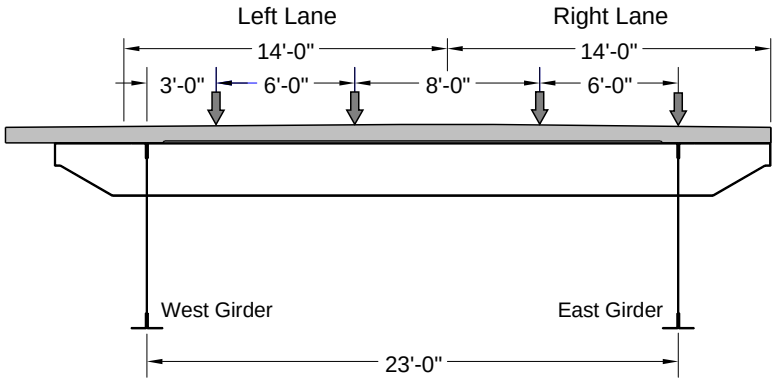

Figure 3.10 Locations of Wheel Loads for Vehicles Centered in Traffic Lanes

The resulting live load distribution factors are reported in Table 3.1 for a single vehicle in each lane. The east girder attracts a larger portion of the live load moment than the west girder because the traffic lanes are not symmetric with respect to the girders, and the outer wheel load is directly above the east girder when the vehicle is in the right lane, while the outer wheel is 3 ft from the west girder when the vehicle is in the left lane.

Table 3.1 Live Load Distribution Factors for Medina River Bridge

Longitudinal Girder	Location of Vehicle*	
	Left Lane	Right Lane
West	0.74	0.13
East	0.26	0.87

* Single vehicle was used in all analyses.

Flexural stresses, σ, can then be calculated from the moments in each longitudinal girder:

$$\sigma = \frac{M_g \cdot c}{I_c} \tag{3.2}$$

where c is the distance from the neutral axis to the extreme fiber of the cross section and I_c is the moment of inertia of the composite cross section. All three parameters on the right side of Eq. 3.2 vary along the length of the longitudinal girders. The composite cross section at midspan of the suspended span is shown in Figure 3.11. An effective flange width of 12 times the concrete slab depth was used in all

calculations. The compressive strength of the concrete was assumed to be 3000 psi and the modulus of elasticity of the concrete was taken as 3120 ksi.

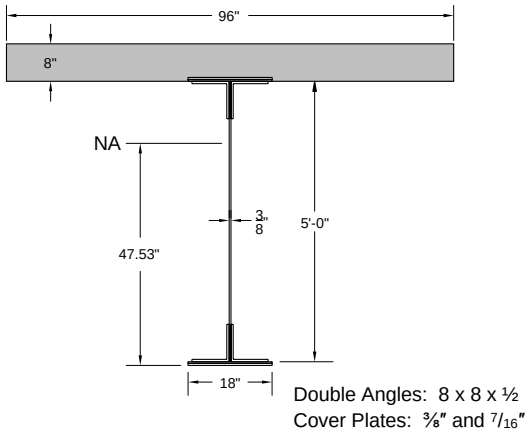

Figure 3.11 Dimensions of Composite Cross Section at Midspan of Suspended Span

The variation of the overall depth of the steel section and the neutral axis depth of the composite cross section is plotted in Figure 3.12. The corresponding variations in the moment of inertia of the composite cross section are shown in Figure 3.13. The moment of inertia over the interior supports is more than five times larger than the moment of inertia at the north and south ends of the bridge.

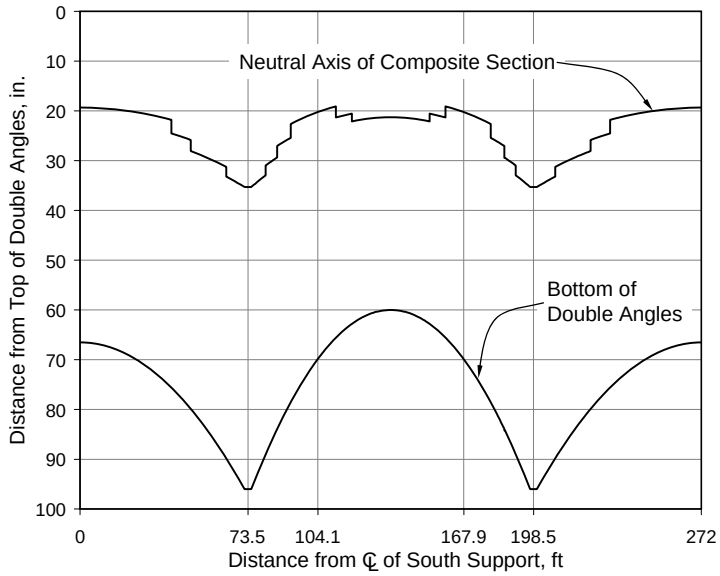

Figure 3.12 Variation of Overall Depth and Neutral Axis Depth along Medina River Bridge

Figure 3.13 Variation of Moment of Inertia of Composite Cross Section along Medina River Bridge

3.1.3 Calculated Live-Load Response

SAP 2000 (CSI 2006) was used to calculate the live-load response of the line girder representation of the Medina River Bridge. A single, HS-20 design vehicle with 14-ft axle spacings (Figure 2.15a) was selected as the loading vehicle. The calculated moment envelope is plotted in Figure 3.14. The end spans experience both positive and negative moments, while only negative moments develop within the cantilevers and only positive moments develop within the suspended span. The maximum moment occurs over the supports and the maximum range in moments occurs within the end spans.

Because the moment of inertia varies along the span, the maximum variation in live-load stress does not occur at the location of the maximum variation in live-load moment. Equation 3.2 was used to calculate the range of live-load stress from the results of the line-girder analysis using the calculated variations of the moment of inertia (Figure 3.13) and neutral axis depth (Figure 3.12) along the span.

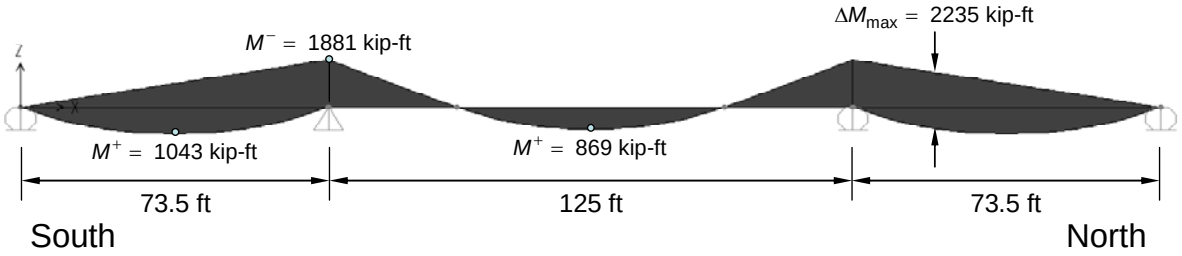

Figure 3.14 Results of Line-Girder Analysis of Medina River Bridge

Results are plotted in Figure 3.15 for the bottom face of the east girder when the HS-20 design vehicle is centered in the right lane. The maximum calculated variation in stress was 17.4 ksi and occurred at the end of the first cover plate (Location X in Figure 3.5). Due to the differences in the live load distribution factors, the maximum calculated variation in stress in the west girder was 14.8 ksi when the HS-20 design vehicle was centered in the left lane.

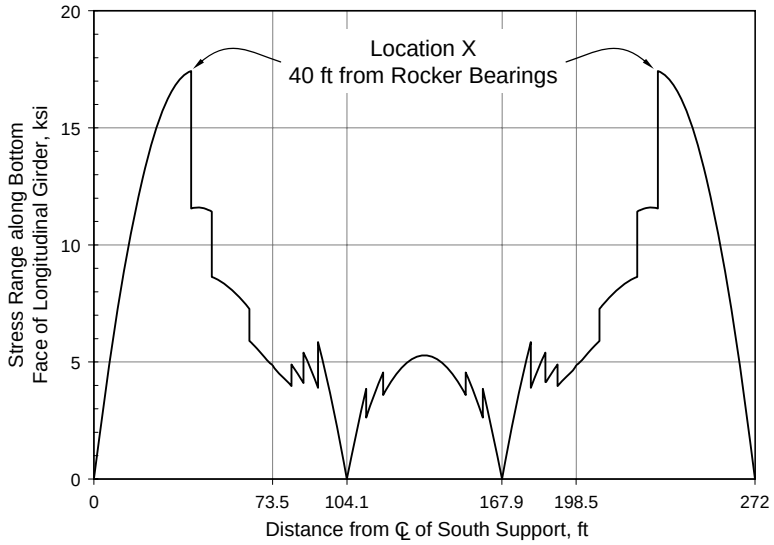

Figure 3.15 Calculated Stress Range in East Girder of Medina River Bridge due to HS-20 Design Vehicle Centered in Right Lane

3.2 12TH STREET EXIT RAMP

The exit ramp from southbound I-35 to 12th Street in downtown Austin (Figure 3.16) carries one lane of traffic over a grade-level entrance ramp to I-35 (Figure 3.17). The bridge was designed in 1971. The geometry of the bridge is discussed in Section 3.2.1 and the structural model used to evaluate the live-load response is discussed in Section 3.2.2. Calculated variations in moment and stress corresponding to a standard design vehicle crossing the bridge are presented in Section 3.2.3.

3.2.1 Geometry

The bridge has an unusual geometry (Figure 3.18) due to the close proximity of the exit ramp to the adjacent entrance ramp. The bridge is supported on a skewed abutment at the north end and on a square abutment at the south end. The abutments are approximately 254 ft apart under the west girder and 154 ft apart under the east girder. A single column is positioned at midspan of the west girder, creating a two-span continuous beam with equal spans.

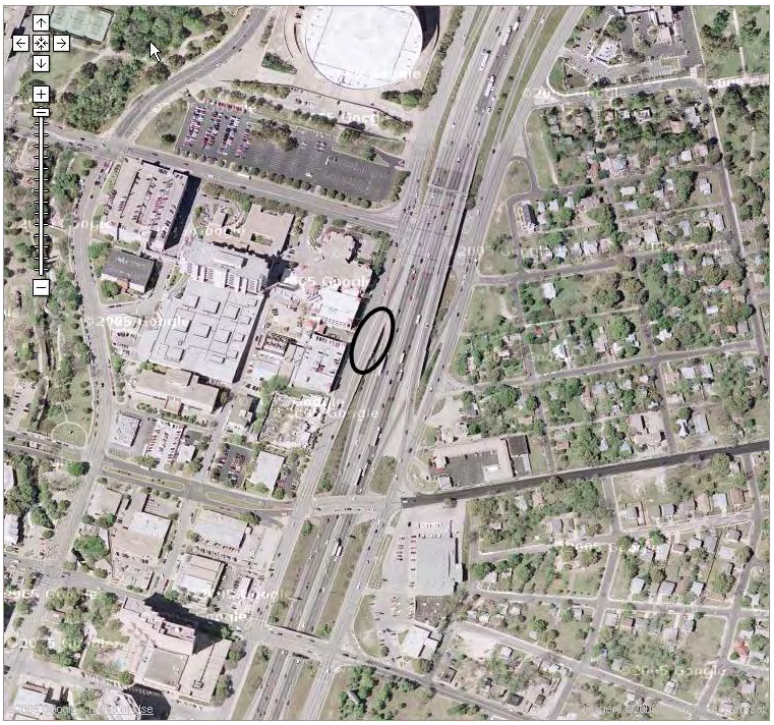

Figure 3.16 Aerial View of 12th Street Exit Ramp in Downtown Austin (www.maps.google.com)

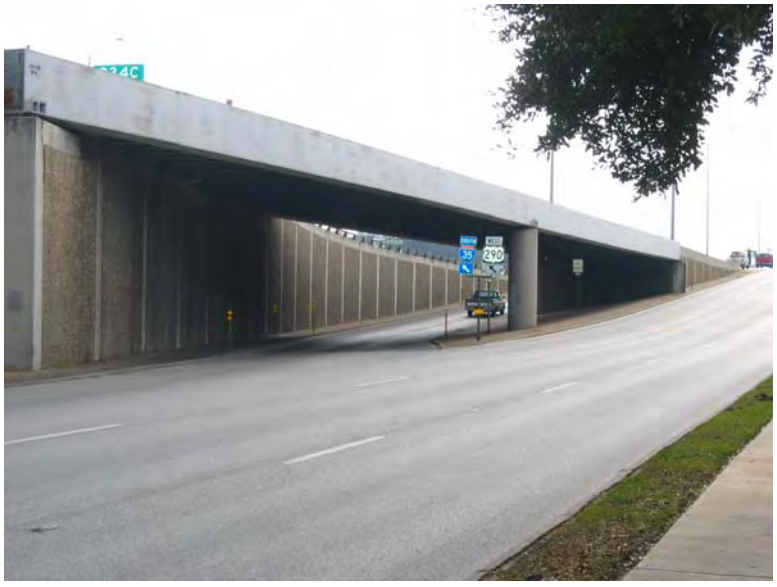

Figure 3.17 12th Street Exit Ramp Crosses Grade-Level Entrance Ramp to I-35

A photograph of the west longitudinal girder is shown in Figure 3.17. The skewed abutment is visible on the left, the column is near the center of the photo, and the square abutment is visible on the right.

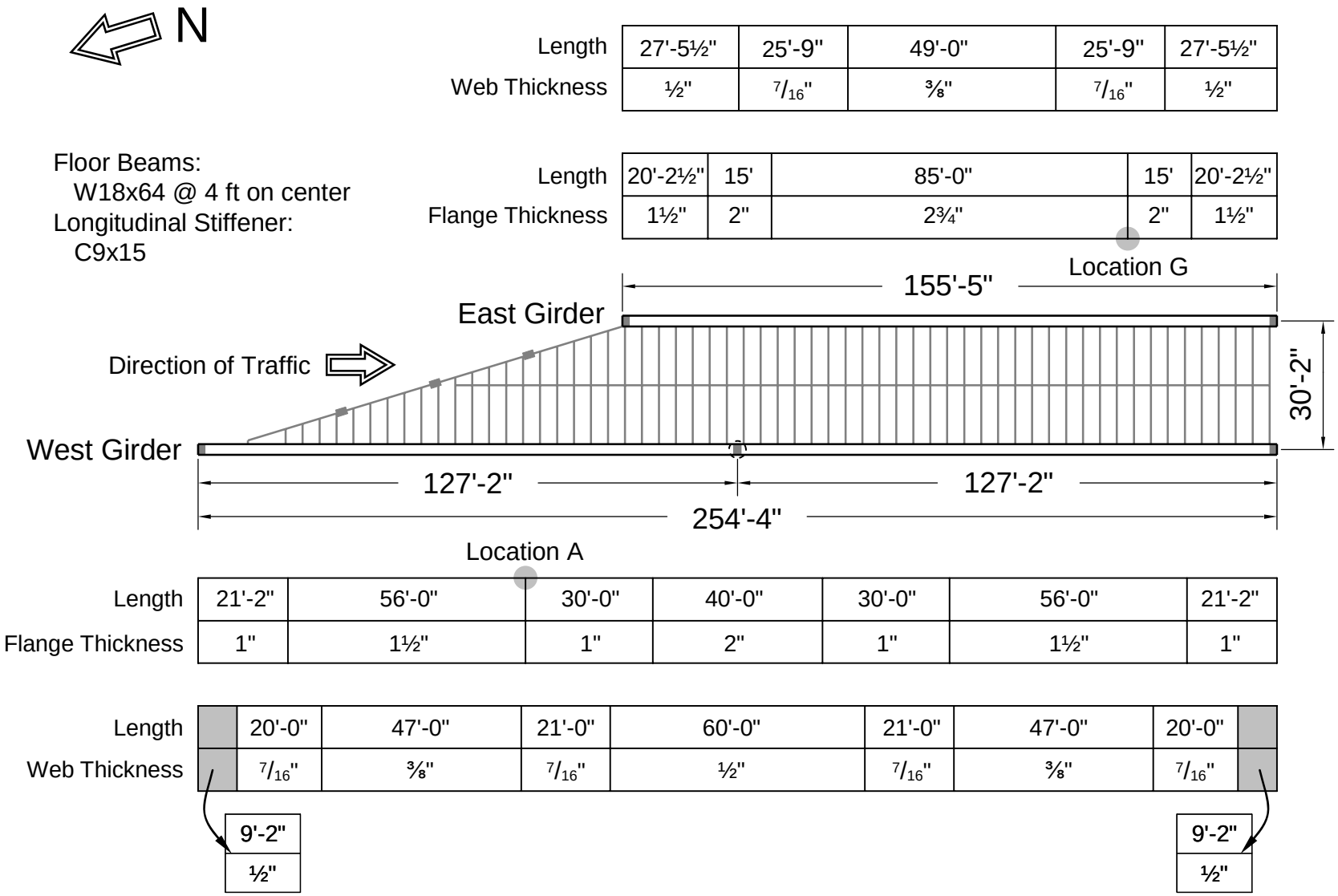

Figure 3.18 Plan of 12th Street Exit Ramp

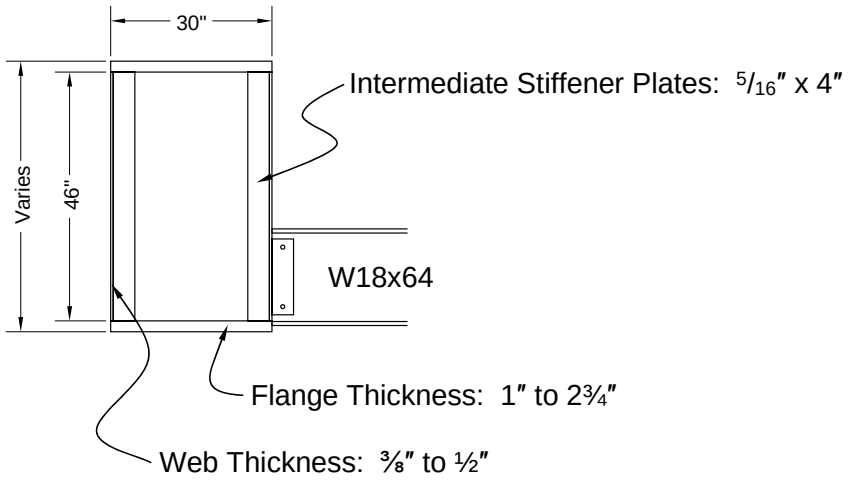

Figure 3.19 Dimensions of Longitudinal Box Girders in 12th Street Exit Ramp

The longitudinal girders are box beams (Figure 3.19). The height of the box, and the thickness of the flanges, varies along the length of the girders, but the width remains constant. The minimum depth is 48″ at the ends of the west girder and the maximum depth is 51½″ at midspan of the east girder. At all locations, the thickness of the top flange is equal to the thickness of the bottom flange.

Transverse floor beams span between the two longitudinal girders and are spaced at 4′-0″ on center. W18x64 sections are used for all floor beams. The floor beams are connected to the box girders near the bottom flange of the box (Figure 3.19). A 4″ wide by ½″ thick plate was welded to the web of the box girder and bolted to the web of the floor beam during erection. The bottom flange of each floor beam was then welded to the bottom flange of the longitudinal girders and the top flange was welded to the inside web of the longitudinal girders. The backing bars used to connect the floor beams to the longitudinal girders were not removed (Figure 3.20).

The 6½″ concrete deck is supported by the floor beams, but is not connected to the longitudinal box girders (Figure 3.21). Pairs of studs were spaced at 12 in. on center along the floor beams to engage the bridge deck.

The west longitudinal girder is supported on three elastomeric bearings and the east longitudinal girder is supported on two elastomeric bearings (Figure 3.22). Three additional elastomeric bearings were used to support the floor beam along the skewed abutment (Figure 3.23).

Figure 3.20 Welded Connections between Floor Beams and Longitudinal Box Girders

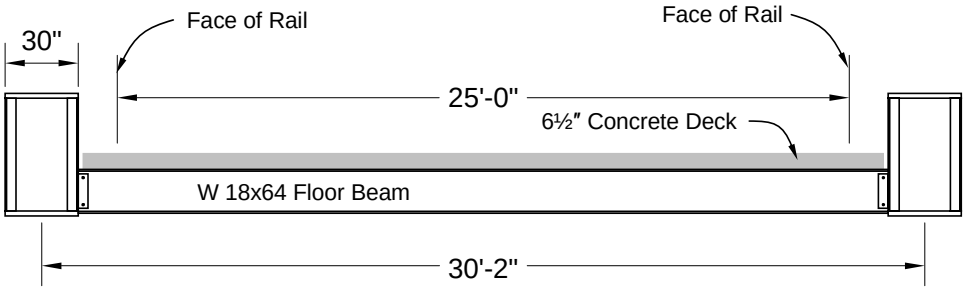

Figure 3.21 Transverse Section

Figure 3.22 Elastomeric Bearing at South End of West Girder

Figure 3.23 Elastomeric Bearings above Skewed Abutment

3.2.2 Structural Model

Due to the complexity of the geometry of the 12th Street Exit Ramp, a two-dimensional model of the longitudinal girders and floor beams (Figure 3.24) was developed using SAP2000 (CSI 2006). The dimensions of the structural members were modeled using the centerline dimensions between supports. The elastomeric bearings at the south end of each girder were idealized as pins and all other bearings were idealized as rollers. The floor slab was not included in the model.

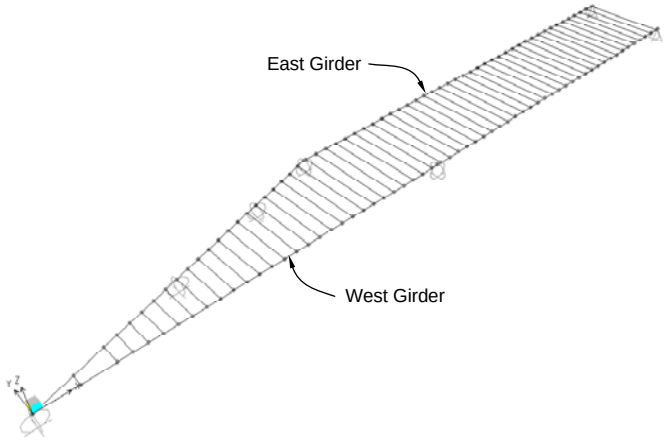

Figure 3.24 Structural Model of 12th Street Exit Ramp

Table 3.2 Variation of Moment of Inertia of Box Girders

Flange Thickness	Web Thickness*	Moment of Inertia
(in.)	(in.)	(in.^{4})
1	½	41,250
1½	½	58,890
2	½	77,270
2¾	½	106,250

* Actual variation in web thickness was ignored.

The variation in the flange thickness of the longitudinal box girders was considered, but the variation in the web thickness was ignored (Table 3.2). Therefore, the west girder was idealized using eight beam elements and the east girder was idealized using five beam elements. The moment of inertia was constant within each beam element. A single beam element was used to model each of the floor beams. Moments in the longitudinal girders were reported at the ends of each beam element and at each point of intersection with the floor beams.

3.2.3 Calculated Live Load Response

As with the line-girder analysis discussed in Section 3.1.3, the HS-20 design vehicle was used to evaluate the live load response of the 12th Street Exit Ramp. The vehicle was idealized using three point loads (Figure 2.15a) and the width of the vehicle was assumed to be zero. Three transverse locations were selected for the loading vehicle: (1) above the west girder, (2) above the east girder, and (3) along the center of the traffic lane. The calculated moment envelopes for the three sets of analyses are plotted in Figure 3.25, Figure 3.26, and Figure 3.27, respectively.

The results of the analyses with the design vehicle positioned above the girders (Figure 3.25 and Figure 3.26) were expected. Most of the moment is carried by the girder directly below the vehicle, but the floor beams transfer a small portion of the load to the opposite girder. When the loading vehicle is positioned along the center of the traffic lane (Figure 3.27); however, significant torsion develops in the floor beams near the skewed abutment. These torsional moments cause variations in the moments at the north end of the west girder, such that the maximum negative moment in this analysis occurs near the third point of the north span. It is expected that the amplitude of the torsional moments are overestimated in the analysis because the stiffness of the concrete deck is not considered in the structural model.

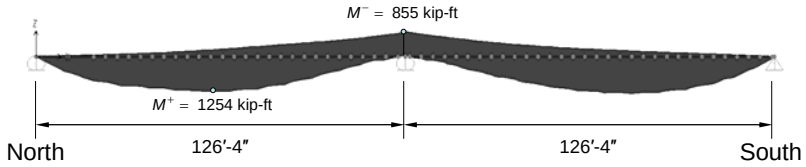

(a) West Girder

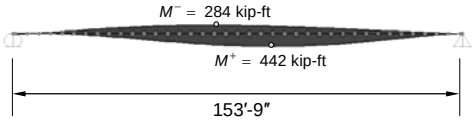

(b) East Girder

Figure 3.25 Calculated Moment Envelopes for HS-20 Vehicle Positioned Along West Girder of 12th Street Exit Ramp

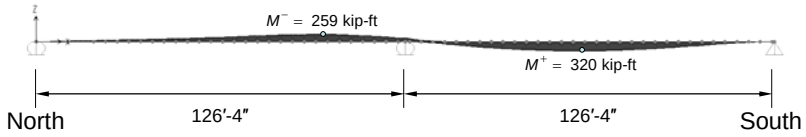

(a) West Girder

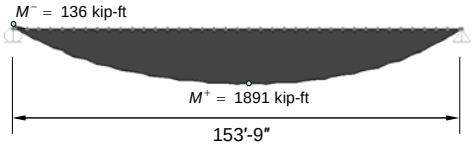

(b) East Girder

Figure 3.26 Calculated Moment Envelopes for HS-20 Vehicle Positioned Along East Girder of 12th Street Exit Ramp

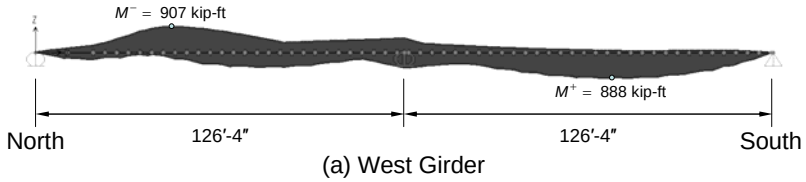

(a) West Girder

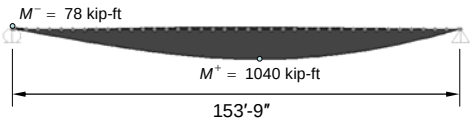

(b) East Girder

Figure 3.27 Calculated Moment Envelopes for HS-20 Vehicle Positioned Along Center of Traffic Lane for 12th Street Exit Ramp

The range of flexural stress in the extreme tension fiber of the box girders were calculated from the moment envelopes using Eq. 3.2. Because the concrete slab was not directly connected to the longitudinal girders, the effective width of the slab was taken as zero. The calculated ranges of stresses in the west and east girders for the moment envelopes in Figure 3.27 are shown in Figure 3.28 and Figure 3.29, respectively.

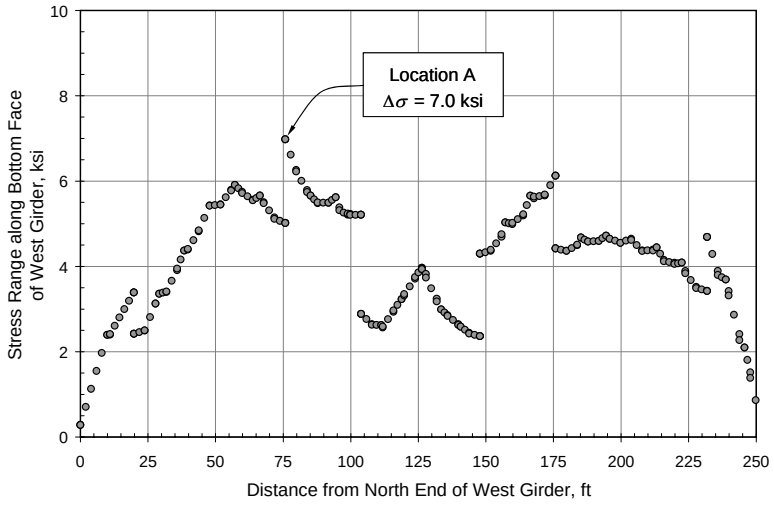

Figure 3.28 Calculated Stress Range in West Girder of 12th Street Exit Ramp due to HS-20 Design Vehicle in Center of Traffic Lane

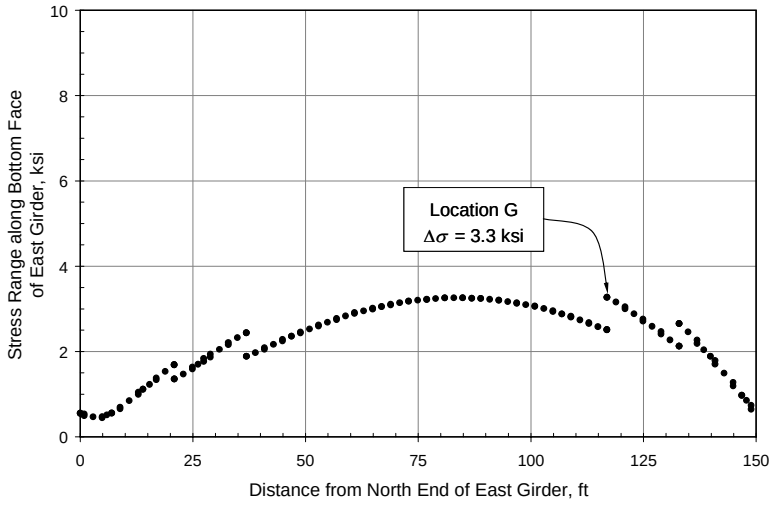

Figure 3.29 Calculated Stress Range in East Girder of 12th Street Exit Ramp due to HS-20 Design Vehicle in Center of Traffic Lane

The maximum calculated stress range in the west girder was 7.0 ksi, which occurred at Location A – the transition from a 1″ flange to a 1½″ flange near the north end of the girder (Figure 3.18). The calculated maximum stress range in the east girder was 3.3 ksi, which occurred at Location G – the transition from a 2″ flange to a 2¾” flange near the south end of the girder (Figure 3.18).

3.3 SUMMARY

Simple models were developed to evaluate the live load response of the Medina River Bridge and the 12th Street Exit Ramp. The Medina River Bridge is statically determinant; therefore, a line-girder analysis is sufficient to determine the distribution of live loads to the longitudinal girders. Due to the skewed abutment, the 12th Street Exit Ramp was more difficult to model. A two-dimensional model of the flexural elements was developed for this bridge.

An HS-20 design vehicle was used to evaluate the live load response of both bridges. The maximum calculated stress range due to a single HS-20 vehicle was 17.4 ksi in the east girder of the Medina River Bridge and 7.0 ksi in the west girder of the 12th Street Exit Ramp. The maximum stress did not occur at the location of maximum calculated moment in either bridge, but occurred at a location where the thickness of the bottom flange changed abruptly.

CHAPTER 4: RESPONSE OF MEDINA RIVER BRIDGE

The live-load response of the Medina River Bridge was monitored during two, 28-day rainflow collection periods. Strain gages were positioned at nine locations on the bridge: eight along the longitudinal girders and one at the end of a transverse floor beam. A tenth strain gage was used to monitor the thermal response of the miniature data acquisition systems. The layout of the strain gages is discussed in Section 4.1, traffic patterns identified from the weigh-in-motion station are summarized in Section 4.2, and the measured rainflow data are presented in Section 4.3.

Rainflow data were not successfully obtained from all ten strain gages. Problems were identified with both the installation of strain gages in the field and the long-term reliability of the miniature data acquisition systems. Therefore, careful evaluation of the rainflow data is required before calculating the fatigue life of the Medina River Bridge.

4.1 LAYOUT OF INSTRUMENTATION

The response of the Medina River Bridge was monitored during two, 28-day periods. Four strain gages were installed along the north cantilever span on 25 August 2004 for the first collection period. TxDOT personnel were conducting a fracture-critical inspection of the bridge at this time, and the research team used a snooper truck to install the instrumentation. Six strain gages were installed along the north anchor span on 25 January 2005 for the second collection period. The research team used a TxDOT bucket truck, which was positioned below the bridge, to install these instruments. In both cases, the strain gages and data acquisition systems were installed in a few hours.

The locations of the ten strain gages were identified using the letters A through J, as shown in Figure 4.1 and documented in Table 4.1. Eight of the gages were attached to the bottom face of the longitudinal girders, one gage was attached to the top flange of a transverse floor beam, and one gage was attached to an aluminum bar, which was not connected to the bridge, but did experience the thermal cycles. More information about the locations of the gages and the expected response of the bridge at these locations is provided in this section.

All strain gages were manufactured by Tokyo Sokki Kenkyujo, Inc. and distributed by Texas Measurements, Inc. Gages attached to the bridge were designated FLA-6-11 (6-mm, 120-Ω, three-wire, foil gages, with temperature compensation for mild steel). Strain gage J was designated FLA-6-23 (6-mm, 120-Ω, two-wire, foil gage, with temperature compensation for aluminum).

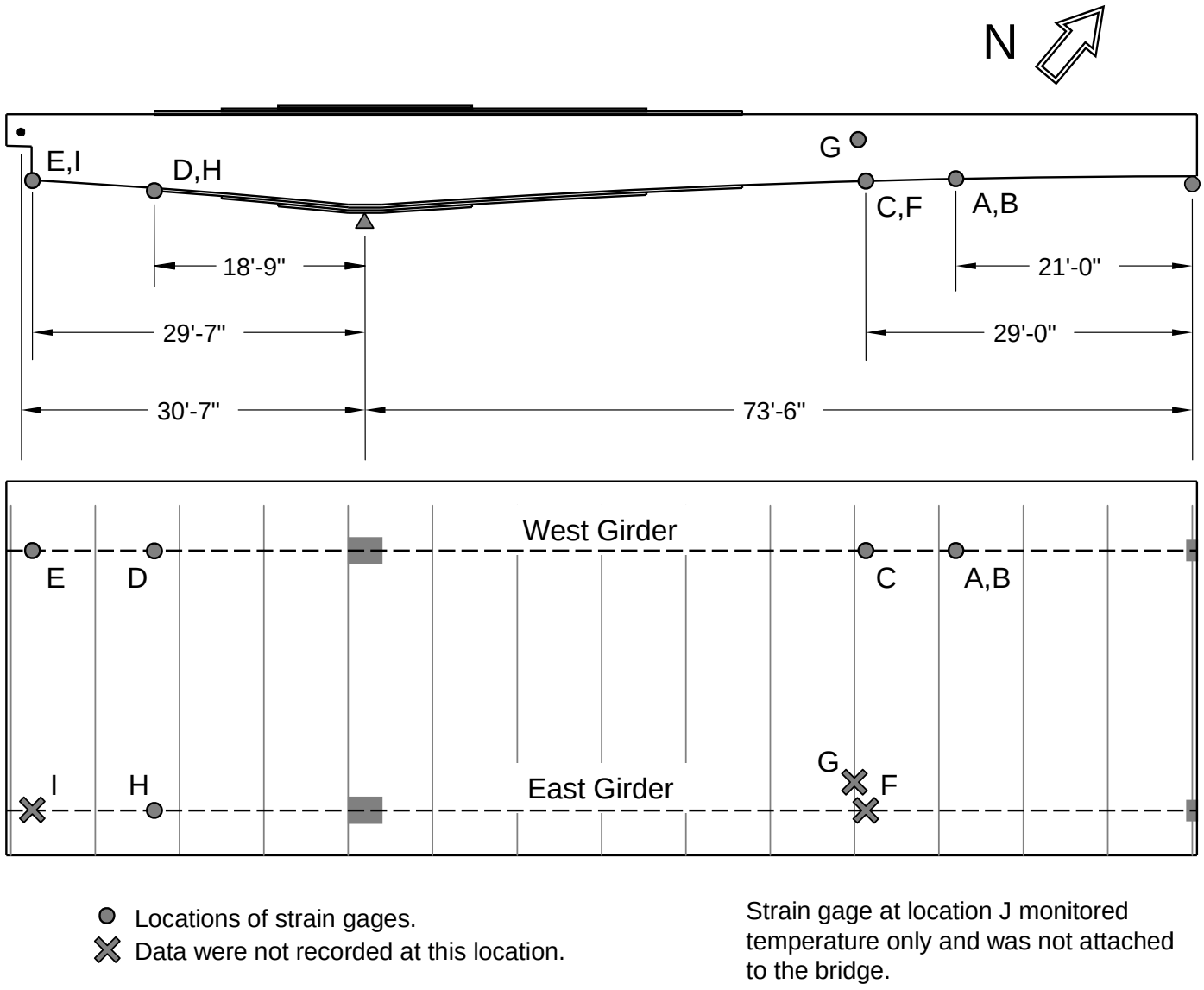

Figure 4.1 Locations of Strain Gages Used to Monitor the Response of the Medina River Bridge

Table 4.1 Locations of Strain Gages Used to Monitor Response of Medina River Bridge

Strain Gage ID	Location	Span	Girder	Data Collection Period
D	18′-9″ south of north fixed bearing	Cantilever	West	Aug 04
H			East	
E	1′ north of north hinge	Cantilever	West	Aug 04
I			East	
A	21′ south of north rocker bearing	Anchor	West	Jan 05
B				
C	29′ south of north rocker bearing	Anchor	West	Jan 05
F			East	
G	30′ south of north rocker bearing	Anchor	Transverse Floor Beam	Jan 05
J	Recorded temperature cycles only	North Rocker Support	West	Jan 05

4.1.1 Thermal Response

During the first rainflow collection period for the Medina River Bridge, one strain cycle was recorded during each 24-hour recording period that exceeded the next largest strain cycle by more than 70 $\mu\varepsilon$. This response was not expected. Therefore, during the second collection period, the rainflow response of an aluminum bar, which was not connected to the bridge, was recorded. The bar was placed near the north rocker support for the west girder and did not experience strain cycles due to the vehicular loads. Because strain gage J had only two wires and because the bar was aluminum, the thermal changes were expected to be larger than those measured using three-wire gages attached to the bridge, but the recorded data were used to confirm that the rainflow counts recorded by the miniature data acquisition systems need to be corrected for thermal cycles.

4.1.2 North Cantilever Span

During the first collection period, two pairs of strain gages were positioned along the longitudinal girders in the north cantilever span. Two areas of interest were identified from the line-girder analyses of the Medina River Bridge (Section 3.1): large negative moments were expected over the interior supports and the moment was expected to be zero at the hinges. Because the depth of the cross section and the thicknesses of the cover plates varied with along the length of the longitudinal girders, the largest live-

load stress range was expected to occur immediately south of the first cover plate (Figure 4.2). Strain gage D was attached to the west girder and strain gage H was attached to the east girder at this location. Strain gages E and I were positioned immediately north of the hinge on the west and east girders, respectively.

Based on the ranges of calculated stresses, the data from the cantilever span were not expected to control the fatigue life of the bridge. Rather, the purpose of the first collection period was to verify that the hinges were working properly.

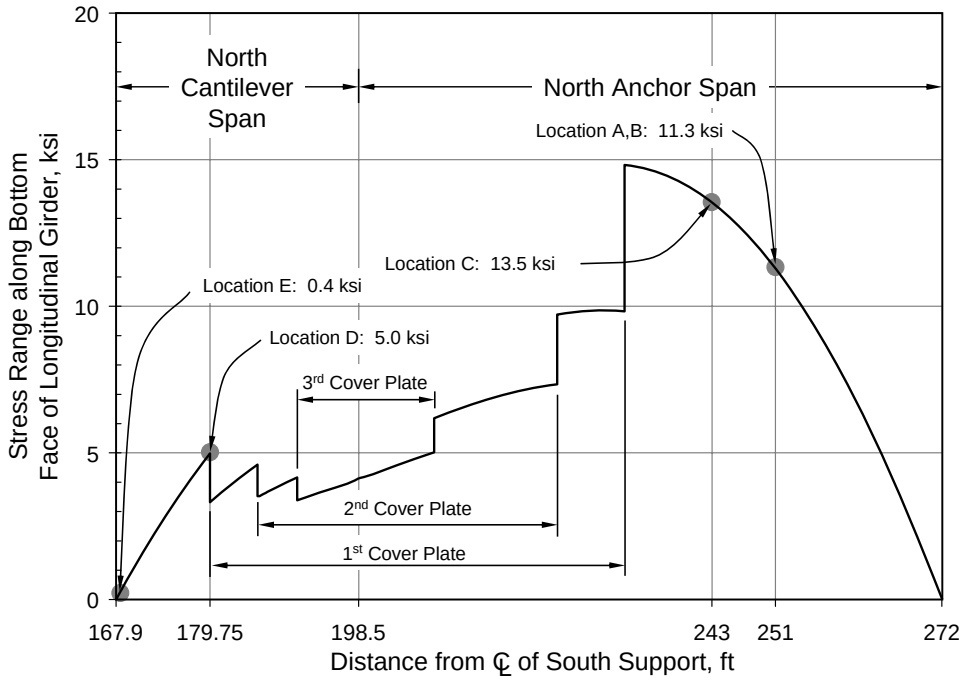

Figure 4.2 Calculated Stress Range in West Girder of North Span of Medina River Bridge due to HS-20 Design Vehicle Centered in Left Lane

The data acquisition systems were programmed prior to installing the units on the bridge and raw data were not collected before the start of the first collection period. The advantage of this approach is that the research team did not need to use the notebook computer in the field. The primary disadvantage is that the research team was not able to verify that the data acquisition units and strain gages were installed properly.

The parameters used to acquire rainflow data during the first collection period are documented in Table 4.2. In retrospect, the bin sizes should have been much smaller for strain gages E and I. The data acquisition system attached to strain gage I failed to collect data during the first rainflow collection period, but the cause of the failure is not known.

Table 4.2 Rainflow Parameters Used during First Collection Period

Strain Gage ID	DAQ ID	Bin Size ($\mu\varepsilon$)	Noise Threshold ($\mu\varepsilon$)	Notes
D	1006	10	5	—
E	1014	20	5	—
H	1007	10	5	—
I	1013	20	5	Rainflow data were not recorded by this unit.

4.1.3 North Anchor Span

During the second rainflow collection period, two pairs of strain gages were positioned along the longitudinal girders in the north anchor span and one strain gage was positioned at the east end of a transverse floor beam. Data were also collected from strain gage J (Section 4.1.1) during the second collection period.

As shown in Figure 4.2, the largest amplitude strain cycles in the longitudinal girders were expected near the middle of the north anchor span and north of the first cover plate. Four strain gages were positioned within the 20-ft region of highest calculated stress. Strain gages A and B were located 21 ft south of the north support on bottom face of the west longitudinal girder. The gages were positioned at the same location in order to evaluate the reliability of the data acquisition units. Strain gages C and F were located 29 ft south of the north support on the bottom face of the west and east longitudinal girders, respectively. Based on the live load distribution factors and the observed traffic patterns (more trucks were observed in the right lane than the left lane, Figure 4.3), higher strain levels were expected in the east girder. This pair of gages was positioned to evaluate those differences. Strain gage G was attached to the bottom face of the top flange of the transverse floor beam immediately south of strain gage F.

During installation of the instrumentation, combined raw strain and rainflow data were collected for 1 to 2 min from each data acquisition unit. The bin sizes and noise thresholds were then set for each unit based on the measured data. Fifteen-second portions of the raw strain records are shown in Figure 4.4 through Figure 4.8, and the maximum strain range during each raw strain record is listed in Table 4.3. The data were not recorded simultaneously by the gages, but all four strain gages attached to the longitudinal girders, and the associated data acquisition systems, seemed to be working properly. In retrospect, the raw strain data recorded by strain gage G never exceeded the noise threshold, and this gage should have been tested more thoroughly in the field before beginning the 28-day collection period.

Figure 4.3 Observed Traffic Patterns on Medina River Bridge

Table 4.3 Rainflow Parameters Used during Second Collection Period

Strain Gage ID	DAQ ID	Maximum Strain Range* ($\mu\varepsilon$)	Bin Size ($\mu\varepsilon$)	Noise Threshold ($\mu\varepsilon$)	Notes
A	1002	55	8	4	Battery failed during collection period.
B	1005	58	8	4	—
C	1004	132	8	4	—
F	1001	220	10	5	DAQ unit recorded one rainflow cycle each day throughout the collection period.
G	1007	8	8	4	DAQ unit failed after 4 hr during first day of collection period.
J	1006	—	8	4	—

* Strains recorded during installation of data acquisition units.

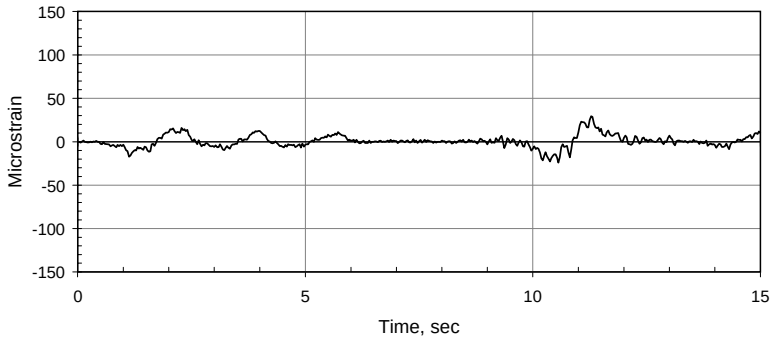

Figure 4.4 Raw Strain Data from Strain Gage A

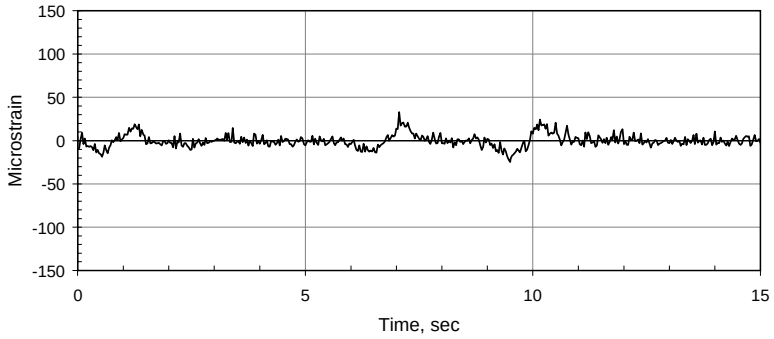

Figure 4.5 Raw Strain Data from Strain Gage B

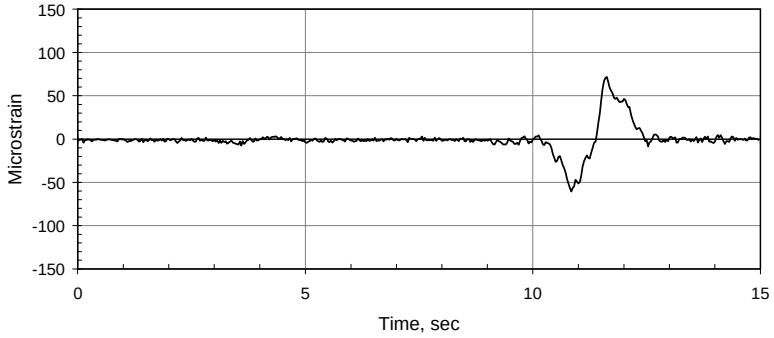

Figure 4.6 Raw Strain Data from Strain Gage C

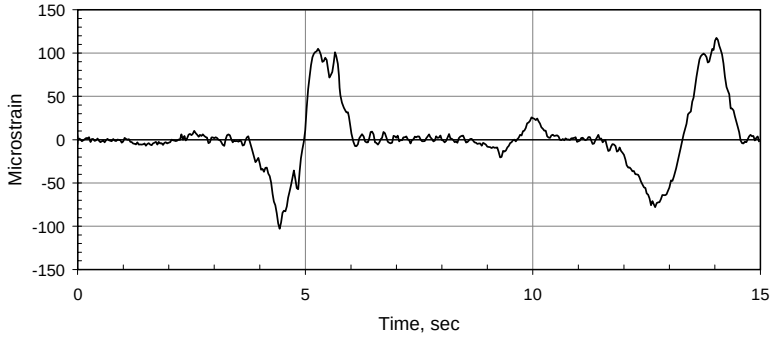

Figure 4.7 Raw Strain Data from Strain Gage F

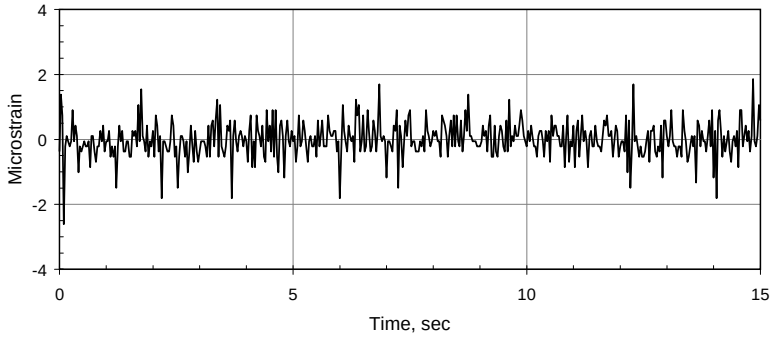

Figure 4.8 Raw Strain Data from Strain Gage G

As expected, the largest amplitude strain cycles were recorded by strain gage F. The bin sizes were selected such that the largest bin (32 times the bin size) was more than 1.5 times the largest strain range recorded during the 1 to 2-min acquisition period. In all cases, the bin sizes proved to be too small. Recommendations for selecting appropriate bin sizes are given in Chapter 7.

In spite of the fact that all data acquisition systems appeared to be working properly at the time of installation, three failed before the end of the second collection period. Twenty-four days of data were recorded for strain gage A before the battery failed. The data acquisition system attached to strain gage F collected data for the entire 28-day collection period, but only one rainflow cycle was recorded per day. Most days the amplitude of the cycle was less than the noise threshold. The data acquisition system attached to strain gage G failed after 4 hr during the first day. The causes of the failures of units 1001 and 1007 are not known.

4.2 OBSERVED TRAFFIC PATTERNS

As discussed in Chapter 2, weight-in-motion station 516 is located approximately 7 miles south of the Medina River Bridge on I-35 (Figure 4.9). The northbound trucks passing the weigh-in-motion station were used to evaluate the measured rainflow response of the Medina River Bridge. The volume of truck traffic is expected to be higher at the weigh-in-motion sensor than the volume crossing the bridge because the outer loop around San Antonio (Loop 1604) intersects I-35 between the weight-in-motion sensor and the Medina River Bridge.

The daily variations in truck traffic during the first rainflow collection period are shown in Figure 4.10. In general, more than 4,500 trucks traveled along this section of I-35 on weekdays. Truck volume dropped to an average of 3,400 trucks on Saturdays and 2,800 trucks on Sundays. Truck traffic was much lower on Labor Day (6 September 2004) than a typical Monday.

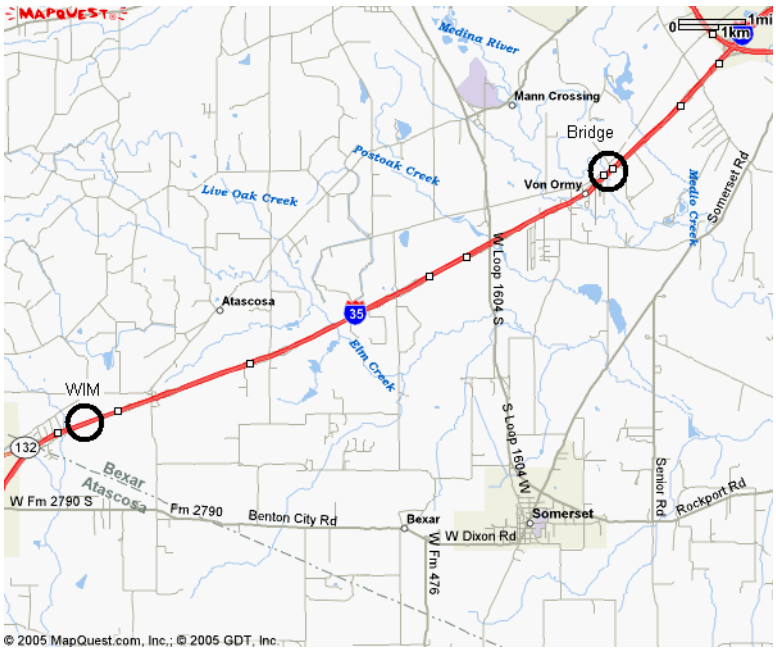

Figure 4.9 Map of I-35 South of San Antonio

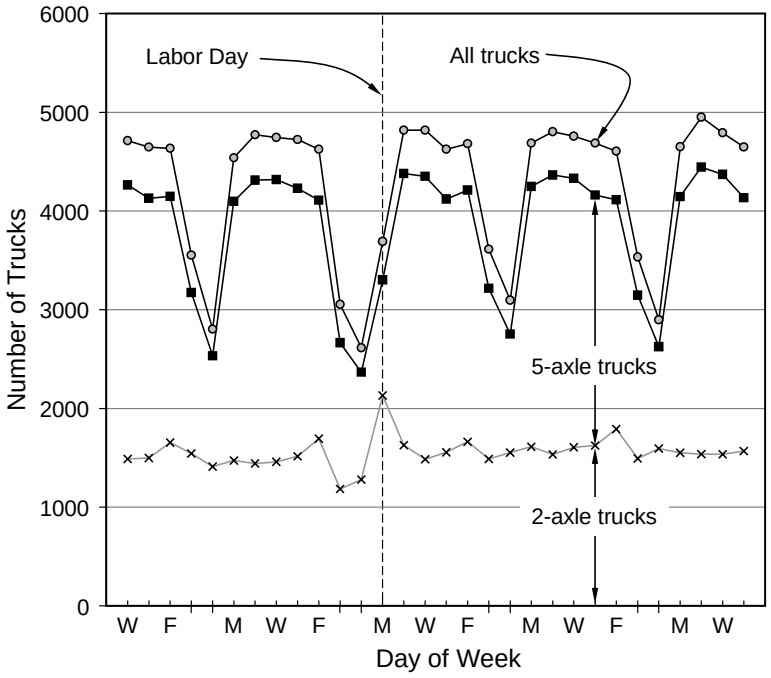

Figure 4.10 Truck Traffic Detected by Weight-in-Motion Station between 25 August and 23 September 2004

Truck traffic recorded during the second rainflow collection period is shown in Figure 4.11. Only twenty days of data are available because the weigh-in-motion station was closed for repairs between 31 January and 4 February and between 10 February and 15 February. The average number of trucks passing the weigh-in-motion station was lower during the second rainflow collection period than the first period. The decrease in traffic volume on the weekends was still evident, but the daily trends were more variable during the second period.

Based on the observed variations in traffic volume, the number of loading cycles recorded each day during the rainflow collection periods was expected to vary considerably.

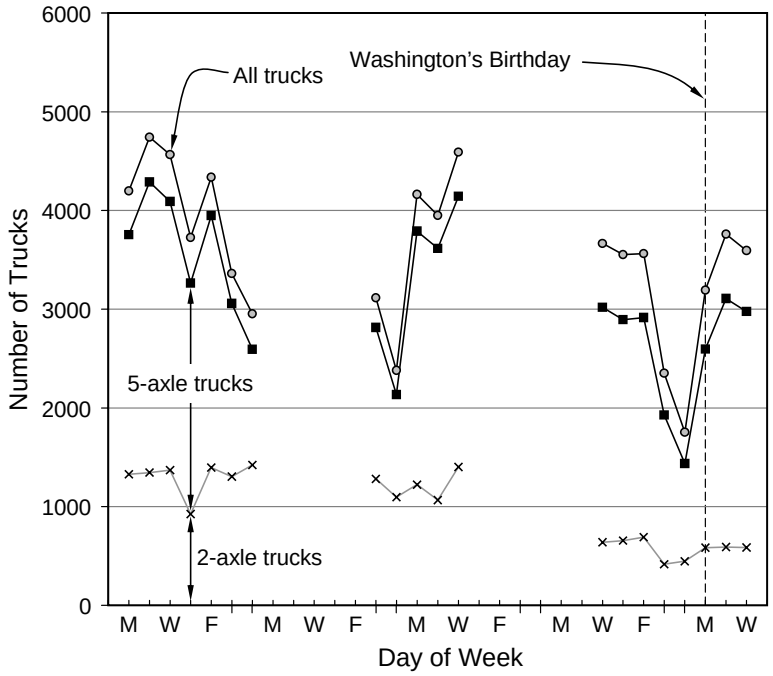

Figure 4.11 Truck Traffic Detected by Weigh-in-Motion Station between 24 January and 23 February 2005

4.3 MEASURED RAINFLOW RESPONSE

As discussed in Section 4.1, rainflow data were only recorded by seven of the ten miniature data acquisition systems. The measured data are summarized in this section. Thermal cycles are discussed in Section 4.3.1. Rainflow cycles along the north cantilever span are discussed in Section 4.3.2 and rainflow cycles along the north anchor span are discussed in Section 4.3.3.

4.3.1 Thermal Response

More than 1.3 million strain cycles were recorded above the noise threshold of 4 $\mu\varepsilon$ by the data acquisition system attached to strain gage J during the 28-day rainflow collection period. On average, more than 46,000 cycles were recorded each day (Figure 4.12). As shown in Figure 4.13, the overwhelming majority of these cycles (99.5%) were in the first bin (4 to 8 $\mu\varepsilon$) and nearly 6,500 cycles were in the second bin (8 to 16 $\mu\varepsilon$). Forty cycles were recorded in the higher bins: on sixteen days a single, large-amplitude cycle was recorded and on twelve days two, large-amplitude cycles were recorded. One or two cycles a day will not influence the calculated fatigue life of the bridge; however, the large-amplitude cycles may exceed the threshold stress level for a given detail category, which could cause a structure with an infinite fatigue life to be evaluated as having a finite fatigue life. Therefore, additional study is warranted.

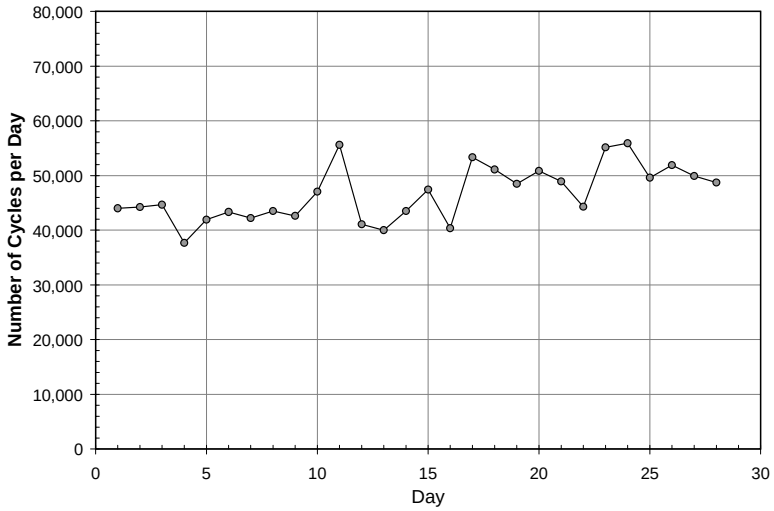

Figure 4.12 Number of Strain Cycles Recorded above Noise Threshold Each Day by Strain Gage J

The relationship between the maximum strain cycle recorded in each 24-hr period and the maximum variation in temperature is shown in Figure 4.14. A strong correlation exists between the maximum recorded strain range and the maximum variation in temperature.

Because the thermal coefficient of expansion of aluminum is higher than that for steel and because three-wire strain gages were used to monitor the response of the Medina River Bridge, the data in Figure 4.14 can not be used directly to correct the measured the rainflow counts for the thermal cycles. Therefore, a second test was conducted at Ferguson Laboratory where an unloaded steel bar was instrumented with four strain gages and monitored over a 7-day period beginning on 8 April 2005. The results from this test provided important results which influenced the interpretation of all rainflow data from the bridge. No loads were applied to the steel bar during the 7-day test period; therefore, all the strain cycles may be attributed to thermal changes and electrical noise.

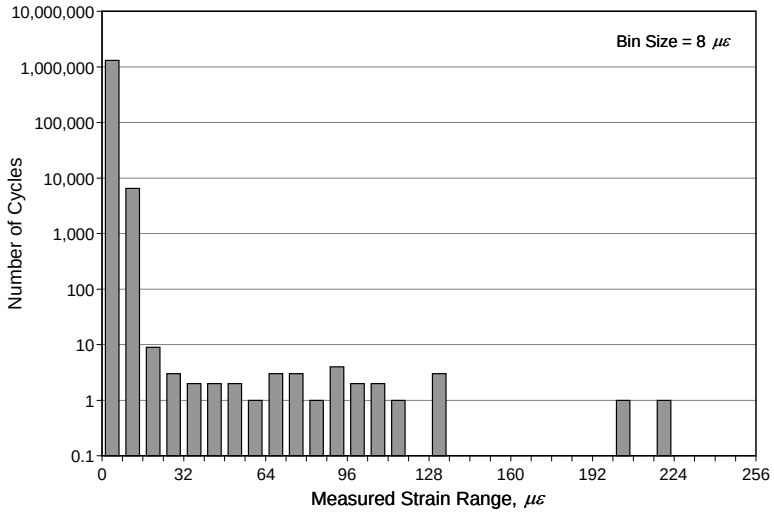

Figure 4.13 Measured Rainflow Response of Strain Gage J

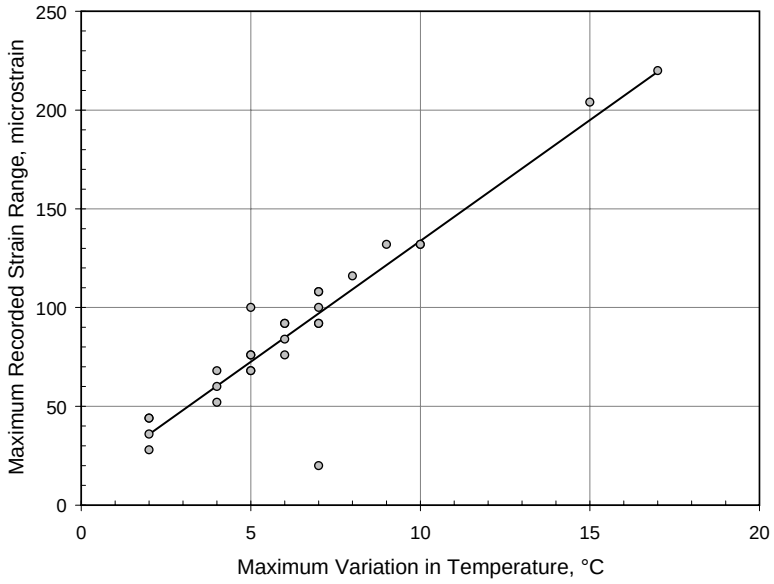

Figure 4.14 Observed Relationship between Maximum Strain Range and Maximum Variation in Temperature for Strain Gage J

The measured rainflow response of the four strain gages is shown in Figure 4.15. All four data acquisition systems recorded strain ranges in excess of 100 $\mu\varepsilon$; however, the response of unit 1005 was clearly very different from the other three. As shown in Figure 4.16, unit 1005 counted approximately 500,000 strain cycles each day, while the other data acquisition system counted 6,000 to 35,000 each day. Based on this information, the rainflow counts collected by unit 1005 were considered to be unreliable. Additional observations to confirm this finding are discussed in Section 4.3.3 and Section 5.2.

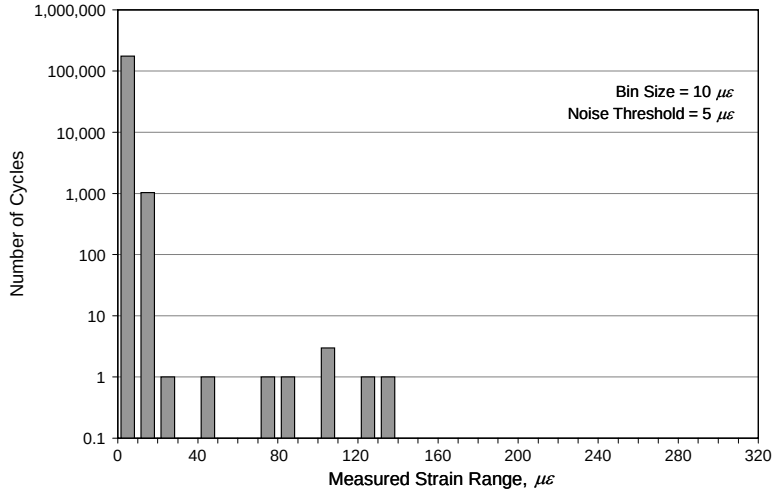

(a) Unit 1001

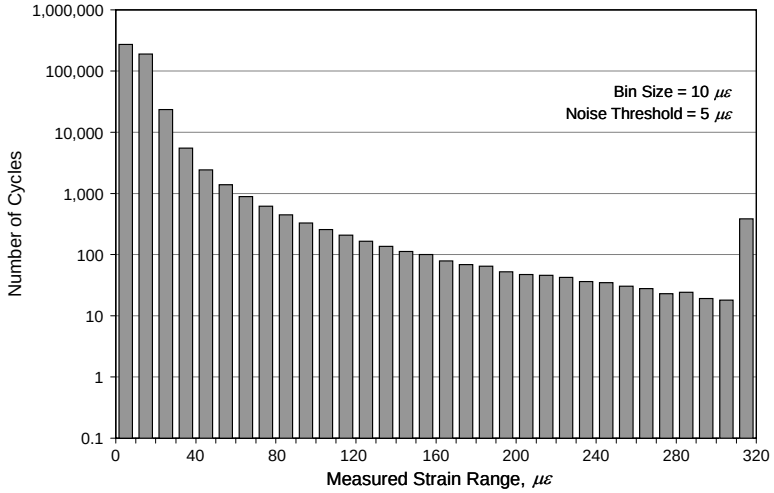

(b) Unit 1005

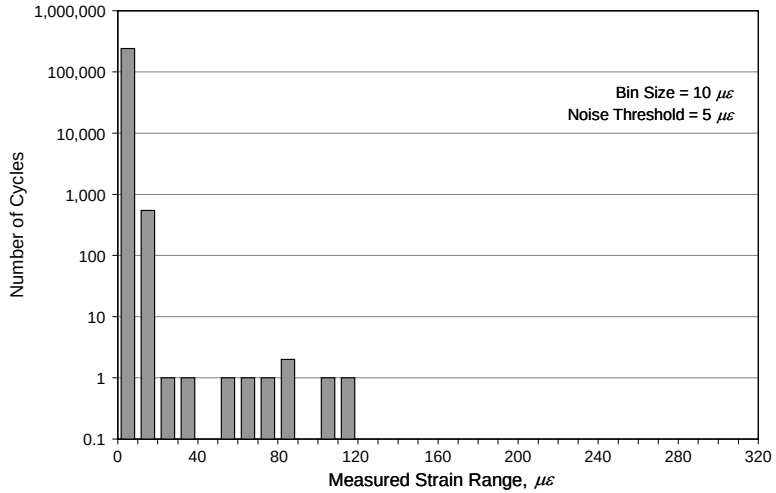

(c) Unit 1007

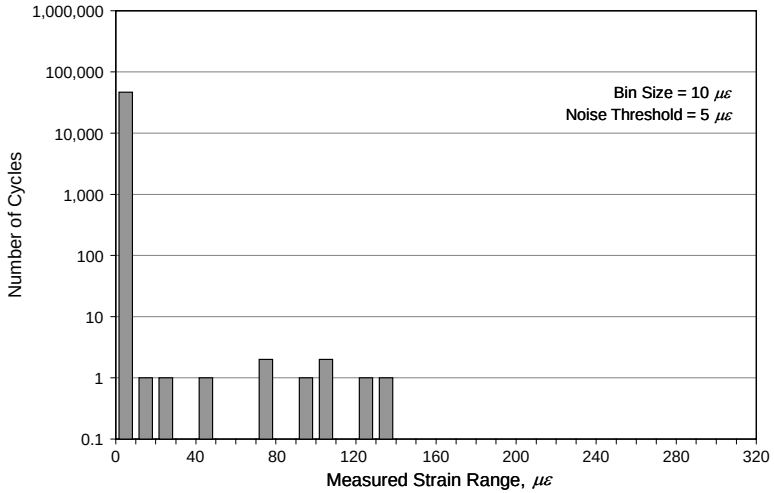

(d) Unit 1013

Figure 4.15 Measured Rainflow Response of Unloaded Steel Bar during Seven-Day Period

As shown in Figure 4.15, the other three data acquisition units counted one or two large-amplitude strain cycles each day. This observation is consistent with the response of strain gage J shown in Figure 4.13. As expected, the largest strain cycles are smaller than those in Figure 4.13 due to the lower coefficient of thermal expansion for steel. In addition, the overwhelming majority of the strain cycles recorded during the 7-day test were in the first bin (5 to 10 $\mu\varepsilon$).

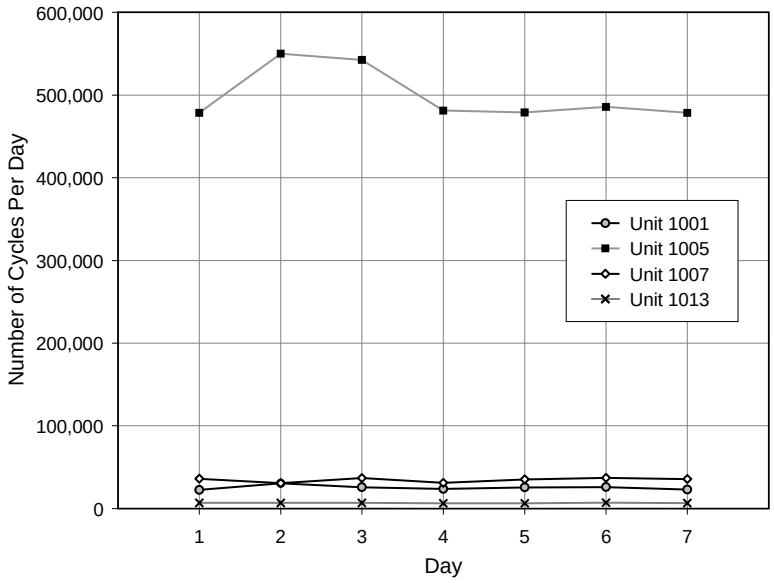

Figure 4.16 Number of Strain Cycles Recorded Above Noise Threshold Each Day during Thermal Test of Steel Bar

These results indicate that the measured rainflow counts must be corrected for thermal cycles. The relationship between the maximum strain range and maximum temperature variation are shown in Figure 4.17 for the two data acquisition units that were connected to three-wire strain gages. Again, a strong linear relationship was observed. The equation for the best-fit line is given in Figure 4.17.

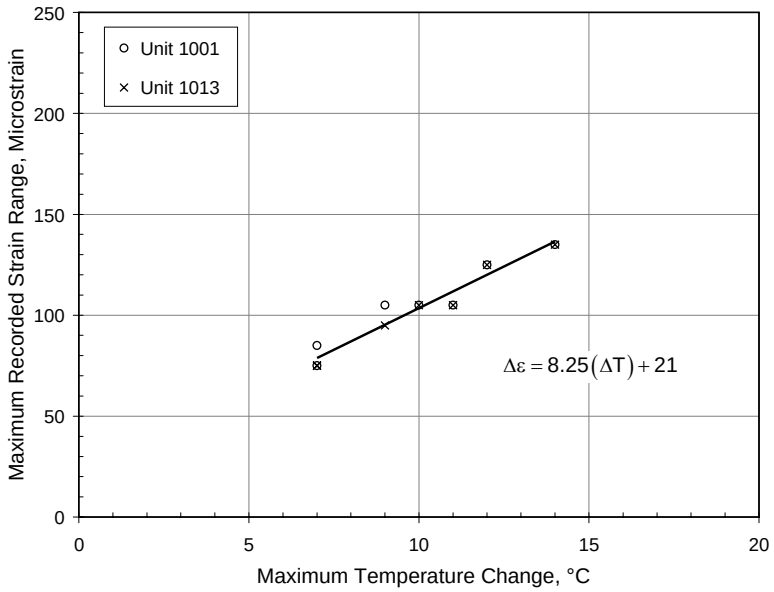

Figure 4.17 Relationship between Maximum Strain Range and Maximum Variation in Temperature for Steel Bar

Although the strain variations due to temperature are easily identified when the strain gage does not experience load-induced strain cycles, the thermal cycles are superimposed on the load fluctuations when the response of the bridge is monitored. Therefore, the strain variation due to the thermal cycles is added to the largest strain variation recorded in the rainflow counts.

The miniature data acquisition units record the temperature once an hour when collecting rainflow data, so the rainflow counts can be modified to remove the influence of temperature. The maximum temperature variation can easily be evaluated for each day, and then the amplitude of the temperature-induced strain cycle can be calculated using the best-fit equation in Figure 4.17.

The procedure used to correct for temperature effects is shown in Table 4.4. The data are representative of cases where zero cycles were recorded in the largest bin. However, a single, large-amplitude cycle was recorded which was more than 70 $\mu\varepsilon$ larger than the next largest cycle. The large-amplitude cycles are highlighted in light grey in the left half of the table. The estimated thermal strain variation was calculated from the maximum temperature variation and then subtracted from the median strain for the bin containing the largest-amplitude cycle for each day. The corrected cycle counts are also highlighted in grey in the right half of the table.

The measured rainflow counts were corrected in this manner whenever the bin sizes had been set to capture the maximum strain range. In cases where the maximum strain range exceeded the largest bin, it was not possible to correct for temperature effects because the amplitude of the maximum strain range is not known.

Table 4.4 Procedure used to Correct Rainflow Counts for Temperature Effects

Median Strain	Raw Rainflow Counts			Corrected Rainflow Counts		
($\mu\varepsilon$)	Day 1	Day 2	Day 3	Day 1	Day 2	Day 3
105	3	1	0	3	1	0
115	1	0	0	1	0	0
125	1	1	0	1	1	0
135	0	0	0	0	0	0
145	2	1	1	2	1	1
155	0	0	0	0	0	0
165	0	0	0	0	1	1
175	0	0	0	1	0	0
185	0	0	0	0	0	0
195	0	0	0	0	0	0
205	0	0	0	0	0	0
215	0	0	0	0	0	0
225	0	0	0	0	0	0
235	0	0	0	0	0	0
245	0	0	0	0	0	0
255	0	0	1	0	0	0
265	0	0	0	0	0	0
275	1	0	0	0	0	0
285	0	1	0	0	0	0
295	0	0	0	0	0	0
ΔT_{max} (°C)	10	12	8	—	—	—
$\Delta\varepsilon$ ($\mu\varepsilon$)	103.5	120	87	—	—	—

4.3.2 North Cantilever Span

Rainflow data were obtained at three locations along the north cantilever span during the first collection period. The recording period began at 5:30 pm each day. The number of rainflow counts recorded each day by strain gages D, E, and H are shown in Figure 4.18. The daily cycle counts were much larger than the number of vehicles crossing the weigh-in-motion station, and the weekly trends in traffic volume were not as pronounced in the measured rainflow data.

Based on the data from the 7-day thermal test (Figure 4.16), a significant portion of the cycles with a strain range less than 10 $\mu\varepsilon$ were expected to be caused by electrical noise and temperature changes. The cycles in the first bin (5 to 10 $\mu\varepsilon$) were removed from the daily totals plotted in Figure 4.19 and the trends more closely represent the observed traffic patterns. Data from strain gage E are not plotted in Figure 4.19 because the bin size was 20 $\mu\varepsilon$ and the number of cycles in the larger bins was quite small.

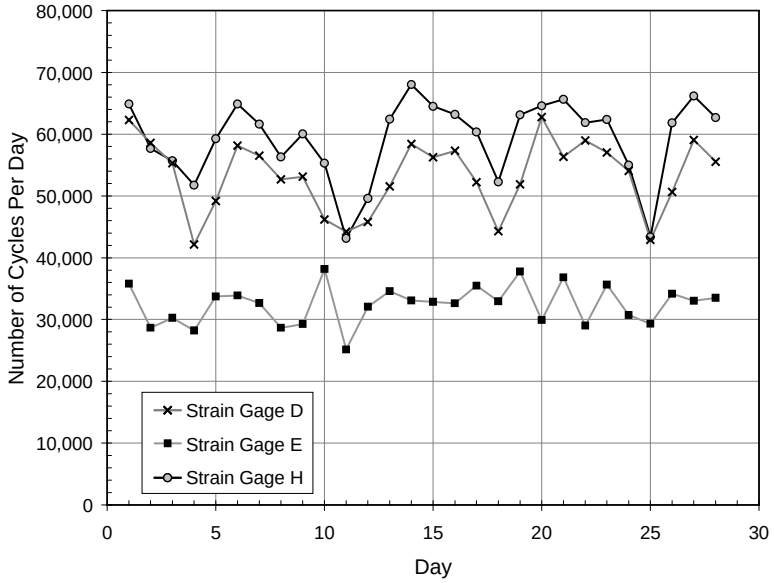

Figure 4.18 Daily Variations in Number of Rainflow Cycles above Noise Threshold Recorded along North Cantilever Span

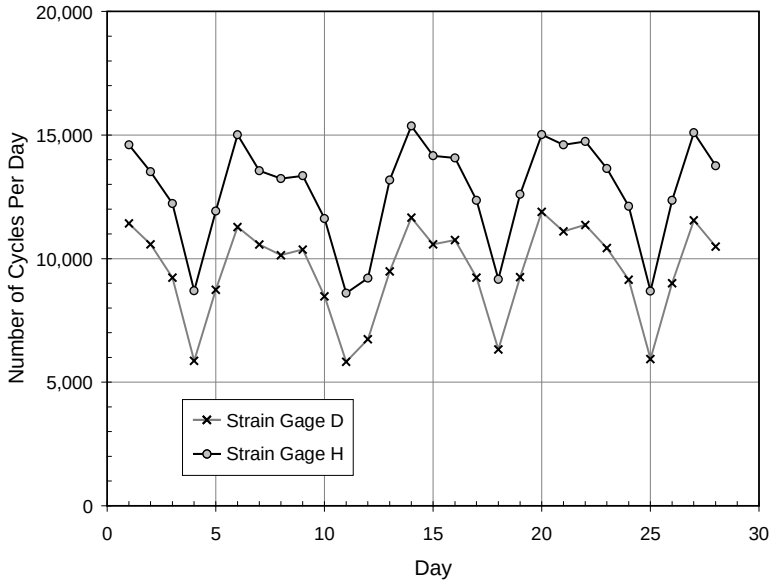

Figure 4.19 Daily Variations in Rainflow Cycles above 10 $\mu\varepsilon$ Recorded along North Cantilever Span

Histograms of the rainflow counts from strain gages D, E, and H are shown in Figure 4.20, Figure 4.21, and Figure 4.22, respectively. Note that the cycle counts corresponding to the first bin are included in the histograms. In all three cases, the maximum strain range was captured because the maximum strain range did not exceed 32 times the bin size.

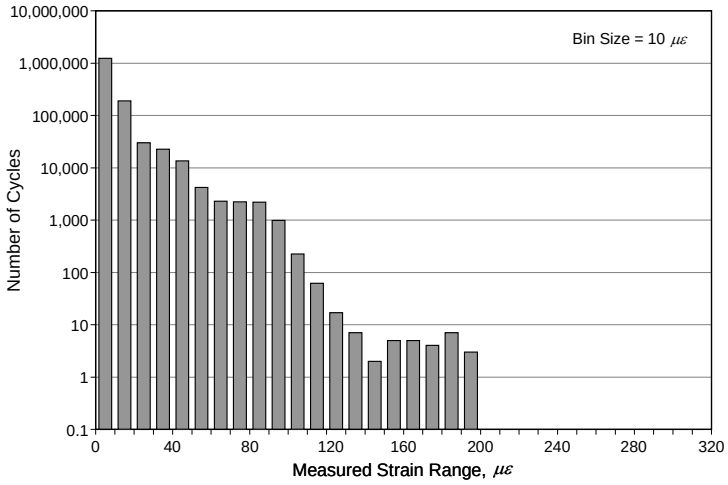

Figure 4.20 Measured Rainflow Response of Strain Gage D

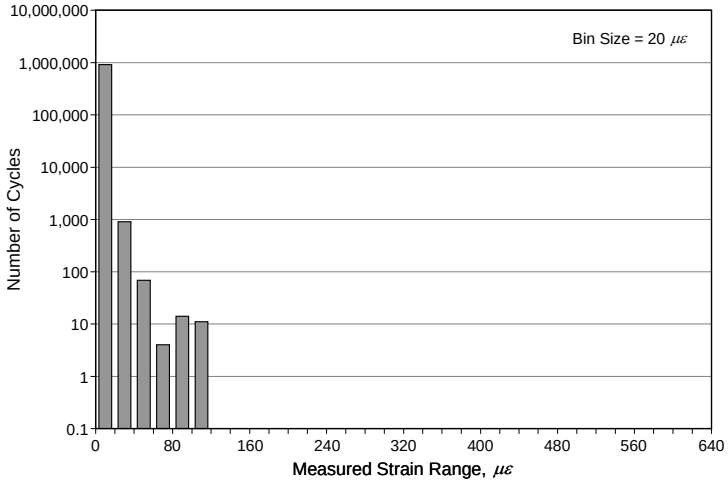

Figure 4.21 Measured Rainflow Response of Strain Gage E

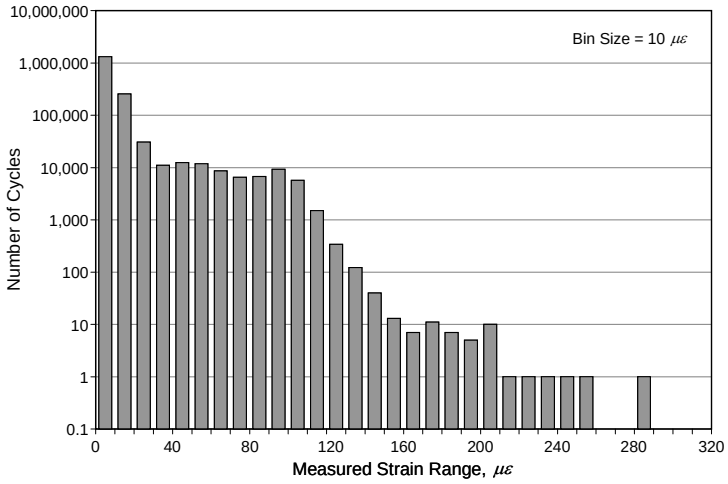

Figure 4.22 Measured Rainflow Response of Strain Gage H

As expected, the number and amplitude of the strain ranges recorded by gages D and H were considerably larger than those recorded by gage E. This is consistent with the trends in Figure 4.2 for the HS-20 design vehicle. Gage H also experienced larger amplitude cycles and a larger number of cycles than gage D. This was also expected, because more trucks cross the bridge in the right than the left lane. A summary of the average number of cycles per day at various strain levels is presented in Table 4.5.

Table 4.5 Average Number of Strain Cycles Recorded per Day during First Collection Period

Strain Range	Stress Range	Strain Gage		
($\mu\varepsilon$)	(ksi)	D	E	H
≥ 5	0.15	53,300	32,400	59,200
≥ 50	1.5	440	2.3	1,800
≥ 100	3.0	12	0.4	280
≥ 150	4.5	0.9	—	2.1
≥ 200	6.0	—	—	0.6
≥ 250	7.5	—	—	0.1
≥ 300	9.0	—	—	—

4.3.3 North Anchor Span

Rainflow data were obtained at three locations along the north anchor span during the second collection period. Data collection began at midnight on Friday, 28 January 2005. The number of rainflow counts recorded each day by strain gages A, B, and C are shown in Figure 4.23. Several inconsistencies are immediately apparent in the recorded data. The battery that powered the data acquisition unit attached to strain gage A failed during the 24th day of the recording period and no cycle counts were recorded during the last four days. In addition, the total number of loading cycles increased dramatically after the 21st day. The MicroSAFE User's Guide (Holman, 2003) states that the units may not operate properly if the battery voltage falls below 3.0 V; therefore, the observed trend is not unexpected. All data recorded on the 22nd, 23rd, and 24th days were ignored when evaluating the rainflow data from strain gage A.

Strain gage B was positioned at the same location as strain gage A; however, the number of cycles recorded each day was significantly higher for the data acquisition unit attached to strain gage B. The same data acquisition unit (1005) recorded very large cycle counts during the 7-day thermal test (Figure 4.16); therefore, the data from strain gage B were considered to be unreliable and were not used to evaluate the fatigue life of the Medina River Bridge.

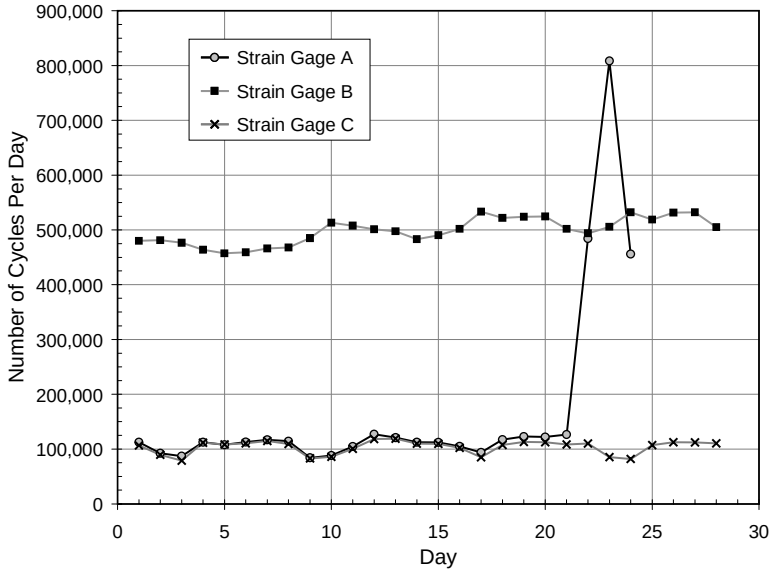

Figure 4.23 Daily Variations in Number of Rainflow Cycles above Noise Threshold Recorded along North Anchor Span

As with the rainflow data from the north cantilever span, the expected traffic patterns may be observed in the rainflow data when the cycles recorded in the first bin (4 to 8 $\mu\varepsilon$) were ignored (Figure 4.24). The number of cycles is nearly identical for strain gages A and C during the first 21 days of the reporting period, which supports the assumption that the readings from these units were reliable.

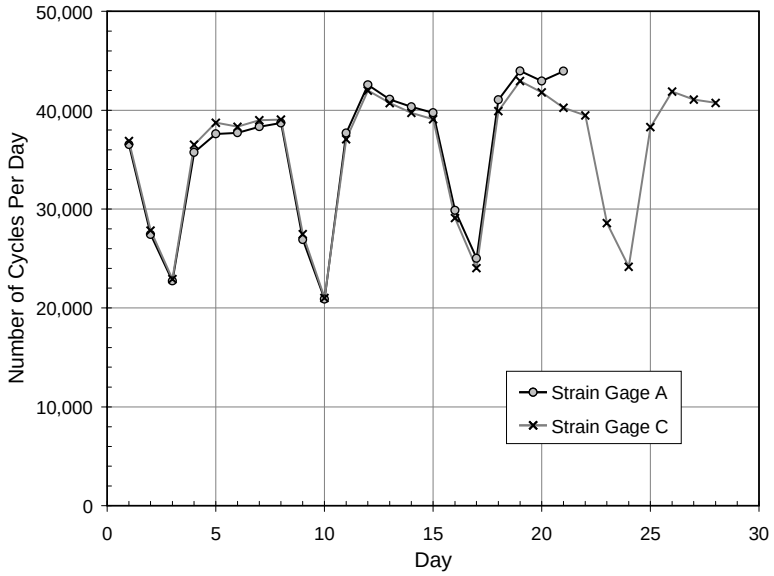

Figure 4.24 Daily Variations in Load-Induced Rainflow Cycles above 8 $\mu\varepsilon$ Recorded along North Anchor Span

Histograms of the rainflow counts from strain gages A, B, and C are shown in Figure 4.25, Figure 4.26, and Figure 4.27, respectively. In all three cases, the maximum strain range was not captured because the maximum strain range exceeded 32 times the bin size. As expected, the numbers of large-amplitude cycles were considerably larger that those recorded along the north cantilever span (Table 4.6). It should be noted that it is not possible to determine that the response from strain gage C is unreliable from the histograms.

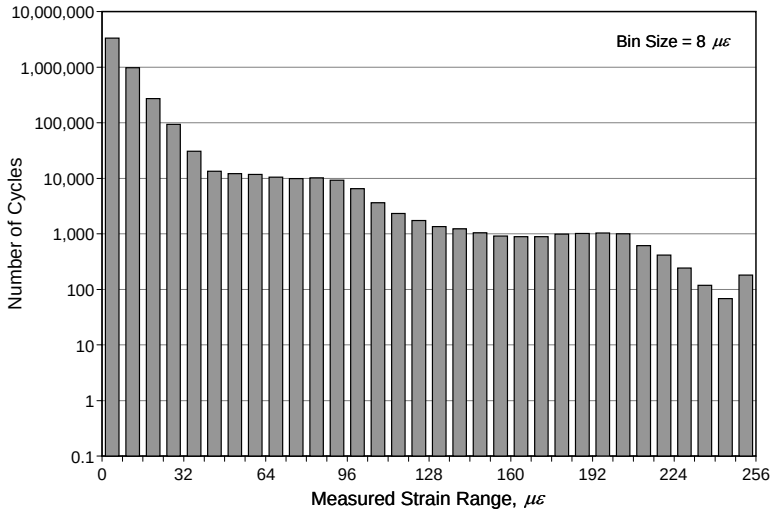

Figure 4.25 Measured Rainflow Response of Strain Gage A (21 Days)

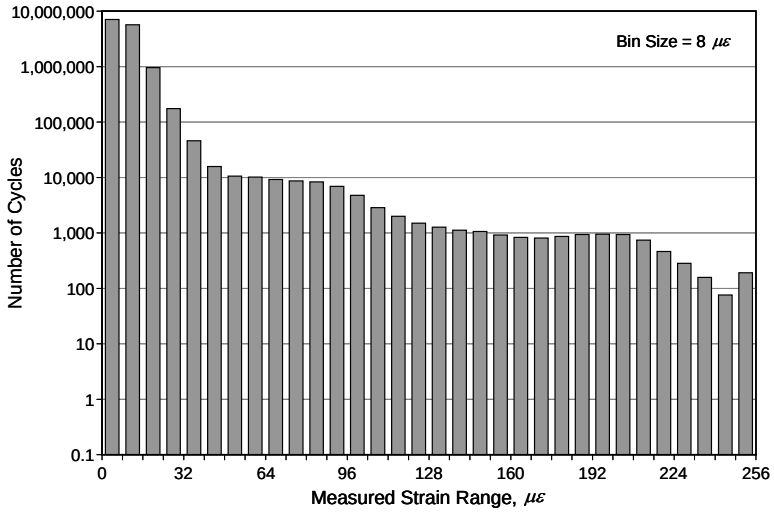

Figure 4.26 Measured Rainflow Response of Strain Gage B

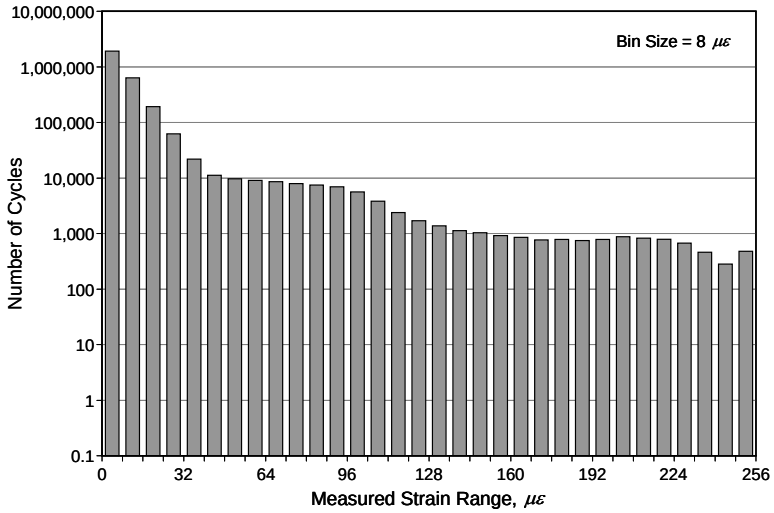

Figure 4.27 Measured Rainflow Response of Strain Gage C

Table 4.6 Average Number of Strain Cycles Recorded per Day during Second Collection Period

Strain Range	Stress Range	Strain Gage	
($\mu\varepsilon$)	(ksi)	A	C
≥ 4	0.12	109,000	103,800
≥ 40	1.2	3,000	3,100
≥ 80	2.4	1,360	1,450
≥ 120	3.6	435	514
≥ 160	4.8	239	295
≥ 200	6.0	86	156
≥ 240	7.2	9	27

4.4 SUMMARY

Ten miniature data acquisition systems were used to monitor the live-load response of the Medina River Bridge. Although all did not function as intended, valuable information was obtained about the response of the bridge and how thermal cycles influence the measured response. It was determined that most of the cycles with a strain range less than 10 $\mu\varepsilon$ can be attributed to electrical noise and/or thermal cycles. When these low-amplitude cycles were removed from the cycle counts, the daily trends in the number of rainflow cycles were similar to the traffic patterns identified from the weigh-in-motion data. In addition, one or two large-amplitude strain cycles were measured during each 24-hr acquisition period and were attributed to thermal variations. These large-amplitude cycles should be removed from the rainflow counts before evaluating the maximum live-load stress range.

The four miniature data acquisition units attached to strain gages C, D, H, and J collected reliable data throughout the entire 28-day rainflow collection period. In retrospect, a larger bin size should have been used for strain gage C to capture the maximum strain range, but otherwise, these units functioned as intended.

The data acquisition units attached to strain gages A, B, and E collected rainflow data, but careful evaluation of the data was required. The battery used to power the unit attached to strain gage A failed during the 28-day acquisition period. Data collected during the first 21 days appear to be reliable, but the data collected during the final 7 days were discarded. As the battery failed, the number of strain cycles counted by the data acquisition system increased significantly. Therefore, the range of reliable data was easy to identify.

At first glance, the data acquisition system attached to strain gage B appeared to measure rainflow data throughout the collection period. However, the number of cycles recorded by this unit was more than an order of magnitude larger than the number of cycles recorded by any of the other data acquisition units. This finding was repeated during a 7-day test of the thermal characteristics of the data acquisition units. Therefore, the data from strain gage B were discarded.

The data acquisition system attached to strain gage E appeared to collect reliable data, but the bin size was too large. More than 99.8% of the rainflow cycles were recorded in the first bin. The consequences of selecting too large a bin size are discussed in Chapter 6.

The largest-amplitude strain cycles were recorded by strain gage F during installation of the data acquisition units. However, this data acquisition unit collected only one rainflow cycle per day during the rainflow collection period. Temperature data were recorded each hour throughout the 28-day period. The cause of this malfunction was not identified.

During installation, the strain cycles recorded by strain gage G never exceeded the noise threshold. In retrospect, this strain gage should have been replaced before attempting to collect rainflow data. The data acquisition unit malfunctioned after 4 hours, and no rainflow data were collected. Rainflow data were also not collected by the data acquisition unit attached to strain gage I. The cause of these malfunctions was not known.

The rainflow data from strain gages A, C, D, E, and H will be used in Chapter 6 to evaluate the remaining fatigue life of the longitudinal girders from the Medina River Bridge.

CHAPTER 5: RESPONSE OF 12TH STREET EXIT RAMP

The live-load response of the 12th Street Exit Ramp was monitored during two rainflow collection periods. Strain gages were positioned at seven locations on the bridge: five along the longitudinal girders and two at the ends of the transverse floor beams. The layout of the strain gages is discussed in Section 5.1 and the measured rainflow data are presented in Section 5.2. As with the Median River Bridge, rainflow data were not successfully obtained from all strain gages. Evaluation of the measured rainflow data is also discussed in Section 5.2.

5.1 LAYOUT OF INSTRUMENTATION

The response of the 12th Street Exit Ramp was monitored during two periods: the first, 28-day collection period began on 21 April 2004 and the second, 7-day collection period began on 6 July 2004. TxDOT personnel were conducting a fracture-critical inspection of the bridge at the beginning of the first collection period, and the research team used the TxDOT scissor lift (Figure 5.1) and bucket truck (Figure 5.2) to install the instrumentation. The strain gages and data acquisition systems were installed in a few hours.

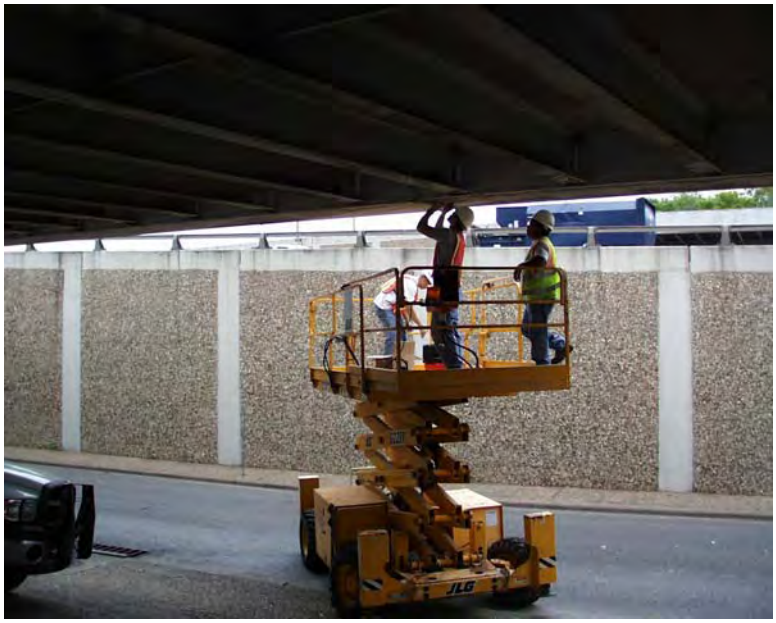

Figure 5.1 Installation of Strain Gages

Figure 5.2 Checking Data from Miniature Data Acquisition Units

The locations of the seven strain gages were identified using the letters A through G, as shown in Figure 5.3 and documented in Table 5.1. Five of the gages were attached to the bottom face of the longitudinal girders and two gages were attached to the bottom face of the top flange of transverse floor beams. All strain gages were manufactured by Tokyo Sokki Kenkyujo, Inc. and distributed by Texas Measurements, Inc. and designated FLA-6-11 (6-mm, 120-Ω, three-wire, foil gages, with temperature compensation for mild steel).

Table 5.1 Locations of Strain Gages Used to Monitor Response of 12th Street Exit Ramp

Strain Gage ID	Location	Girder	Span
A	Transition from 1″ to 1½″ flange thickness, north of column	West	North
B	West end of first transverse floor beam north of column	—	North
C	West end of first transverse floor beam south of column	—	South
D	Midspan of south span	West	South
E	Transition from 1″ to 1½″ flange thickness, north of south support	West	South
F	Midspan	East	—
G	Transition from 2″ to 2¾″ flange thickness, north of south support	East	—

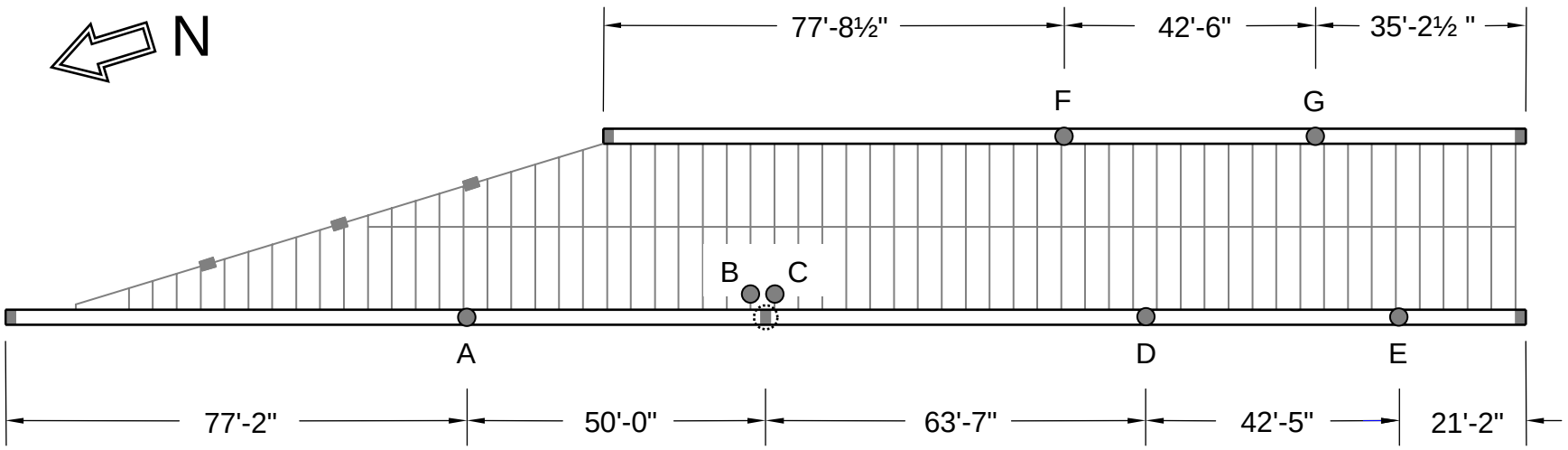

● Locations of strain gages.

Figure 5.3 Locations of Strain Gages Used to Monitor the Response of the 12th Street Exit Ramp

As discussed in Section 3.2.2, the largest live-load moments in the longitudinal box girders were expected to occur near midspan and the largest live-load stress ranges were expected to occur at locations where the thicknesses of the top and bottom flanges of the longitudinal box girders changed. Strain gage D was positioned at midspan of the south span of the west girder and strain gage F was positioned at midspan of the east girder. Strain gages A, E, and G were positioned near flange thickness changes. In all cases, the strain gages were attached to the thinner plate (Figure 5.4). Strain gages B and C were attached to the top flanges of adjacent transverse floor beams near the west end. The beams nearest the intermediate column were selected for instrumentation.

Data were collected from the same set of strain gages during both rainflow collection periods, but the bin sizes were increased during the second period. The parameters used during the two periods are discussed below.

Figure 5.4 Installation of Strain Gage near Transition in Flange Thickness

5.1.1 First Collection Period

During installation of the instrumentation for the first collection period, combined raw strain and rainflow data were collected for 1 to 2 min from each data acquisition unit. The bin sizes and noise thresholds were then set for each unit based on the measured data. Fifteen-second portions of the raw strain records are shown in Figure 5.5 through Figure 5.11, and the maximum strain range during each raw strain record is listed in Table 5.2.

Table 5.2 Rainflow Parameters Used during First Collection Period

Strain Gage ID	DAQ ID	Maximum Strain Range* ($\mu\varepsilon$)	Bin Size ($\mu\varepsilon$)	Noise Threshold ($\mu\varepsilon$)
A	1006	21	5	3
B	1005	28	5	3
C	1013	14	10	5
D	1002	23	4	3
E	1003	17	4	3
F	1001	26	4	3
G	1004	22	4	3

* Strains recorded during installation of data acquisition units.

All seven strain gages, and the associated data acquisition systems, seemed to be working properly, although the noise level for strain gage B is considerably higher than the noise level for the other gages. The amplitudes of the recorded strain histories were much smaller than those recorded at the Medina River Bridge (Figure 4.4 through Figure 4.8). The largest amplitude strain cycle recorded on the 12th Street Exit Ramp was 28 $\mu\varepsilon$, while the largest amplitude strain cycle recorded on the Medina River Bridge was 220 $\mu\varepsilon$. The load-induced strain cycles were most pronounced in the response from strain gage F (Figure 5.10).

As will be discussed in Section 5.2, the bin sizes were too small to capture the maximum amplitude strain cycles from most of the strain gages during the first collection period. All seven data acquisition systems acquired 28 days of data during the first rainflow collection period.

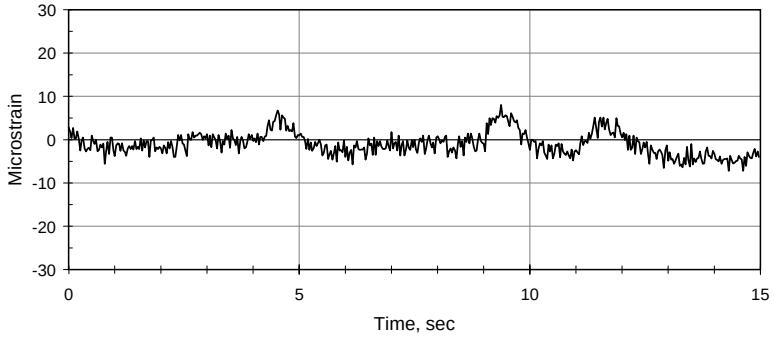

Figure 5.5 Raw Strain Data from Strain Gage A

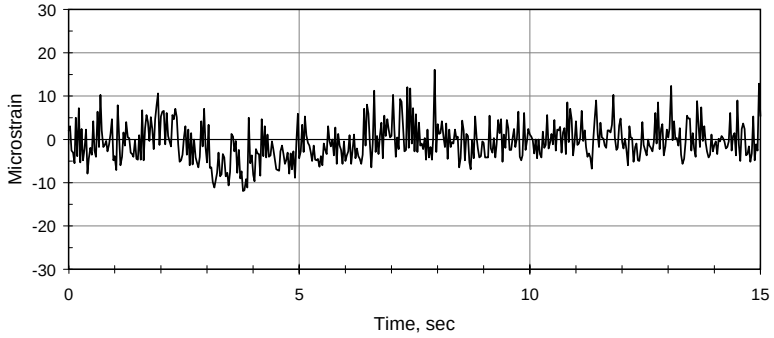

Figure 5.6 Raw Strain Data from Strain Gage B

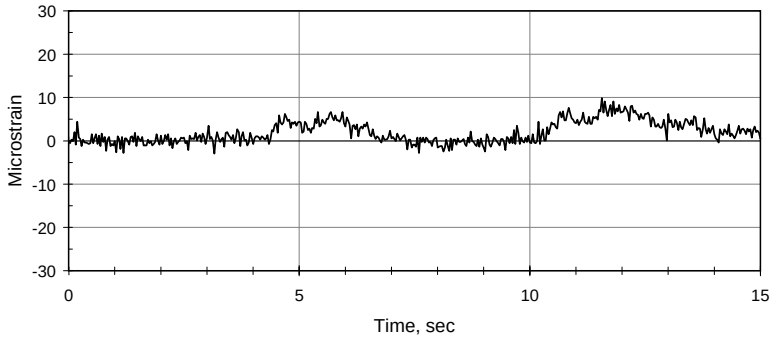

Figure 5.7 Raw Strain Data from Strain Gage C

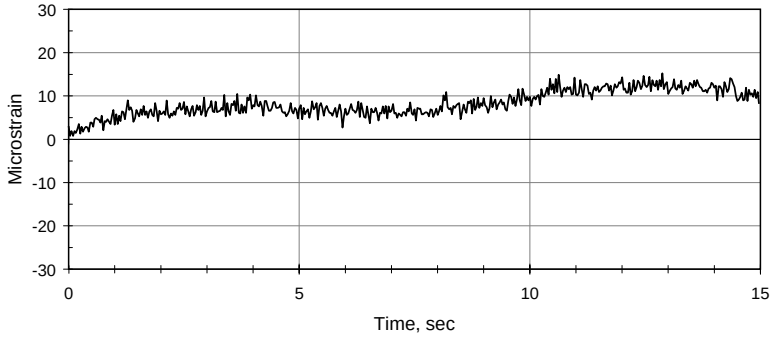

Figure 5.8 Raw Strain Data from Strain Gage D

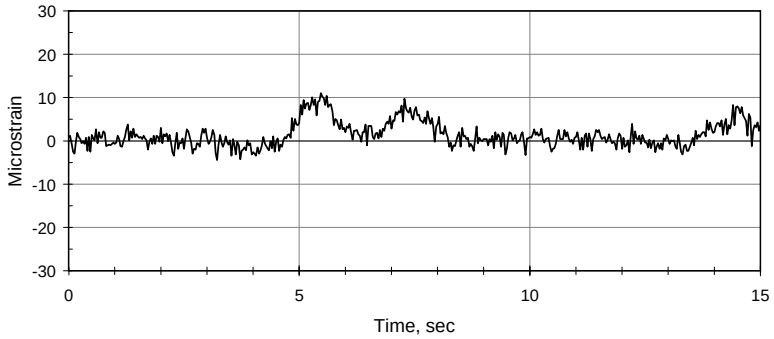

Figure 5.9 Raw Strain Data from Strain Gage E

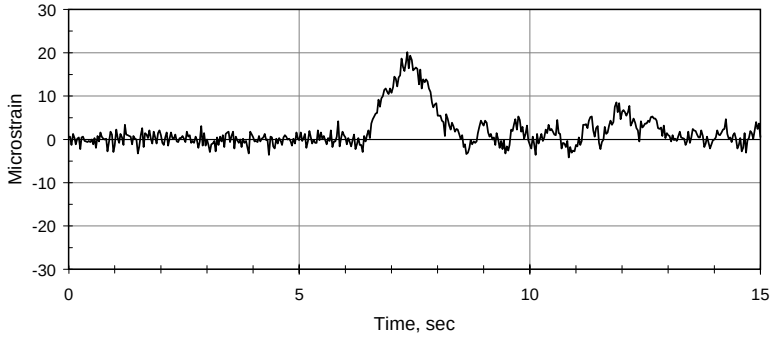

Figure 5.10 Raw Strain Data from Strain Gage F

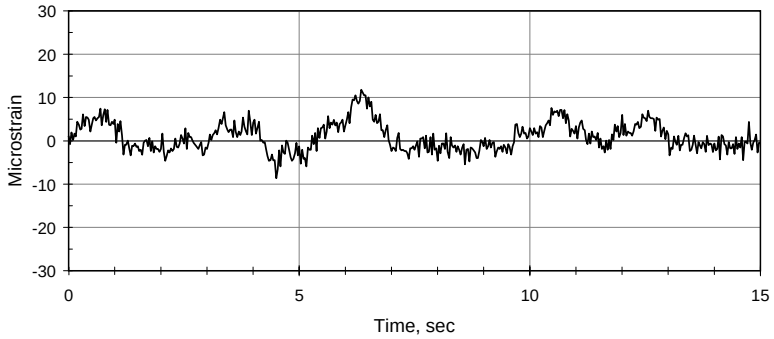

Figure 5.11 Raw Strain Data from Strain Gage G

5.1.2 Second Collection Period

For the second collection period, the data acquisition systems were programmed prior to installing the units on the bridge. The noise thresholds in the second collection period were the same as those used in the first, but the bin sizes were increased by a factor of 2.5, except for strain gage C, where the bin size was increased by a factor of 2 (Table 5.3). Raw data were not collected before the start of the second collection period.

Five of the seven data acquisition units recorded rainflow data for the entire 7-day collection period. Only 5 days of data were collected from strain gage A and no data were collected from strain gage G. The causes of the failures of units 1004 and 1006 are not known.

Table 5.3 Rainflow Parameters Used during Second Collection Period

Strain Gage ID	DAQ ID	Bin Size ($\mu\varepsilon$)	Noise Threshold ($\mu\varepsilon$)	Notes
A	1006	12.5	3	Early termination of rainflow recording.
B	1005	12.5	3	—
C	1013	20	5	—
D	1002	10	3	—
E	1003	10	3	—
F	1001	10	3	—
G	1004	10	3	Rainflow data were not recorded by the unit.

5.2 MEASURED RAINFLOW RESPONSE

The measured rainflow data are summarized and evaluated in this section. Data acquired during the first collection period are presented and evaluated in Section 5.2.1 and data acquired during the second collection period are presented and evaluated in Section 5.2.2. The measured data were corrected for temperature effects using the procedure described in Section 4.3.1.

5.2.1 First Collection Period

Rainflow data were obtained from all seven data acquisition units during the first collection period. The number of rainflow counts recorded each day by each strain gage are shown in Figure 5.12. Based on this information, three trends in the data may be observed: (1) the number of cycles recorded by strain gages A, C, D, and F did not vary appreciably during the 28-day recording period, (2) strain gage B recorded many more cycles than the other strain gages, and (3) the number of cycles recorded each day by strain gages E and G varied considerably.

Data acquisition unit 1005 was attached to strain gage B. As discussed in Section 4.3, this unit records many more strain cycles than the other data acquisition units (Figure 4.14b). A procedure is not available to identify the load-induced strain cycles from the measured response; therefore, the data from strain gage B were considered to be unreliable and were not be used to evaluate the fatigue life of the 12th Street Exit Ramp.

As discussed in Section 4.3, the traffic patterns were apparent in the rainflow data measured from the Medina River Bridge when the low-amplitude strain cycles were subtracted from the daily totals. The number of strain cycles above 8 $\mu\varepsilon$ from strain gages E and G are plotted in Figure 5.13. The number of larger amplitude cycles varied considerably for both strain gages, and the trends were not consistent with expected traffic patterns. Therefore, data from strain gages E and G recorded during the first collection period were considered to be unreliable and were not be used to evaluate the fatigue life of the 12th Street Exit Ramp.

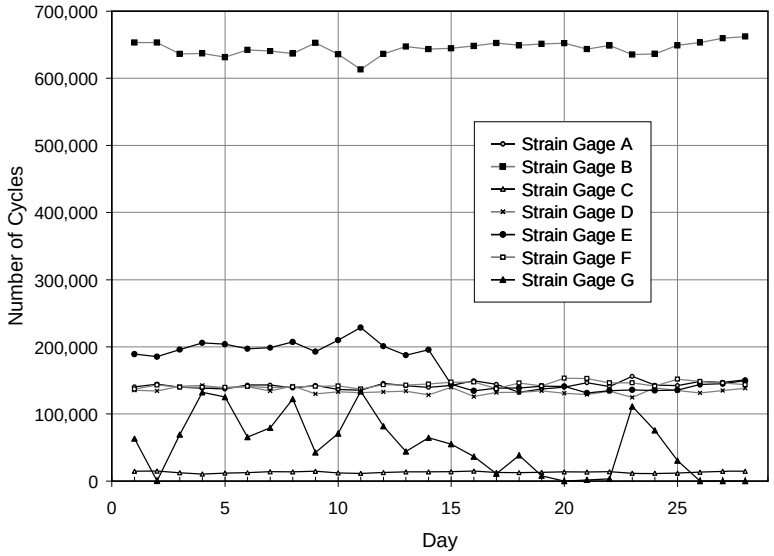

Figure 5.12 Daily Variations in Number of Rainflow Cycles Recorded above Noise Threshold during First Collection Period

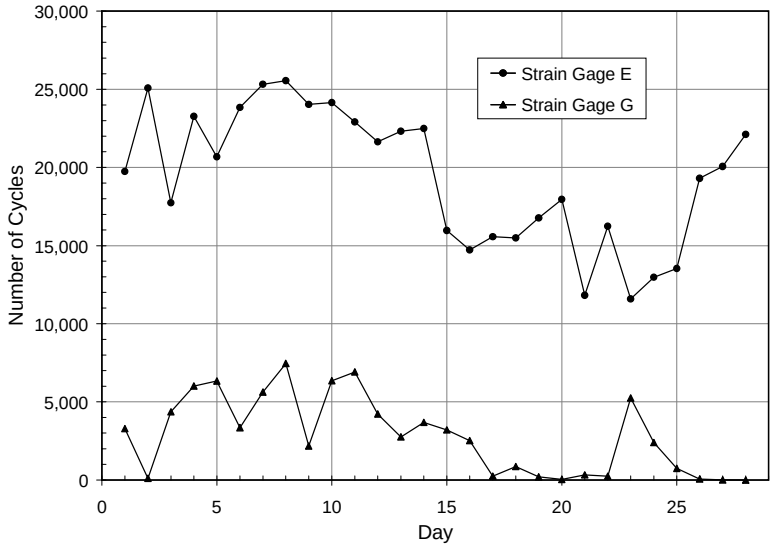

Figure 5.13 Daily Variations in Number of Rainflow Cycles above 8 $\mu\varepsilon$ Recorded by Strain Gages E and G during First Collection Period

The number of strain cycles above 8 $\mu\varepsilon$ from strain gages D and F are plotted in Figure 5.14. The number of cycles recorded each day by the two gages were similar and exhibited a 7-day traffic pattern. The number of strain cycles above 10 $\mu\varepsilon$ from strain gages A and C are also plotted in Figure 5.14. The bin sizes were larger for these gages A and C than for gages D and F; therefore, a direct comparison among the four gages is not possible. It is not possible to determine if the number of traffic-induced cycles was less at the locations of strain gages A and C, or if the difference in the number of cycles may be attributed to strain cycles between 8 and 10 $\mu\varepsilon$. With the exception of one unexpected point (day 23 from strain gage A), 7-day traffic patterns were also observed in the data from gages A and C.

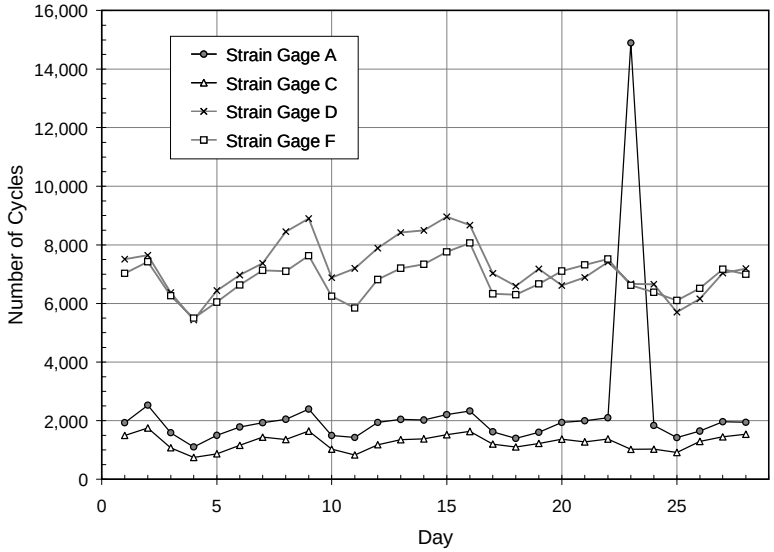

Figure 5.14 Daily Variations in Number of Rainflow Cycles above 8 $\mu\varepsilon$ Recorded by Strain Gages D and F and above 10 $\mu\varepsilon$ Recorded by Strain Gages A and C during First Collection Period

Further investigation of the data recorded by strain gage A was required to evaluate the response during day 23. As shown in Figure 5.15, the number of cycles recorded in each bin were more than an order of magnitude larger on day 23 than on any other day in the collection period. This trend was not repeated in the response of any of the other strain gages, and therefore, could not be attributed to a change in the normal traffic patterns (such as a detour due to an accident or construction on I-35) on this day. The strain cycles recorded during day 23 were considered to be caused by a malfunction of the data acquisition unit, and data from day 23 were ignored when evaluating the rainflow data from strain gage A. The cause of the malfunction was not known, but sudden changes in the number of cycles can be caused by a low battery (Holman, 2003).

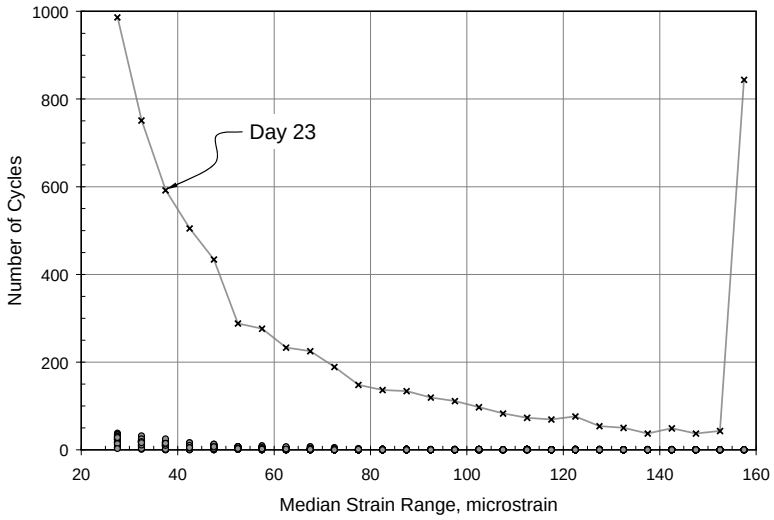

Figure 5.15 Daily Variations in Number of Rainflow Cycles above 25 $\mu\varepsilon$ Recorded by Strain Gage A during First Collection Period

Histograms of the rainflow counts from all seven strain gages are shown in Figure 5.16 through Figure 5.22. Note that it is not possible to distinguish the unreliable data from the reliable data using only the histograms. Evaluation of the daily cycle counts is needed to identify the unreliable data.

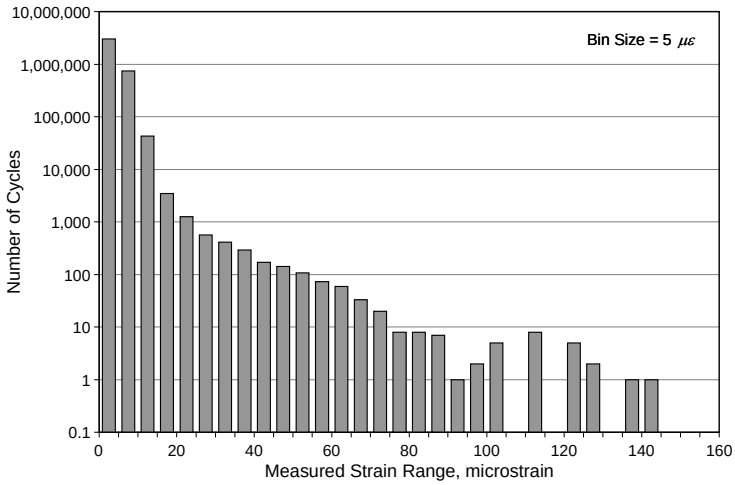

Figure 5.16 Measured Rainflow Response of Strain Gage A – Phase 1 (Ignoring Day 23)

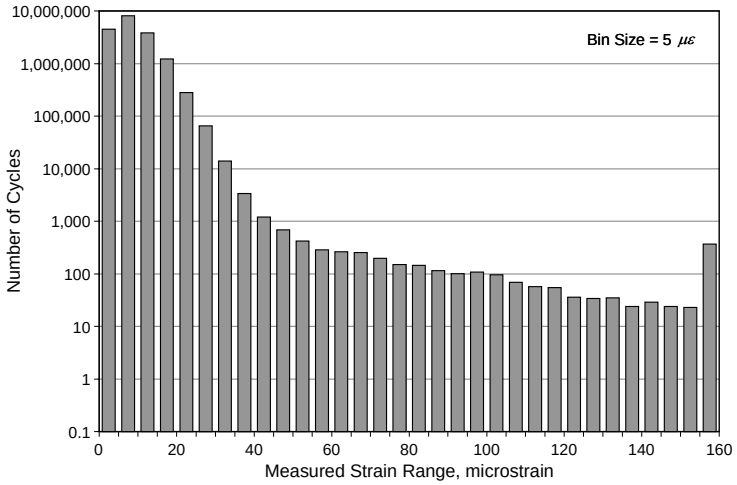

Figure 5.17 Measured Rainflow Response of Strain Gage B – Phase 1

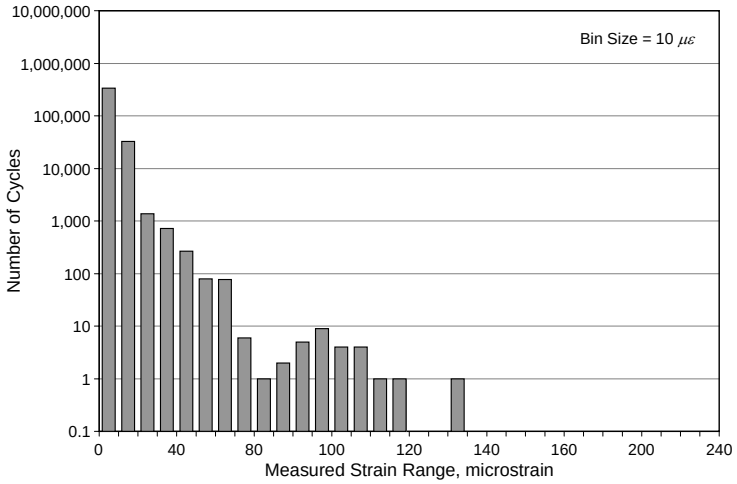

Figure 5.18 Measured Rainflow Response of Strain Gage C – Phase 1

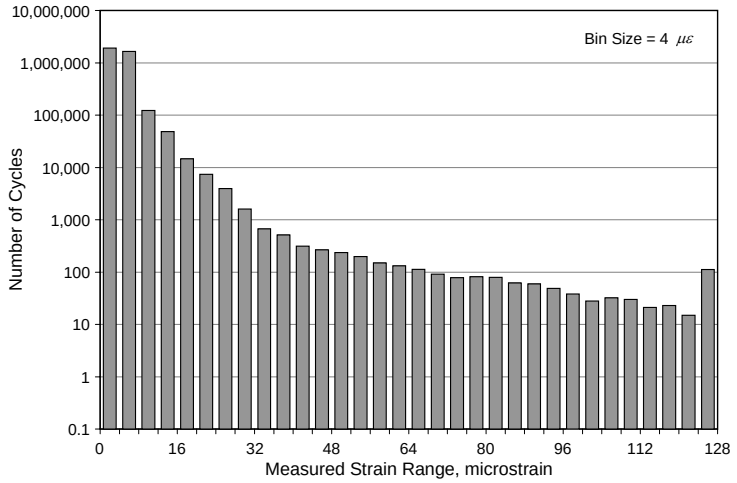

Figure 5.19 Measured Rainflow Response of Strain Gage D – Phase 1

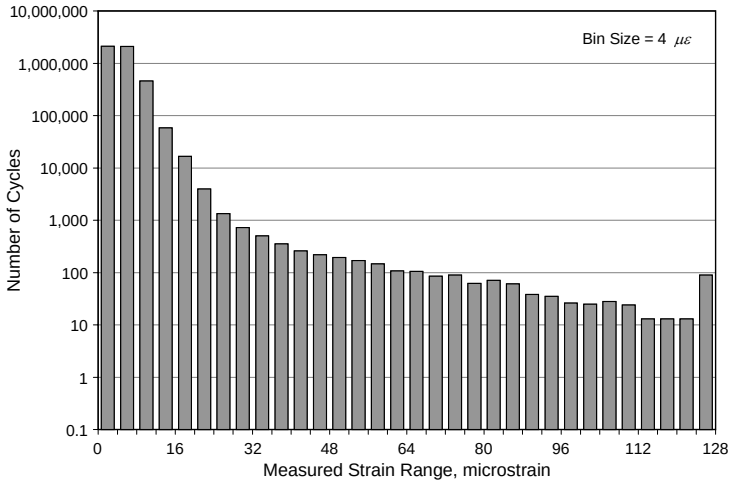

Figure 5.20 Measured Rainflow Response of Strain Gage E – Phase 1

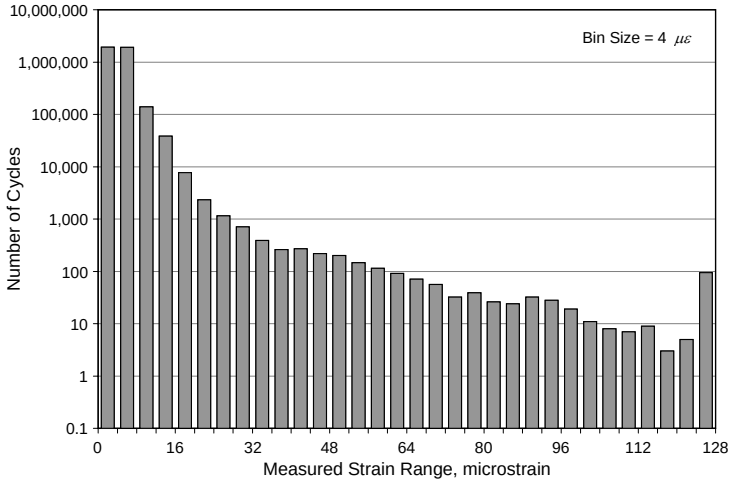

Figure 5.21 Measured Rainflow Response of Strain Gage F – Phase 1

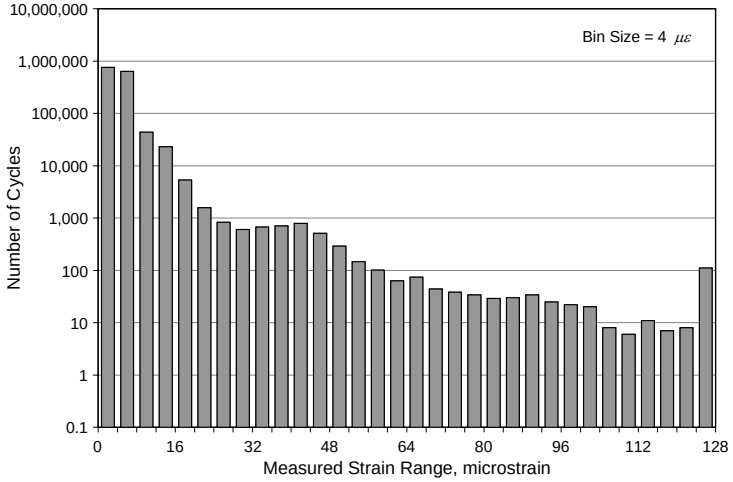

Figure 5.22 Measured Rainflow Response of Strain Gage G – Phase 1

The maximum strain range was captured for strain gages A and C. A summary of the average number of cycles per day at various strain levels is presented in Table 5.4 for these two gages. For the other two strain gages that collected reliable data – strain gages D and F – more than 100 cycles were recorded in the largest bin. A summary of the average number of cycles per day at various strain levels is presented in Table 5.5 for these two gages.

Table 5.4 Average Number of Strain Cycles Recorded per Day by Strain Gages A and C during First Collection Period

Strain Range	Stress Range	Strain Gage	
($\mu\varepsilon$)	(ksi)	A	C
≥ 5	0.15	29,500	13,200
≥ 20	0.6	118	91
≥ 40	1.2	24	16
≥ 60	1.8	5.9	4.0
≥ 80	2.4	1.5	1.0
≥ 100	3.0	0.8	0.9
≥ 120	3.6	0.3	0.4
≥ 140	4.2	—	0.1

Table 5.5 Average Number of Strain Cycles Recorded per Day by Strain Gages D and F during First Collection Period

Strain Range	Stress Range	Strain Gage	
($\mu\varepsilon$)	(ksi)	D	F
≥ 4	0.12	65,800	74,800
≥ 20	0.6	583	226
≥ 40	1.2	79	54
≥ 60	1.8	37	20
≥ 80	2.4	20	10
≥ 100	3.0	9.3	4.9
≥ 120	3.6	4.5	3.6

5.2.2 Second Collection Period

Because the maximum strain ranges were not captured for five of the seven strain gages during the first collection period, rainflow data were collected during the second reporting period using larger bin sizes. The number of rainflow counts recorded each day by the six strain gages (no data were collected from strain gage G) are plotted in Figure 5.23. The trends are essentially the same as those in Figure 5.12, except that the data from strain gage E appear to be reliable, as the daily fluctuations were consistent with the other strain gages. Only 5 days of data were collected from strain gage A. Once again, the data acquisition system attached to strain gage B (unit 1005) recorded many more strain cycles than the other units.

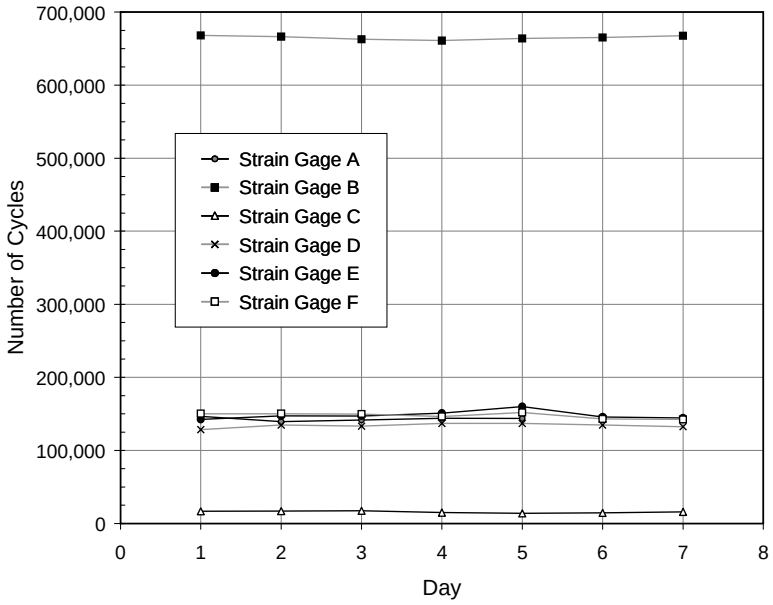

Figure 5.23 Daily Variations in Number of Rainflow Cycles Recorded above Noise Threshold during Second Collection Period

Histograms of the rainflow counts from the strain gages Figure 5.24 through Figure 5.29. The maximum strain range was captured for all strain gages. In retrospect, the bin size was too large for strain gage C because all the strain cycles were grouped into the lowest seven bins. A summary of the average number of cycles per day at various strain levels is presented in Table 5.6 for strain gages A, D, E, and F. Data from strain gage C are not included due to differences in the bin sizes. The maximum strain range was less than 200 $\mu\varepsilon$ for all five strain gages.

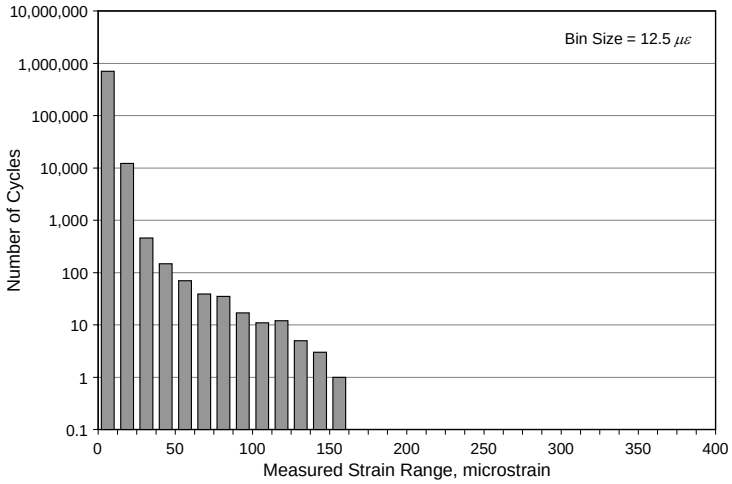

Figure 5.24 Measured Rainflow Response of Strain Gage A – Phase 2

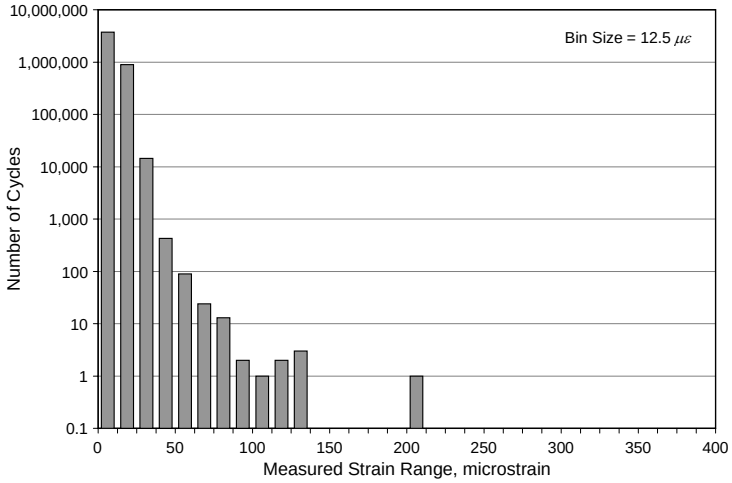

Figure 5.25 Measured Rainflow Response of Strain Gage B – Phase 2

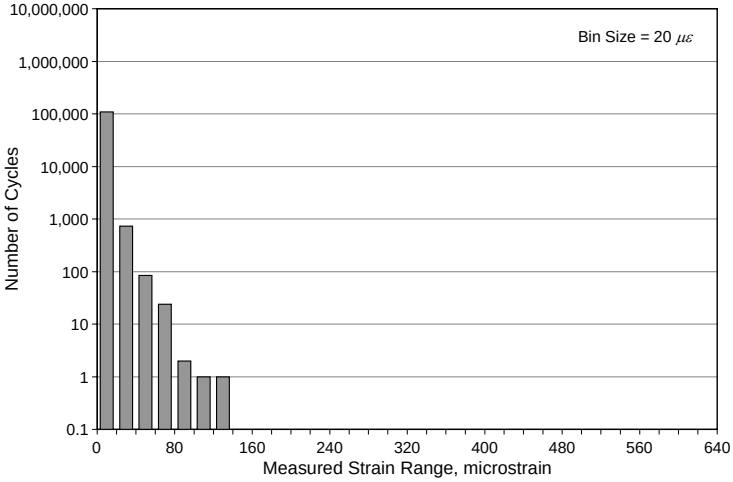

Figure 5.26 Measured Rainflow Response of Strain Gage C – Phase 2

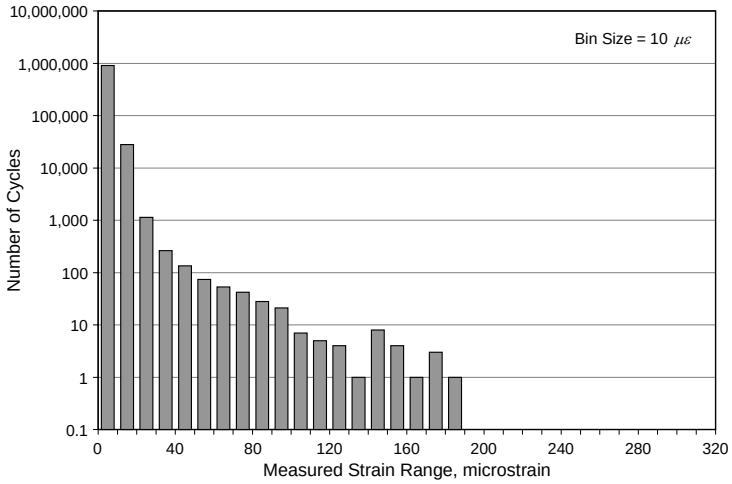

Figure 5.27 Measured Rainflow Response of Strain Gage D – Phase 2

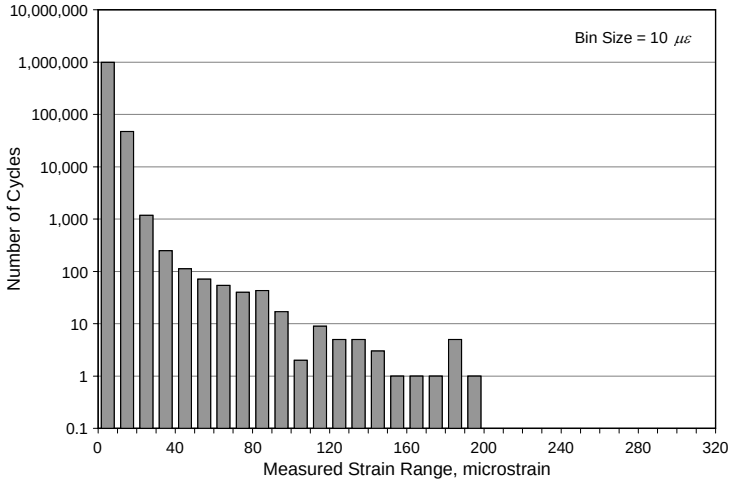

Figure 5.28 Measured Rainflow Response of Strain Gage E – Phase 2

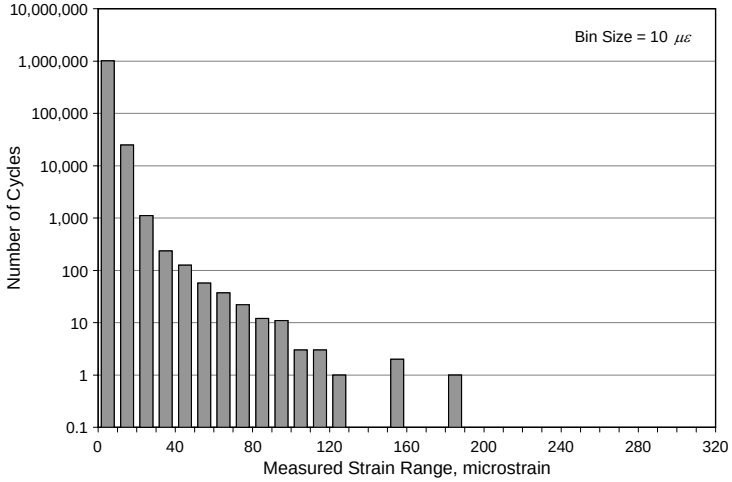

Figure 5.29 Measured Rainflow Response of Strain Gage F – Phase 2

Table 5.6 Average Number of Strain Cycles Recorded per Day by Strain Gages A, D, E, and F during Second Collection Period

Strain Range	Stress Range	Strain Gage			
($\mu\varepsilon$)	(ksi)	A	D	E	F
≥ 3	0.09	143,000	134,000	148,000	148,000
≥ 50	1.5	39	36	37	21
≥ 100	3.0	6.4	4.9	4.7	1.4
≥ 150	4.5	0.2	1.3	1.3	0.4
≥ 200	6.0	—	—	—	—

5.3 SUMMARY

Seven miniature data acquisition systems were used to monitor the live-load response of the 12th Street Exit Ramp. Although all did not function as intended, valuable information was obtained about the live-load response of the bridge.

The three miniature data acquisition units attached to strain gages C, D, and F collected reliable data during both rainflow collection periods. In retrospect, a larger bin size should have been used for strain gages D and F during the first collection period and a smaller bin size should have been used for strain gage C during the second collection period, but otherwise, these units functioned as intended.

The data acquisition units attached to strain gages A, B, E, and G recorded rainflow data, but careful evaluation of the data was required. Because it is not possible to distinguish the unreliable data from the reliable data using only the rainflow histograms, evaluation of the daily cycle counts is needed to identify the unreliable data.

The data acquisition unit attached to strain gage A exhibited unexpected response during both rainflow collection periods. During the first period, an unusually high number of strain cycles was recorded on one day, while the rainflow data from the other 27 days appeared to be reliable. During the second period, the data acquisition unit did not collect rainflow cycles during the last two days, but the rainflow data from the first five days appeared to be reliable.

At first glance, the data acquisition unit attached to strain gage B appeared to measure rainflow data throughout both collection periods. However, the number of cycles recorded by this unit was more than an order of magnitude larger than the number of cycles recorded by the other data acquisition units. Therefore, the rainflow data from strain gage B were discarded.

The data acquisition unit attached to strain gage E recorded rainflow data during both collection periods, but large daily variations in the number of cycles were observed during the first collection period. Therefore, the rainflow data from strain gage E recorded during the first collection period were discarded.

The rainflow data from strain gage E recorded during the second collection period were considered to be reliable.

The data acquisition unit attached to strain gage G recorded rainflow data during the first collection period, but large variations in the number of cycles recorded each day were observed. These rainflow data were discarded. No rainflow data were recorded by this unit during the second collection period.

The reliable rainflow data from strain gages A, D, E, and F will be used in Chapter 6 to evaluate the remaining fatigue life of the longitudinal girders from the 12th Street Exit Ramp.

CHAPTER 6: EVALUATION OF FATIGUE LIFE FROM MEASURED RAINFLOW DATA

The measured rainflow data were presented and evaluated in Chapters 4 and 5 for the Medina River Bridge and the 12th Street Exit Ramp, respectively. The data considered to be reliable are used in this chapter to evaluate the remaining fatigue life of the two bridges. Measured rainflow data are evaluated in Section 6.1 to determine the sensitivity of the calculated fatigue life to the parameters selected by the research team (bin size and noise threshold) when collecting the rainflow data. The possibility of reproducing the measured rainflow response using the truck configurations identified by the weigh-in-motion station is addressed in Section 6.2. Rainflow data from the longitudinal girders are used to estimate the remaining fatigue life of the Medina River Bridge and the 12th Street Exit Ramp in Section 6.3.

In all fatigue life calculations, the longitudinal girders from the Medina River Bridge were classified as Detail Category D due to the riveted connections and the longitudinal box girders from the 12th Street Exit Ramp were classified as Detail Category E due to the geometry of the welded connections with the floor beams.

6.1 SENSITIVITY OF FATIGUE LIFE TO PARAMETERS USED TO COLLECT RAINFLOW DATA

The procedures used to calculate the fatigue life of a bridge from the measured rainflow data were presented in Section 2.3 and Section 2.4. However, the nature of the measured rainflow data presented in Chapter 4 for the Medina River Bridge and in Chapter 5 for the 12th Street Exit Ramp highlighted two issues that must be addressed before calculating the remaining fatigue life of the bridges:

(1) As shown in Figure 4.15, the miniature data acquisition systems recorded a large number of low-amplitude strain cycles that can be attributed to electrical noise and thermal cycles, in addition to the live-load response of the bridge. The sensitivity of the calculated fatigue life to these low-amplitude cycles is discussed in Section 6.1.1.

(2) At several locations on each bridge, the bin size used to collect the rainflow data was too small to capture the maximum strain range. At other locations, the bin size used to collect the rainflow data was too large, and the measured strain cycles were grouped in a few bins. The sensitivity of the calculated fatigue life to the choice of bin size is addressed in Section 6.1.2.

Rainflow data from both bridges were used to evaluate the sensitivity of the calculated fatigue life to both parameters.

Calculating the fatigue life from a strain histogram is a two-step process: first the effective stress range, S_{re}, must be calculated (Section 2.3) and then the fatigue life can be determined (Section 2.4). For the calculations discussed in this section, the fatigue life, *m*, is expressed in years and the annual rate of traffic growth, *r*, was assumed to be 2%.

6.1.1 Low-Amplitude Strain Cycles

As discussed in Chapters 4 and 5, the measured rainflow response of the bridge has three components: electrical noise, thermal cycles, and load-induced cycles. The fatigue life of the bridge depends only on the number and magnitude of the load-induced cycles, but it is not possible to separate these from the measured rainflow response. The data in Figure 4.13 and Figure 4.15 indicate that most of cycles attributed to electrical noise and thermal variations have a range less than 20 $\mu\varepsilon$. Therefore, the focus of this section is determining the sensitivity of the calculated fatigue life to the low-amplitude cycles caused by electrical noise and thermal cycles.

When recording rainflow data, the miniature data acquisition systems report the number of strain cycles below the noise threshold and the number of strain cycles in each of the 32 bins for each 24-hr collection period. The sensitivity of the calculated fatigue life to the number of low-amplitude strain cycles can be determined by increasing the minimum strain range used in the fatigue life calculations, $S_{r,\min}$. For example, if the cycles below the noise threshold and the cycles in the 32 bins are included in the fatigue life calculations, all strain cycles with a range above 0 $\mu\varepsilon$ are considered. If, however, the cycles in the first bin are ignored in the fatigue life calculations, then only the cycles with a range above the bin size are considered. By varying the minimum strain range considered in the fatigue life calculations, the same set of measured rainflow data can be used to evaluate the sensitivity of the calculated fatigue life to the number of low-amplitude cycles.

The results of these calculations are summarized in Table 6.1 for the strain gages attached to the longitudinal girders of the Medina River Bridge and in Table 6.2 for the strain gages attached to the longitudinal girders of the 12th Street Exit Ramp. The duration of the rainflow collection period, *D*; total number of cycles recorded, N_{tot}; calculated effective stress range, S_{re}; calculated fatigue life in cycles, *N*; and calculated fatigue life in years, *m*, are also listed for each value of minimum strain range considered.

The variation of the effective stress range with the minimum level of strain range considered in the fatigue life calculations is plotted in Figure 6.1. In all cases the effective stress range increased as the minimum strain range considered increased.

Table 6.1 Sensitivity of Calculated Fatigue Life of Longitudinal Girders from Medina River Bridge to Minimum Stress Range Considered

Strain Gage	D (days)	$S_{r,\min}$ (ksi)	N_{tot} (cycles)	S_{re} (ksi)	N (cycles)	m^* (years)
A	21	0	16.6×10^6	0.50	17.3×10^9	87.3
		4	2.30×10^6	0.97	2.40×10^9	87.3
		8	0.75×10^6	1.41	0.79×10^9	87.5
C	28	0	21.8×10^6	0.54	13.8×10^9	78.6
		4	2.91×10^6	1.06	1.85×10^9	78.7
		8	1.00×10^6	1.51	0.64×10^9	78.8
D	28	0	23.5×10^6	0.22	209×10^9	201
		5	1.49×10^6	0.54	13.8×10^9	203
		10	0.27×10^6	0.94	2.63×10^9	206
E	28	0	24.9×10^6	0.13	921×10^9	272
		10	0.91×10^6	0.38	40.4×10^9	282
H	28	0	23.2×10^6	0.34	56.9×10^9	138
		5	1.66×10^6	0.81	4.11×10^9	139
		10	0.36×10^6	1.35	0.90×10^9	140

* Assumed annual rate of traffic growth = 2%

Table 6.2 Sensitivity of Calculated Fatigue Life of Longitudinal Girders from 12th Street Exit Ramp to Minimum Stress Range Considered

Strain Gage	D (days)	$S_{r,\min}$ (ksi)	N_{tot} (cycles)	S_{re} (ksi)	N (cycles)	m^* (years)
A	27	0	23.9×10^6	0.10	1110×10^9	246
		3	3.83×10^6	0.18	193×10^9	250
		5	0.80×10^6	0.28	52.8×10^9	264
		10	0.05×10^6	0.55	6.76×10^9	300
	5	0	4.39×10^6	0.15	319×10^9	184
		3	0.72×10^6	0.27	53.1×10^9	185
D	28	0	24.5×10^6	0.13	493×10^9	206
		3	3.76×10^6	0.24	78.2×10^9	208
		4	1.84×10^6	0.30	40.0×10^9	210
		8	0.20×10^6	0.59	5.42×10^9	220
	7	0	6.14×10^6	0.14	436×10^9	200
		3	0.94×10^6	0.25	68.6×10^9	201
		10	0.03×10^6	0.65	3.95×10^9	231
E	7	0	6.14×10^6	0.14	373×10^9	192
		3	1.04×10^6	0.26	64.7×10^9	193
		10	0.05×10^6	0.60	5.21×10^9	220
F	28	0	24.5×10^6	0.12	670×10^9	221
		3	4.02×10^6	0.21	115×10^9	224
		4	2.10×10^6	0.26	63.7×10^9	227
		8	0.19×10^6	0.51	8.38×10^9	245
	7	0	6.14×10^6	0.13	515×10^9	208
		3	1.03×10^6	0.23	90.0×10^9	210
		10	0.03×10^6	0.58	5.60×10^9	255

* Assumed annual rate of traffic growth = 2%

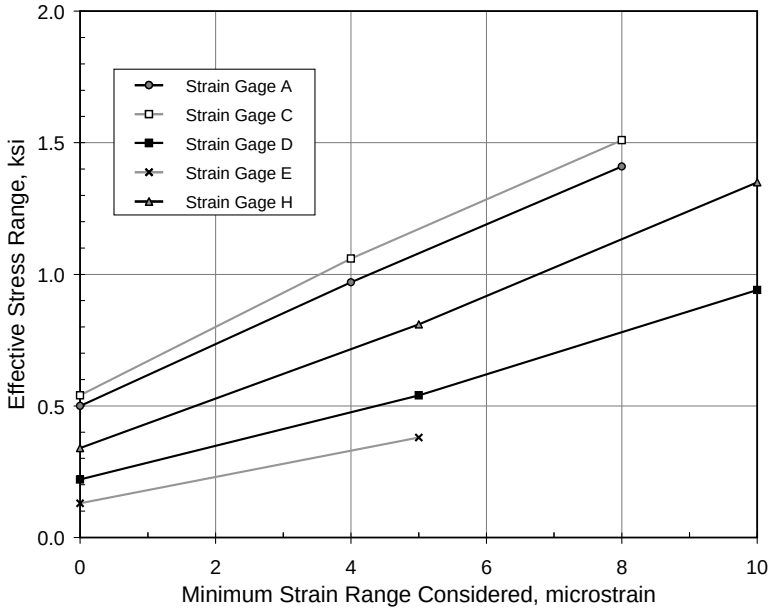

(a) Medina River Bridge

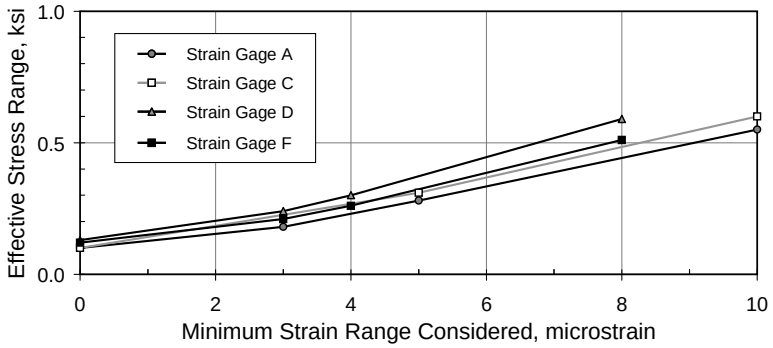

(b) 12th Street Exit Ramp – First Collection Period

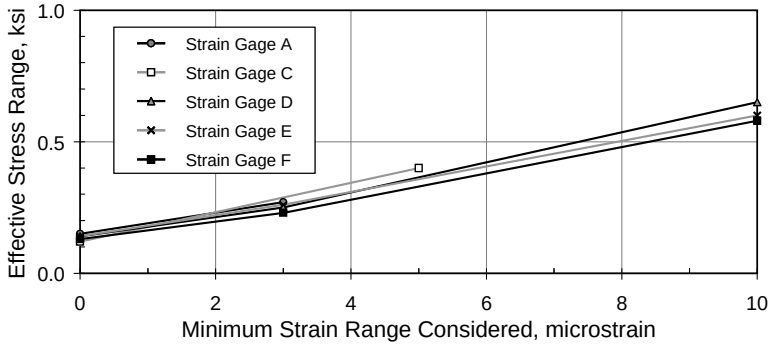

(c) 12th Street Exit Ramp – Section Collection Period

Figure 6.1 Variation of Effective Stress Range with Minimum Strain Range Considered in Calculations

Because the number of cycles recorded during the rainflow collection period decreased as the minimum strain range considered increased, the calculated fatigue life was not as sensitive to the minimum strain range considered in the calculations (Figure 6.2). For the Medina River Bridge, the results are almost independent of the minimum strain range used in the calculations. However, for the 12th Street Exit Ramp, the calculated fatigue life increased when the minimum strain range considered exceeded the noise threshold.

This difference in sensitivity is likely due to the differences in the traffic patterns on the two bridges. Because many more trucks cross the Medina River Bridge each day, the number of large-amplitude strain cycles is larger, and these large-amplitude strain cycles dominate the fatigue life calculations. In contrast, the live-load induced strain ranges are much lower for the 12th Street Exit Ramp, and therefore, the calculated fatigue life is sensitive to strain ranges less than 10 $\mu\varepsilon$.

Based on the results of these calculations, the fatigue life of the bridges will be calculated using all strain cycles above the noise threshold specified for each of the data acquisition units. This is expected to provide a conservative estimate of the remaining fatigue life of each bridge.

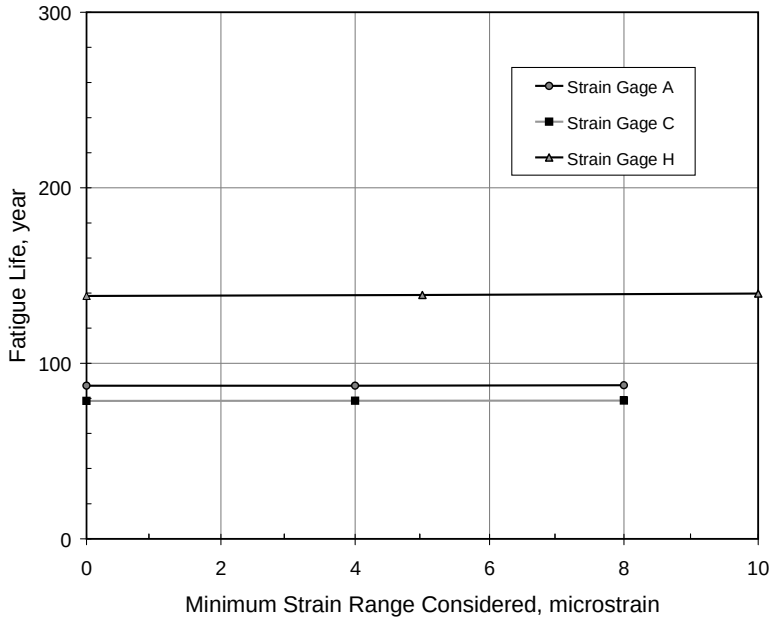

(a) Medina River Bridge

Figure 6.2 Variation of Calculated Fatigue Life with Minimum Strain Range Considered in Calculations

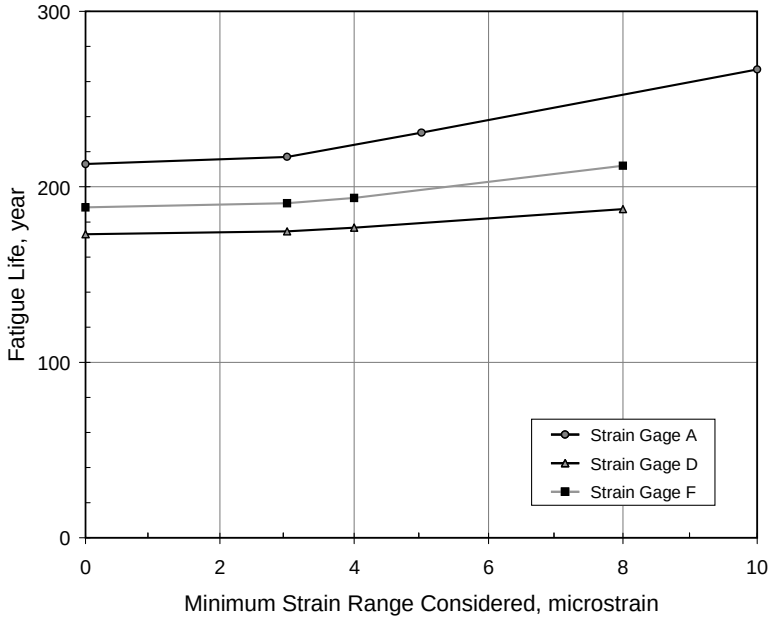

(b) 12th Street Exit Ramp – First Collection Period

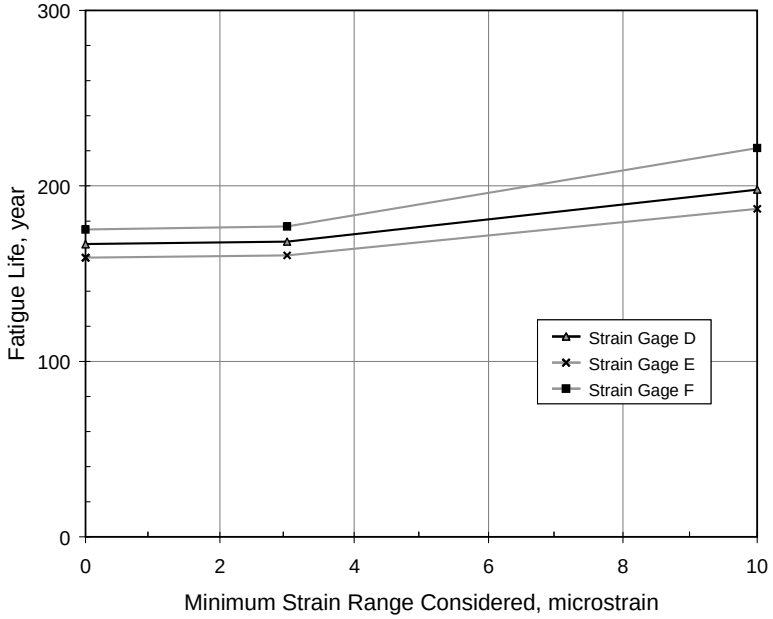

(c) 12th Street Exit Ramp – Section Collection Period

Figure 6.2 (cont.) Variation of Calculated Fatigue Life with Minimum Strain Range Considered in Calculations

6.1.2 Bin Size

As discussed in Chapters 4 and 5, the research team selected too small a bin size for several strain gages and too large a bin size for several others. As a result, the maximum strain range could not be determined from the rainflow data at some locations and the measured rainflow data were grouped in only a few bins at other locations. The consequences of using too small a bin size are addressed first. Data from strain gages A and C from the Medina River Bridge and from strain gages D and F from the 12th Street Exit Ramp are used in these calculations.

For strain gage A from the Medina River Bridge, 130 cycles were recorded in the largest bin (>248 $\mu\varepsilon$) and for strain gage C, 475 cycles were recorded in the largest bin. Based on the results of the calculations presented in Section 6.2, these cycles were distributed into bins between 248 and 352 $\mu\varepsilon$ for strain gage A and between 248 and 408 $\mu\varepsilon$ for strain gage C. Four distributions of strain ranges were considered: (1) measured distribution – all cycles in a single bin between 248 and 256 $\mu\varepsilon$, (2) uniform distribution of cycles in bins exceeding 248 $\mu\varepsilon$, (3) linear distribution of cycles in bins exceeding 248 $\mu\varepsilon$, and (4) parabolic distribution of cycles in bins exceeding 248 $\mu\varepsilon$. For distributions (3) and (4), the largest number of cycles was assigned to the bin between 248 and 256 $\mu\varepsilon$. The measured distributions of cycles for strain ranges less than 248 $\mu\varepsilon$ were used in all four distributions.

The calculated values of effective stress range and fatigue life are summarized for each distribution of strain cycles in Table 6.3. The lowest effective stress range and longest fatigue life was calculated using distribution (1), the measured strain histogram with a large number of cycles in the 32nd bin. The effective stress ranges were higher for the other three strain histograms; however, the maximum differences in fatigue life were quite small.

Table 6.3 Sensitivity of Calculated Fatigue Life to Distribution of Large-Amplitude Cycles

Distribution	Strain Gage A+		Strain Gage C+	
	Effective Stress Range (ksi)	Fatigue Life* (year)	Effective Stress Range (ksi)	Fatigue Life* (year)
(1) Measured	0.971	87.3	1.060	78.7
(2) Uniform	0.977	86.5	1.087	75.7
(3) Linear	0.975	86.8	1.077	76.8
(4) Parabolic	0.974	87.0	1.076	76.9

+ Rainflow data from Medina River Bridge
* Assumed annual rate of traffic growth = 2%

For the 12th Street Exit Ramp, rainflow data were recorded at the same locations using different bin sizes during the two collection periods. A bin size of 4 $\mu\varepsilon$ was used for strain gages D and F during the first collection period. At the conclusion of the 28-day rainflow collection period approximately 100 cycles were recorded in the largest bin (>124 $\mu\varepsilon$) for each gage. The bin size was increased to 10 $\mu\varepsilon$ for each gage during the second collection period. A single cycle was recorded by each gage in the bin between 180 and 190 $\mu\varepsilon$ during the second, 7-day rainflow collection period.

Key parameters from the two strain gages are summarized in Table 6.4. On average, more large-amplitude cycles were recorded each day during the first collection period than the second collection period. However, the calculated effective stress ranges were slightly larger for the second collection period, and therefore, the corresponding fatigue lives were less when the maximum strain range was captured.

Table 6.4 Sensitivity of Calculated Fatigue Life to Maximum Strain Range

Parameters	Strain Gage D+		Strain Gage F+	
	First Collection Period	Second Collection Period	First Collection Period	Second Collection Period
Noise Threshold, $\mu\varepsilon$	3	3	3	3
Bin Size, $\mu\varepsilon$	4	10	4	10
Duration, day	28	7	28	7
Cycles above 120 $\mu\varepsilon$	127	22	100	4
Average Cycles per Day above 120 $\mu\varepsilon$	4.5	3.1	3.6	0.6
Effective Stress Range, ksi	0.24	0.25	0.21	0.23
Fatigue Life*, year	208	201	224	210

+ Rainflow data from 12th Street Exit Ramp
* Assumed annual rate of traffic growth = 2%

The rainflow data from both bridges indicated that the fatigue life is over-estimated when the bin size is too small to capture the maximum bin size. The differences in fatigue life tended to be larger for the 12th Street Exit Ramp.

The consequences of using too large a bin size were investigated using data from the same four strain gages. The effective stress range was calculated for each gage using the measured distribution of strain cycles. Adjacent bins were then combined to create a histogram with a bin size that was two times the original. The process was repeated, such that the histogram had a bin size four times the original.

The results are summarized in Table 6.5. A bin size of 8 $\mu\varepsilon$ was used to capture the response of strain gages A and C from the Medina River Bridge and a bin size of 4 $\mu\varepsilon$ was used to capture the response of strain gages D and F from the 12th Street Exit Ramp. When the original bin size was doubled, the measured strain ranges were grouped into 16 bins and when the original bin size was quadrupled, the measured strain ranges were grouped into 8 bins. The calculated fatigue lives were very similar for the histograms with the original and doubled bin sizes. However, the calculated fatigue lives were considerably shorter when calculated using the histograms with the quadrupled bin sizes. Again, the differences in fatigue life were larger for the 12th Street Exit Ramp.

Table 6.5 Sensitivity of Calculated Fatigue Life to Bin Size

Bridge	Strain Gage	Parameter	Bin Size			
			4 $\mu\varepsilon$	8 $\mu\varepsilon$	16 $\mu\varepsilon$	32 $\mu\varepsilon$
Medina River Bridge	A	Effective Stress Range, ksi	—	0.971	0.978	1.016
		Fatigue Life*, year	—	87.3	86.5	81.7
	C	Effective Stress Range, ksi	—	1.060	1.065	1.098
		Fatigue Life*, year	—	78.7	78.1	74.5
12th Street Exit Ramp	D+	Effective Stress Range, ksi	0.241	0.250	0.320	—
		Fatigue Life*, year	208	203	166	—
	F+	Effective Stress Range, ksi	0.212	0.222	0.303	—
		Fatigue Life*, year	234	217	171	—

* Assumed annual rate of traffic growth = 2%
+ Data recorded during first collection period.

Two conclusions may be drawn from these analyses: (1) the calculated fatigue life is over-estimated when the bin size is too small and the maximum strain range can not be determined from the rainflow data, and (2) the calculated fatigue life is conservative when the bin size is too large and the strain cycles are grouped in a few bins. The calculations described in this section highlight the importance of selecting an appropriate bin size when collecting rainflow data.

6.2 USE OF WEIGH-IN-MOTION DATA TO CALCULATE LIVE-LOAD RESPONSE

As discussed in Chapter 4, the maximum strain range was not captured from the strain gages positioned along the north anchor span of the Medina River Bridge. The possibility of using the vehicle data from the weigh-in-motion station to calculate the distribution of the large-amplitude strain cycles for this bridge is discussed in this section.

The analytical model developed for this purpose is discussed is Section 6.2.1 and the measured rainflow response is compared with the calculated distribution of strain cycles in Section 6.2.2. The limitations of using the measured weigh-in-motion data to calculate the rainflow response are summarized in Section 6.2.3.

6.2.1 Analytical Model

As discussed in Chapter 3, a line girder model was used to calculate the live-load response of the Medina River Bridge due to the simple geometry. A special-purpose computer program was developed to determine the flexural response at any location along either longitudinal girder to the traffic loads detected by the weigh-in-motion station. The bridge was modeled as a statically-determinant beam using the boundary conditions shown in Figure 3.5. The analysis may be divided into four steps:

(1) The influence line for moment was calculated at each specified location. A unit load was positioned at 0.1-ft intervals along the girder, and the corresponding moments were calculated at the specified locations.

(2) The moment induced at the specified locations by a given truck was calculated by superimposing the influence lines, which were multiplied by the axle loads and offset horizontally by the axle spacing. Each vehicle recorded by the weigh-in-motion station was considered independently.

(3) Maximum and minimum moments were selected from the calculated moment histories. The moments were distributed to the girders using the live load distribution factors given in Table 3.1 and converted to flexural stress using Eq. 3.2. The values of stress were then converted to strain using Hooke's Law.

(4) A rainflow counting routine was then used to determine the corresponding live-load strain ranges for each vehicle.

Steps (2) through (4) were repeated using as many vehicles as desired, and the resulting strain histograms were compared with the measured rainflow response of the bridge.

A representative moment history (step 2) calculated at the location of strain gage C is shown in Figure 6.3. An idealized 5-axle truck, positioned in the left lane, was used in these calculations. The characteristics of the idealized truck are listed in Table 6.6 and are similar to the median T5-1 truck from the weigh-in-motion data (Table 2.6). The idealized loading vehicle induced two strain cycles at this location: the large-amplitude cycle had a range between 192 and 200 $\mu\varepsilon$ and the low-amplitude cycle had a range between 8 and 16 $\mu\varepsilon$.

Table 6.6 Idealized Five-Axle Truck

Axle Weight, kip					GVW	Axle Spacing, ft				Total Length
A	B	C	D	E	(kip)	AB	BC	CD	DE	(ft)
10	10	10	10	10	50	17	4	33	4	58

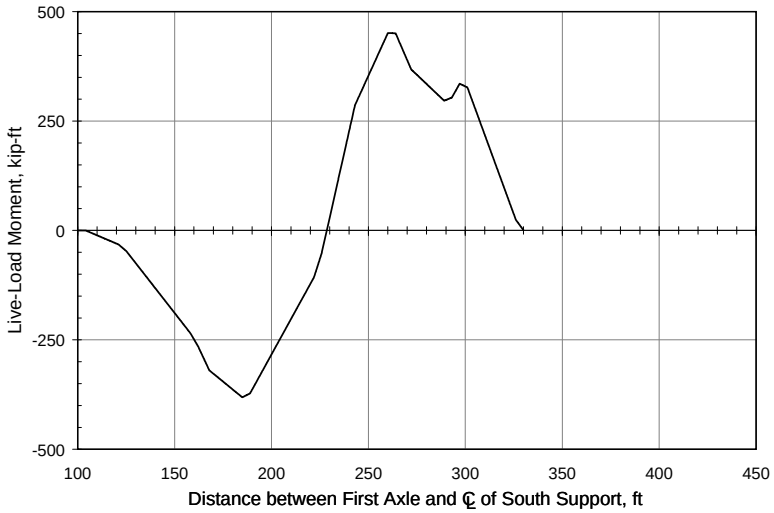

Figure 6.3 Calculated Variation of Live-Load Moment at Strain Gage C for Idealized Five-Axle Truck

Inherent to this analysis is the assumption that one truck crosses the Medina River Bridge at a time. As shown in Figure 4.3, the truck traffic was sufficient that multiple trucks often crossed the bridge simultaneously. The calculated moment histories are sensitive to the number of trucks, as shown in Figure 6.4 where the live-load response at the location of strain gage C was calculated for two idealized five-axle trucks, which crossed the bridge in the left lane separated by 50 ft. Four strain cycles were calculated for this situation: one cycle with a range between 192 and 200 $\mu\varepsilon$, one cycle with a range between 80 and 88 $\mu\varepsilon$, and two cycles with a range between 8 and 16 $\mu\varepsilon$.

The results of this simple analysis indicate that the maximum strain range is not sensitive to the number of trucks crossing the bridge in the same lane simultaneously, but that the number of large-amplitude cycles will be over-estimated compared with the measured rainflow response using the analysis described in this section, where the trucks are assumed to cross the bridge one at a time. The possibility of trucks crossing the bridge simultaneously in both lanes is also not considered.

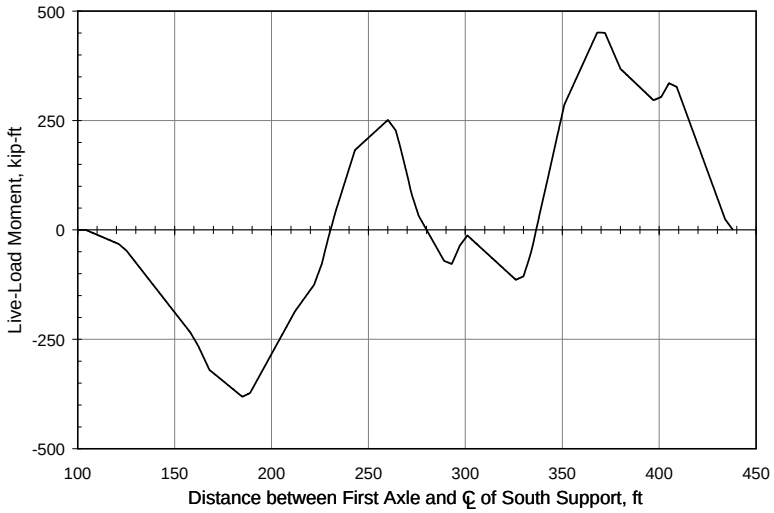

Figure 6.4 Calculated Variation of Live-Load Moment at Strain Gage C for Two Idealized Five-Axle Trucks Separated by 50 ft

6.2.2 Calculated Distribution of Strain Cycles

Based on the results discussed in Section 6.2.1, it is clear that differences exist between the measured rainflow response of the Medina River Bridge and the response calculated using the weigh-in-motion data. Traffic patterns, including the distribution of trucks among the lanes of traffic and the number of trucks crossing the bridge simultaneously, influence the measured strain response, and this can not be represented using the simple analytical model. However, the combination of measured rainflow and weigh-in-motion data presents a rare opportunity to determine which aspects of the measured rainflow response can be reproduced analytically. Data recorded by strain gages D and H are used for this analysis.

Rainflow and weigh-in-motion data from Tuesday, 31 August 2004 were used to compare the calculated and measured response of strain gages D and H. The 24-hr data acquisition periods began at 5:30 pm each day during the first collection period. The weigh-in-motion data are identified by the hour that the truck passed the station, but not the minute. Therefore, the 4,769 trucks that crossed the weigh-in-motion station between 5:00 pm on 31 August 2004 and 5:00 pm on 1 September 2004 were considered in this analysis. The actual number of trucks that crossed the Medina River Bridge – and their transverse positions – was not known.

The sensitivity of the calculated rainflow response to the percent of trucks in the right lane is shown in Figure 6.5. The number of cycles within a given strain range varied with the transverse position of the trucks. The number of large-amplitude cycles increased in the west girder when more trucks were assumed to be in the left lane and the number of large-amplitude cycles increased in the east girder when more trucks were assumed to be in the right lane. However, the maximum strain range, $S_{r,\max}$, was nearly independent of the transverse position of the trucks. A single cycle was recorded in the same bin for all three truck distributions shown in Figure 6.5.

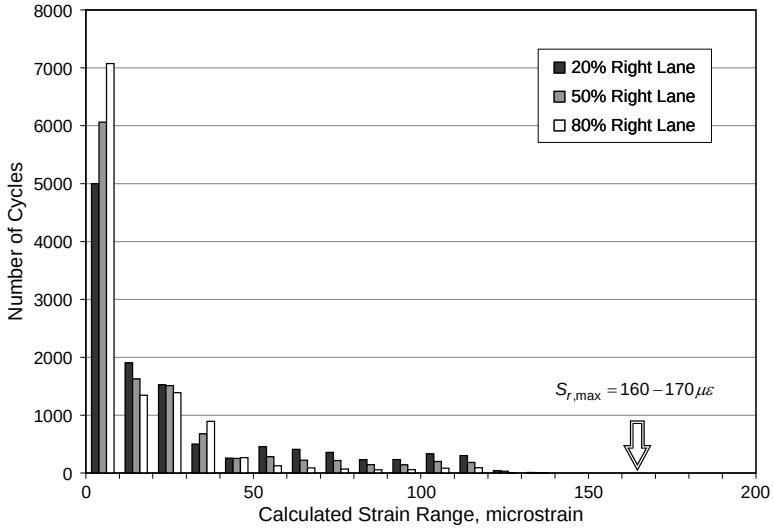

(a) Strain Gage D – West Girder

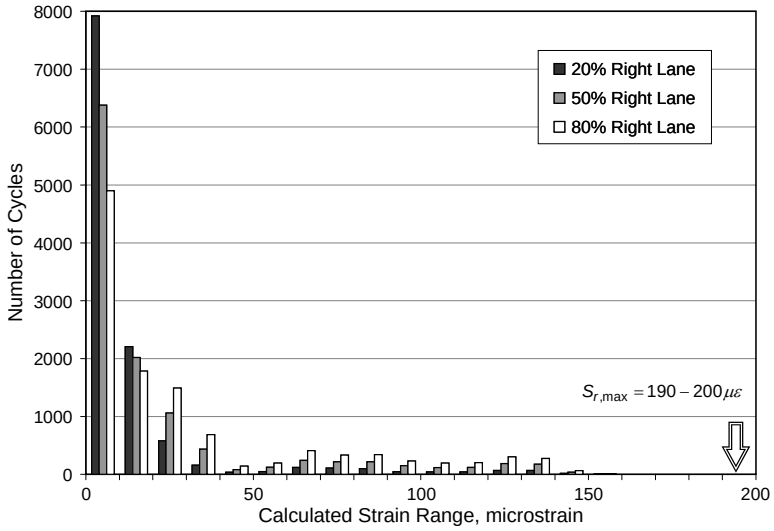

(b) Strain Gage H – East Girder

Figure 6.5 Sensitivity of Strain Cycles to Transverse Position of Trucks

The calculated strain histograms are compared with the measured strain histograms for 31 August 2004 in Figure 6.6. Seventy percent of the trucks were assumed to cross the bridge in the right lane. As expected, the number of measured low-amplitude cycles exceeded the calculated number and the number of calculated large-amplitude cycles exceeded the measured number for both girders. However, the range of measured strain cycles was well represented by the calculations.

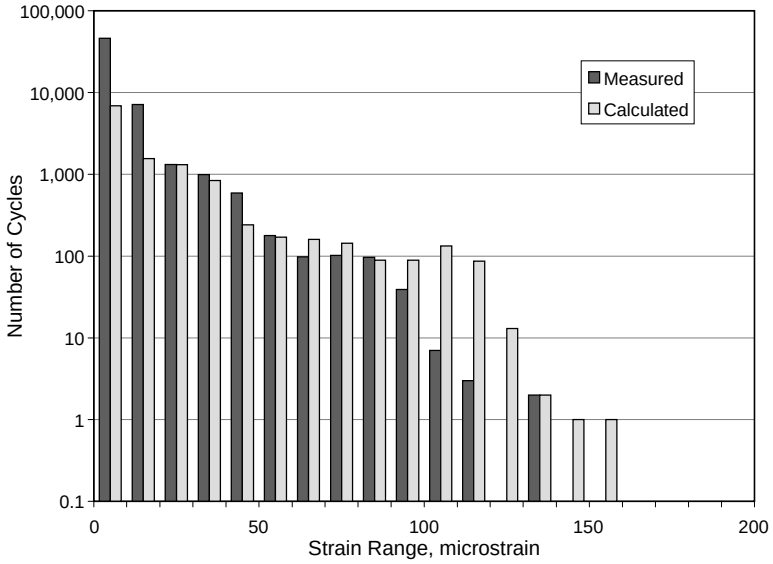

(a) Strain Gage D – West Girder

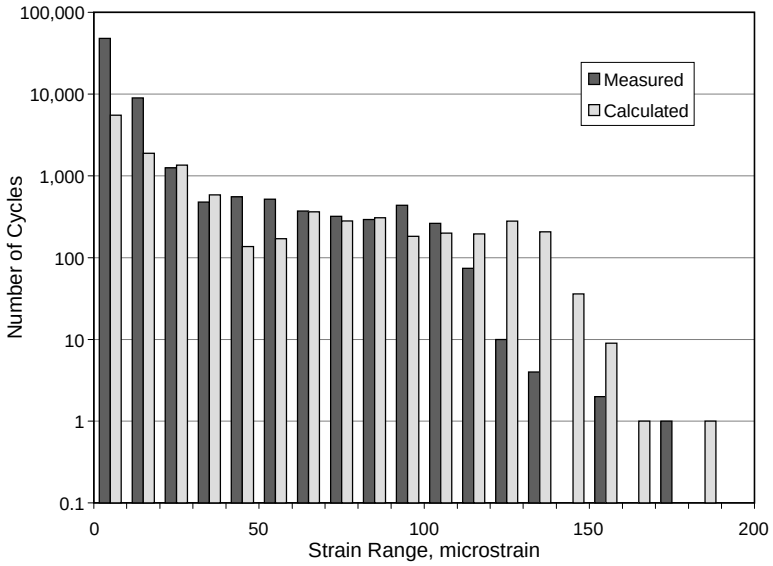

(b) Strain Gage H – East Girder

Figure 6.6 Comparison of Measured and Calculated Rainflow Cycles for Gages D and H on 31 August 2004

The calculations were repeated using the 118,932 trucks that passed the weigh-in-motion station during the 28-day period that began at midnight on 26 August 2004. The results are compared with the measured data from the first collection period in Figure 6.7. The trends were essentially the same as those shown in Figure 6.6 using the larger truck population; however, in this case the amplitude of the maximum measured strain range exceeded the calculated values. The differences in the number of cycles in the largest few bins appear to be significant on the log scale, but never exceeded 10 cycles.

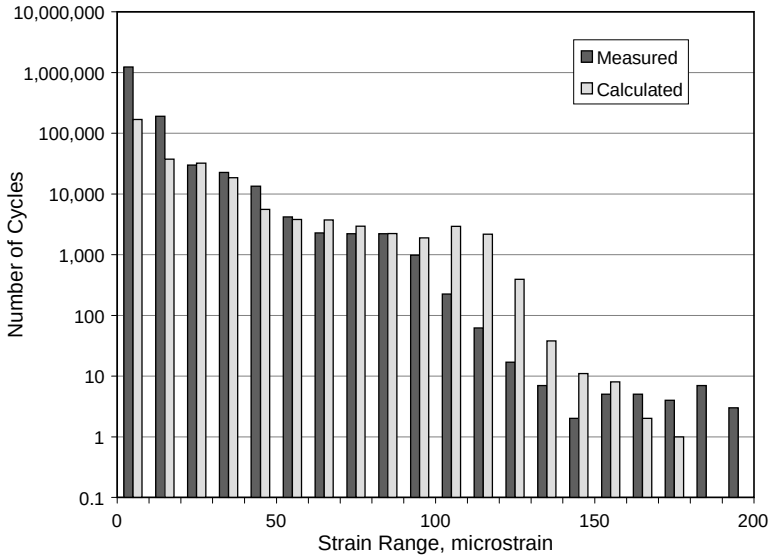

(a) Strain Gage D – West Girder

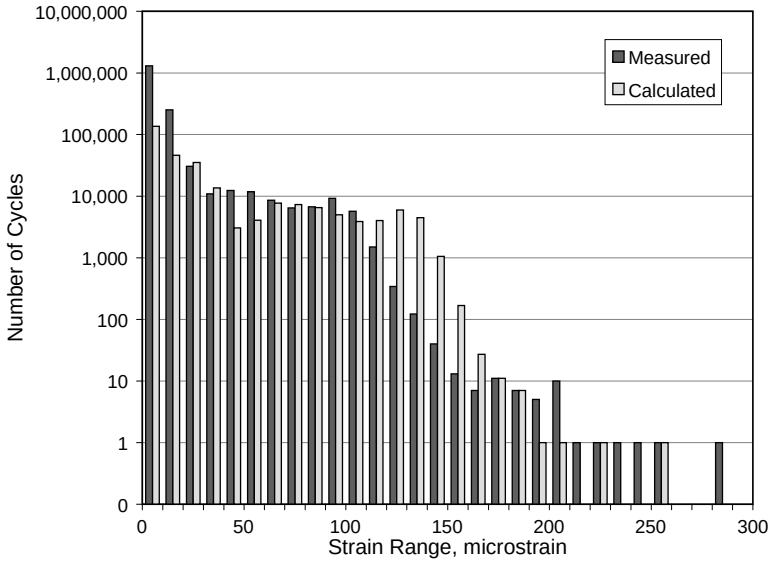

(b) Strain Gage H – East Girder

Figure 6.7 Comparison of Measured and Calculated Rainflow Cycles for Gages D and H during First Collection Period

The same data are summarized in Table 6.7. The total number of strain cycles recorded above the noise threshold of 5 $\mu\varepsilon$ was more than five times larger than the total number of calculated strain cycles for both strain gages. Differences in the total number of cycles were expected because the calculations can not reproduce electrical noise, thermal cycles, and the dynamic response of the bridge. When evaluating the percentage of cycles with strain ranger larger than 50 $\mu\varepsilon$ (1.5 ksi), the calculated percentages were typically considerably larger than the measured values. As a result of these two differences between the measured and calculated response, the effective stress ranges for the calculated strain histograms were more than a factor of two times larger than the values calculated from the measured data and the corresponding fatigue lives were considerably shorter.

Table 6.7 Comparison of Measured and Calculated Rainflow Response of Strain Gages D and H from Medina River Bridge

Parameter	Strain Gage D		Strain Gage H	
	Measured	Calculated	Measured	Calculated
Total Number of Cycles	1,493,359*	283,272+	1,657,652*	283,272+
Cycles ≥ 50 $\mu\varepsilon$	4.3%	7.1%	3.0%	17.7%
Cycles ≥ 100 $\mu\varepsilon$	0.12%	2.0%	0.47%	6.9%
Cycles ≥ 150 $\mu\varepsilon$	0.0085%	0.0039%	0.0036%	0.077%
Cycles ≥ 200 $\mu\varepsilon$	—	—	0.0010%	0.0011%
Cycles ≥ 250 $\mu\varepsilon$	—	—	0.00012%	0.00035%
Cycles ≥ 300 $\mu\varepsilon$	—	—	—	—
Effective Stress Range (ksi)	0.54	1.14	0.81	1.72
Fatigue Life (cycles)	13.8×10^9	1.49×10^9	4.11×10^9	0.44×10^9
Fatigue Life (year)†	203	175	139	117

* Measured number of cycles exceeding noise threshold of 5 $\mu\varepsilon$.

+ Calculated number of cycles exceeding 0 $\mu\varepsilon$.

† Assumed annual rate of traffic growth = 2%.

These comparisons demonstrate that the measured weigh-in-motion data can not be used to reproduce the measured rainflow response. Therefore, it is not possible to calculate the rainflow response of the bridge at a location where a data acquisition system failed to collect date or at another location of interest where the research team did not position a strain gage. However, for both strain gages, the calculated number of large-amplitude cycles was similar to the measured number. Therefore, the measured weigh-in-motion data were used to approximate the distribution of large-amplitude cycles for strain gages A and C, where the bin size was too small to capture the maximum strain range.

Measured weigh-in-motion data from Friday, 28 January 2005 were used to evaluate the response of strain gages A and C. As before, seventy percent of the trucks were assumed to cross the Medina River Bridge in the right lane. The rainflow collection periods began at midnight during the second collection period; therefore, no adjustment of the weigh-in-motion data was required. On this day, 2,942 trucks crossed the weigh-in-motion station. Five cycles were recorded in the largest bin (248-256 $\mu\varepsilon$) for strain gage A and 15 cycles were recorded in the largest bin for strain gage C.

Measured and calculated data are compared in Figure 6.8. For strain ranges less than 40 $\mu\varepsilon$, the number of measured cycles exceeded the number of calculated cycles by a factor of more than 20. For strain ranges between 40 and 200 $\mu\varepsilon$, the number of measured and calculated cycles was approximately the same. Above 200 $\mu\varepsilon$, the number of calculated strain cycles exceeded the measured number of cycles by a factor of more than 3. For strain gage A, the maximum calculated strain range exceeded the maximum bin size by five bins (40 $\mu\varepsilon$); however, the maximum calculated strain range exceeded the maximum bin size by thirteen bins (104 $\mu\varepsilon$) for strain gage C.

These results are consistent with those from strain gages D and H, and therefore, the model was considered to be appropriate for evaluating the distribution of the large-amplitude strain cycles. A larger population of vehicles was used in this analysis. During the 50 days for which weigh-in-motion data were available, more than 198,000 five-axle trucks were detected. This population of vehicles was used to calculate the strain response at the locations of gages A and C.

For strain gage A, 130 cycles were recorded in the largest bin (248 to 256 $\mu\varepsilon$) during the 21-day collection period. When the population of 5-axle trucks was considered, 16,500 cycles were calculated with a strain range larger than 248 $\mu\varepsilon$ and a single cycle was recorded in the bin between 392 and 400 $\mu\varepsilon$. The 130 measured strain cycles were then distributed among the larger bins based on the calculated distribution. Because an integer number of cycles must be assigned to each bin, the largest amplitude strain cycle attributed to strain gage A during the 21-day collection period was between 344 and 352 $\mu\varepsilon$. The complete strain histogram with the extrapolated data for strain gage A is shown in Figure 6.9.

For strain gage C, 475 cycles were recorded in the largest bin (248 to 256 $\mu\varepsilon$) during the 28-day collection period. When the population of 5-axle trucks was used, nearly 27,300 cycles were calculated with a strain range larger than 248 $\mu\varepsilon$ and a single cycle was recorded in the bin between 472 and 480 $\mu\varepsilon$. The 475 cycles were distributed among the larger bins, and the largest amplitude strain cycle attributed to strain gage C during the 28-day collection period was between 400 and 408 $\mu\varepsilon$ (Figure 6.10).

When combined with the measured strain histograms, the extrapolated, large-amplitude strain cycles (Figure 6.9 and Figure 6.10) were fairly uniformly distributed above the maximum measured bin size. While this may not be the most realistic distribution, but as indicated in Table 6.3, this distribution should lead to a conservative estimate of the fatigue life.

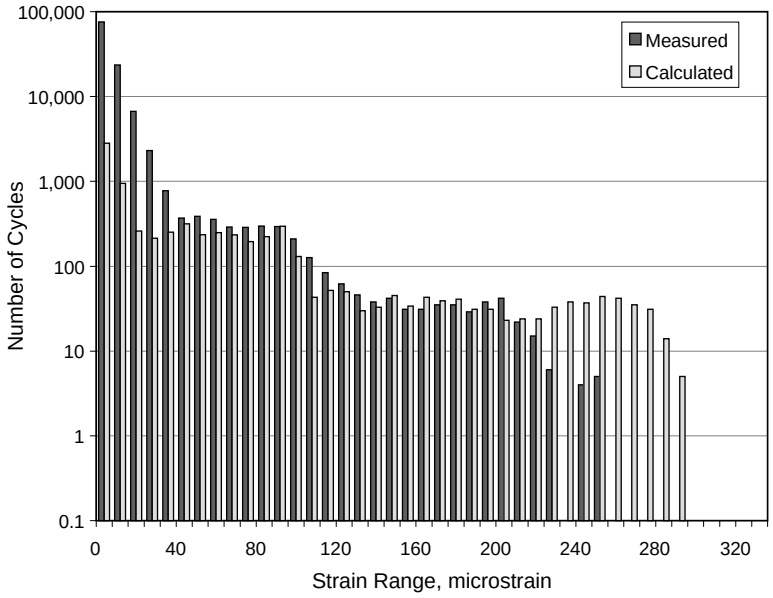

(a) Strain Gage A – West Girder

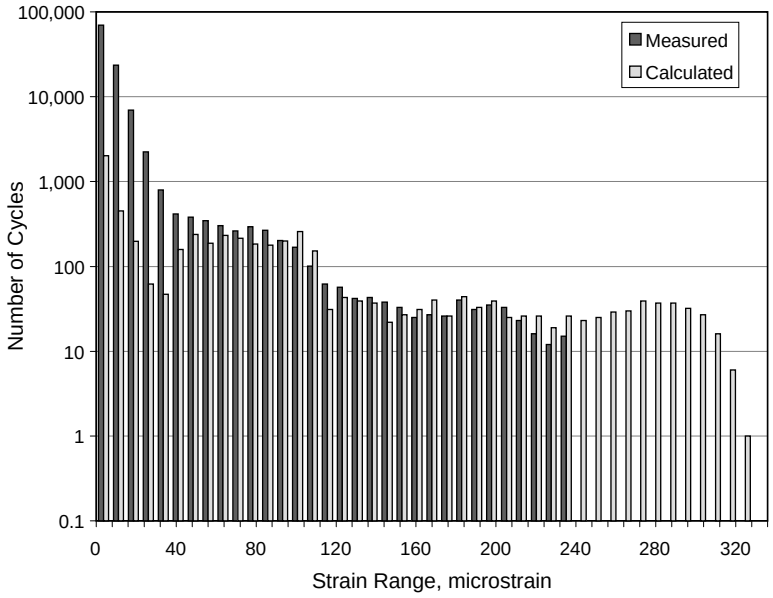

(b) Strain Gage C – West Girder

Figure 6.8 Comparison of Measured and Calculated Rainflow Cycles for Gages A and C on 28 January 2005

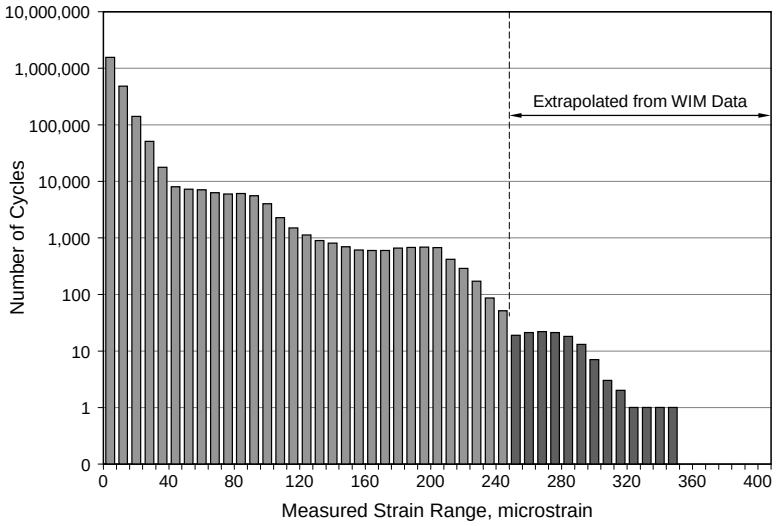

Figure 6.9 Strain Histogram for Strain Gage A with Large-Amplitude Cycles Extrapolated from Weigh-in-Motion Data

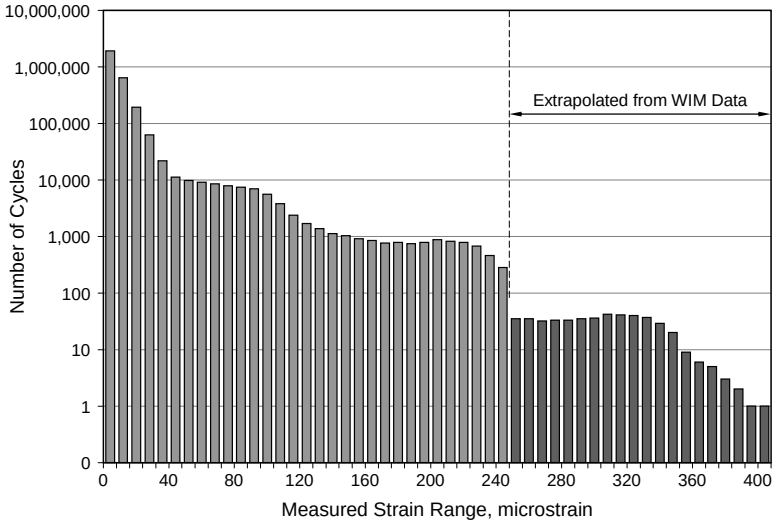

Figure 6.10 Strain Histogram for Strain Gage C with Large-Amplitude Cycles Extrapolated from Weigh-in-Motion Data

6.2.3 Limitations of Approach

The analyses described in this section provide a reasonable estimate of the range of strain cycles measured at various locations along the longitudinal girders of the Medina River Bridge due to vehicular loads. However, the calculations tended to underestimate the total number of strain cycles and over-estimate the number of large-amplitude strain cycles. As a result, the effective stress range for the calculated strain histogram is significantly larger than the effective stress range calculated from the measured data, which leads to a conservative estimate of the fatigue life. Therefore, this procedure should not be used to calculate the live-load response of the bridge at locations where the strain response

was not measured. However, the procedure provides a reasonable means of estimating the distribution of large-amplitude strain cycles when the selected bin size was too small.

6.3 REMAINING FATIGUE LIFE

The fatigue life of the longitudinal girders of the Medina River Bridge and 12th Street Exit Ramp at the location of each strain gage was calculated from the strain histograms using the procedures described in Sections 2.3 and 2.4. All rainflow cycles above the noise threshold were included in the calculations, and the large-amplitude cycles extracted from the weigh-in-motion data were used to evaluate the fatigue life of the west girder along the north anchor span of the Medina River Bridge.

The calculated effective stress ranges are summarized in Table 6.8 for the strain gages attached to the Medina River Bridge and in Table 6.9 for the strain gages attached to the 12th Street Exit Ramp. The results are also plotted in Figure 6.11. In all cases, the effective stress ranges for the 12th Street Exit Ramp were less than the effective stress ranges for the Medina River Bridge – even for the strain gage located nearest the pin at the end of the north cantilever span (strain gage E). The fatigue life of the girders, expressed in number of cycles, is also reported at the location of each strain gage in Table 6.8 and Table 6.9.

The maximum measured stress ranges are reported in Table 6.8 and Table 6.9 and plotted in Figure 6.12 and Figure 6.13. At three locations (strain gages D and E along the west girder of the Medina River Bridge and strain gage A along the west girder of the 12th Street Exit Ramp), the maximum stress range was less than the threshold stress for the corresponding fatigue detail category. Therefore, the fatigue life of the longitudinal girders was assumed to be infinite at these locations.

At the locations of the other strain gages, the maximum measured stress range exceeded the threshold stress, and the fatigue life of the longitudinal girders was considered to be finite. The fatigue life is reported in terms of years for assumed annual rates of traffic growth of 2% and 6%. The shortest fatigue life was calculated at the location of strain gage C on the Medina River Bridge – approximately 80 years. The calculated fatigue life exceeded 100 years at the locations of all instruments along the 12th Street Exit Ramp. Note that due to the age of the Medina River Bridge, the calculated fatigue life is not sensitive to the assumed value of annual traffic growth. The differences in the calculated fatigue life are much greater for the 12th Street Exit Ramp because this bridge has not been in service as long.

Table 6.8 Calculated Fatigue Life of Longitudinal Girders for Medina River Bridge

Location	N_{tot}	D	S_{re}	$S_{r,\max}$	$N^{\dagger}$	$m^{\ddagger}$	
						r = 0.02	r = 0.06
	(cycles)	(days)	(ksi)	(ksi)	(cycles)	(years)	(years)
A	2,294,315	21	0.97	12.0*	2.38×10^9	87	90
C	2,906,113	28	1.08	14.4*	1.76×10^9	77	86
D	1,493,359	28	0.54	6.0+	13.8×10^9	Infinite	Infinite
E	908,030	28	0.38	3.6+	40.4×10^9	Infinite	Infinite
H	1,657,652	28	0.81	8.7	4.11×10^9	139	110

† Fatigue detail category D.
* Maximum stress range estimated using weigh-in-motion data.
+ $S_{r,\max}$ < threshold stress.
‡ Remaining fatigue life = Calculated fatigue life (m) – years of service.

Table 6.9 Calculated Fatigue Life of Longitudinal Girders for 12th Street Exit Ramp

Location	N_{tot}	D	S_{re}	$S_{r,\max}$	$N^{\dagger}$	$m^{\ddagger}$	
						r = 0.02	r = 0.06
	(cycles)	(days)	(ksi)	(ksi)	(cycles)	(years)	(years)
A	3,830,192	27	0.18	4.4+	193×10^9	Infinite	Infinite
D	937,215	7	0.25	5.7	68.6×10^9	201	108
E	1,037,899	7	0.26	6.0	64.7×10^9	193	105
F	1,034,535	7	0.23	5.7	89.9×10^9	210	111

† Fatigue detail category E.
+ $S_{r,\max}$ < threshold stress.
‡ Remaining fatigue life = Calculated fatigue life (m) – years of service.

The calculated stress ranges for a single, HS-20 design vehicle crossing the bridge are also shown in Figure 6.12 and Figure 6.13. For strain gage locations A, C, and D along the west longitudinal girder of the Medina River Bridge, the maximum measured stress range was 10 to 20% larger than the calculated stress range for the design vehicle. The maximum measured stress range was approximately 50% larger than the calculated stress range at the location of strain gage H, along the east longitudinal girder. The largest difference between the measured and calculated response was observed near the pin at the end of the cantilever, location E. The measured maximum stress range at the location of strain gage E was less than the threshold stress for detail category D, so fatigue damage is not expected at this location. However, the larger than expected flexural stresses indicate that the pins at the ends of the suspended span may not be free to rotate and that the bridge is not statically determinant, as assumed.

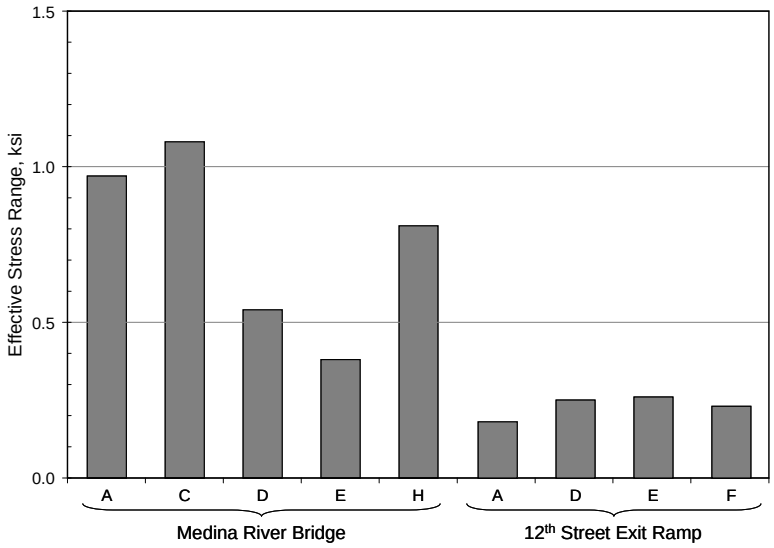

Figure 6.11 Comparison of Effective Stress Range at Locations of Strain Gages along Longitudinal Girders

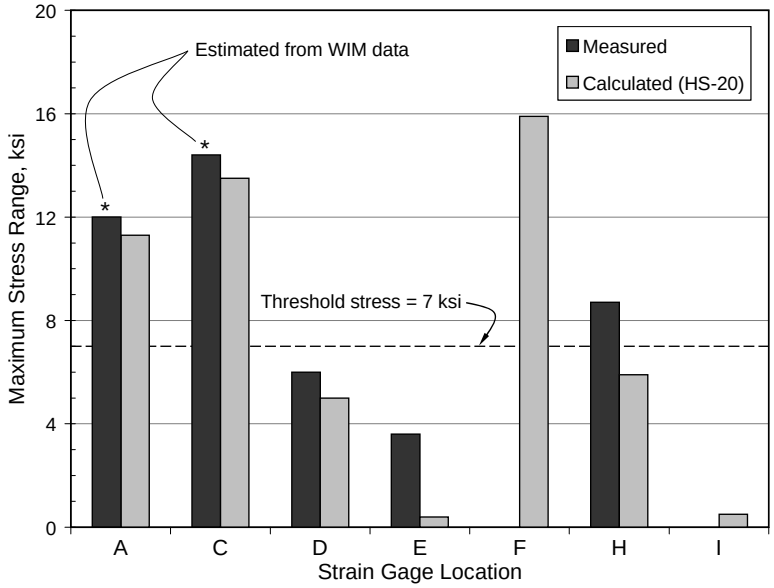

Figure 6.12 Distribution of Maximum Stress Ranges for Medina River Bridge

For the 12th Street Exit Ramp, the distribution of maximum measured stresses was not consistent with the calculated response. The largest stress range was expected at the location of strain gage A, yet the lowest maximum stress range and the lowest effective stress range were recorded at this location. This observation indicates that the analytical model discussed in Chapter 3 does not provide an accurate representation the load path for the bridge. This finding is not surprising, as large torsional moments were calculated at the north end of the west girder because the stiffness of the concrete deck was not included in the analytical model.

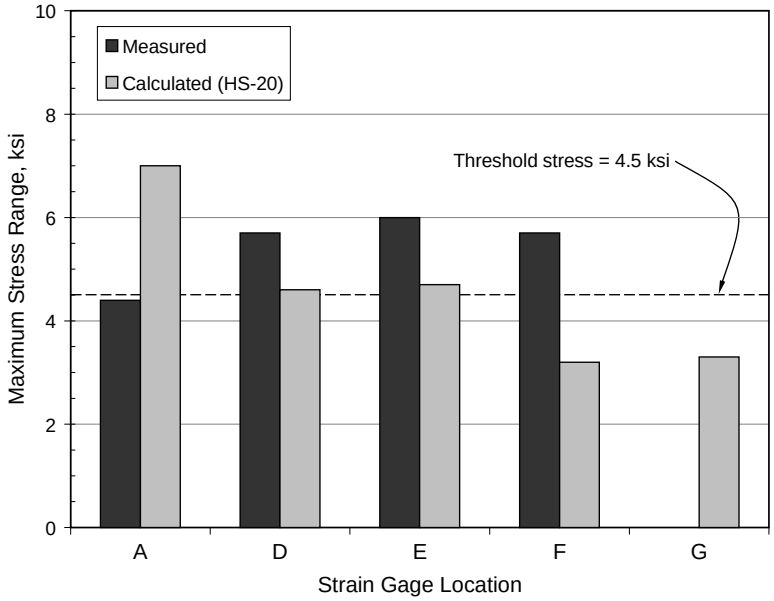

Figure 6.13 Distribution of Maximum Stress Ranges for 12th Street Exit Ramp

The Medina River Bridge was constructed in 1935, and had been in service 69 years in 2004 when the rainflow data were recorded. The critical calculated fatigue life was approximately 80 years (location C along the west girder), but the fatigue life was expected to be shorter at location F along the east girder. Unfortunately, rainflow data were not recorded at this location and it is not possible to estimate the fatigue life at this location from the available data.

The 12th Street Exit Ramp was constructed in 1971 and had been in service 33 years in 2004 when the rainflow data were recorded. The estimated fatigue life of this bridge ranges from 100 to 200 years, depending on the actual rate of traffic growth. Based on this information, the service life of the 12th Street Exit Ramp is not expected to be limited by fatigue damage.

6.4 SUMMARY

The analyses discussed in this chapter demonstrated that the calculated fatigue life of a steel girder bridge is sensitive to the parameters used to collect the rainflow cycles, and therefore, these parameters must be selected carefully. The calculated values of effective stress range were sensitive to the noise threshold for both bridges. As the minimum strain range used in the calculations increased, the effective stress range increased. However, the calculated fatigue life was mush less sensitive to this parameter. The calculated fatigue life of the Medina River Bridge was nearly independent of noise threshold, while the calculated fatigue life of the 12th Street Exit ramp was more sensitive to this parameter. A noise threshold of 5 $\mu\varepsilon$ is considered to be appropriate for most applications.

If too small a bin size is used to collect the rainflow data and the maximum strain range is not captured, the calculated fatigue life is over-estimated. If too large a bin size is used and the rainflow

counts are grouped in a few bins, the calculated fatigue life is conservative. These trends were observed for both bridges, but the calculated fatigue life of the 12th Street Exit Ramp was more sensitive to the choice of bin size. The increased sensitivity of the 12th Street Exit Ramp to the two parameters used to collect rainflow data is likely due to the relatively low traffic loads.

An analytical model was developed to use the measured weigh-in-motion data to calculate the rainflow response of the Medina River Bridge. In the analyses, one truck was assumed to cross the bridge at a time. The calculated distributions of strain cycles were sensitive to the percentage of trucks assumed to cross the bridge in each lane, but the maximum strain range was not sensitive to this parameter. When compared with measured strain data, the calculations provided a good approximation of the range of live-load strains, but the calculated number of strain cycles was considerably less than the number of measured cycles. In addition, the calculations tended to over-estimate the number of large-amplitude strain cycles. These differences were attributed to two primary causes: (1) cycles caused by the dynamic response of the bridge, electrical noise, and thermal changes were not captured in the analyses but were measured by the miniature data acquisition systems, and (2) when multiple trucks cross the bridge in the same lane, the maximum strain range is the same as if the trucks crossed the bridge separately, but the number of large-amplitude strain cycles is reduced. Therefore, it is not possible to recreate the measured rainflow response using the analytical model, but the model was used to distribute strains to larger bins when the maximum strain range was not captured in the measured data.

After adjusting the measured rainflow data to include large-amplitude strain cycles, the remaining fatigue life of the two bridges was calculated. The minimum fatigue life for the Medina River Bridge was calculated at the location of strain gage C on the west girder. Values ranged from 77 to 86 years, depending on the assumed annual rate of traffic growth. Because more trucks cross the bridge in the right lane than the left lane, the fatigue life of the east girder is expected to control for this bridge. In addition, the location of strain gage C did not correspond to the largest calculated stress range (Figure 4.2). Therefore, it is unlikely that the remaining fatigue life of the Medina River Bridge exceeds 10 years.

The minimum fatigue life for the 12th Street Exit Ramp was calculated at the location of strain gage E near the south end of the west girder. Due to the shorter service life and lower traffic loads crossing this bridge, the calculated fatigue life was much more sensitive to the assumed annual rate of traffic growth: 193 years for 2% growth and 105 years for 6% growth. The measured distribution of strains was not well represented by the analytical model discussed in Section 3.2, but it is unlikely that the service life of this bridge will be limited by fatigue.

CHAPTER 7: RECOMMENDED PROCEDURES FOR COLLECTING AND EVALUATING RAINFLOW DATA

The recommendations presented in this chapter represent the opinion of the research team, based on their experiences collecting rainflow data from the Medina River Bridge and 12th Street Exit Ramp. If the research team were charged with evaluating the same two bridges today, the layout of the strain gages, the parameters used to program the miniature data acquisition systems, and the procedures used to ensure that the rainflow data were collected successfully would be different. Therefore, the benefit of hindsight is reflected in these recommendations. Four topics are addressed in this chapter: preliminary analysis of the bridge (Section 7.1), instrumentation of the bridge (Section 7.2), collection of rainflow data (Section 7.3), and evaluation of rainflow data (Section 7.4).

7.1 PRELIMINARY ANALYSIS OF BRIDGE

Developing a structural model of the fracture critical bridge before embarking on an instrumentation program is of paramount importance. The analytical model is used to identify the locations that experience the largest variation of stress under live loads. If the strain gages are positioned at the wrong location along the bridge, the calculated fatigue life will over-estimate the actual fatigue life of the bridge.

For bridges with simple geometries, a line girder model should sufficient to identify the locations that experience the largest variations in moment under vehicle loads. The live load distribution factors defined in the AASHTO LRDF Design Specifications (2004) are considered to be appropriate for this analysis.

For bridges with skewed abutments, a more detailed structural model is required. The stiffness provided by the bridge deck must be included in the structural model, even though this increases the level of complexity of the model significantly.

It is important to capture the maximum strain range during the rainflow collection period. Therefore, it is recommended that the HS-20 design vehicle be used to evaluate the live-load response of the each longitudinal girder. The live-load response should be calculated for a single design vehicle in each lane. As shown in Figure 6.11, 1.5 times the calculated stress ranges using the HS-20 vehicle provided a reasonable approximation of the maximum measured stress ranges for both bridges.

The bridge deck should be assumed to be composite with the girders when calculating the live-load stress range from the moments in each girder, unless the bridge has a very unusual geometry, such as

the 12th Street Exit Ramp. Using the specified compressive strength of the concrete and the effective flange width defined in the AASHTO LRFD Design Specifications (2004) are reasonable approximations.

The locations that experience the largest moment ranges due to live load are often not the locations that experience the largest stress ranges. Particular attention should be paid to locations where the geometry of the cross section of the longitudinal girders changes, as the largest live-load stress ranges are expected at these locations. The locations with the highest calculated stress ranges should be selected for instrumentation. It is recommended that all girders be instrumented at these locations. Depending on the configuration of the bridge, it may also be appropriate to select instrument locations where the live-load moments are expected to be zero, such as hinges and pinned supports. The rainflow data from these locations will provide direct evidence that the boundary conditions are behaving as assumed.

The final number of locations selected for instrumentation will depend on the geometry of the bridge under consideration and the calculated live-load stress distribution. Recommended instrument locations for the Medina River Bridge are shown in Figure 7.1. A total of nine locations were selected. Six correspond to locations where the thickness of the cover plates changes (S1, S2, S3, N1, N2, and N3), two correspond to locations where the live-load moment is expected to be zero (C1 and C3), and one corresponds to the location of maximum live-load moment (C2). Strain gages should be attached to both longitudinal girders at each location and in all cases, the strain gages should be attached to the bottom flange with the thinner cover plate.

Ten recommended instrument locations for the 12th Street Exit Ramp are shown in Figure 7.2. Six are positioned along the west girder and four are positioned along the east girder. All correspond to locations where the thickness of the top and bottom flanges changed. Strain gages should be attached to the bottom flange of each longitudinal girder, and in all cases, the strain gages should be attached to thinner flange.

Not all the instruments shown in Figure 7.1 and Figure 7.2 are of the same relative importance. Strain gages at locations with the highest calculated stress ranges are critical for evaluating the fatigue life of the bridge, while the other locations are used to evaluate the distribution of live-load stresses and the boundary conditions. Locations S1 and N3 on the Medina River Bridge and locations W2, W5, W6, and E3 on the 12th Street Exit Ramp are considered to be more important than the other locations. If the number of data acquisition systems is limited, strain gages should be placed at these locations first. Therefore, a minimum of four strain gages should be used to evaluate the fatigue life of each bridge.

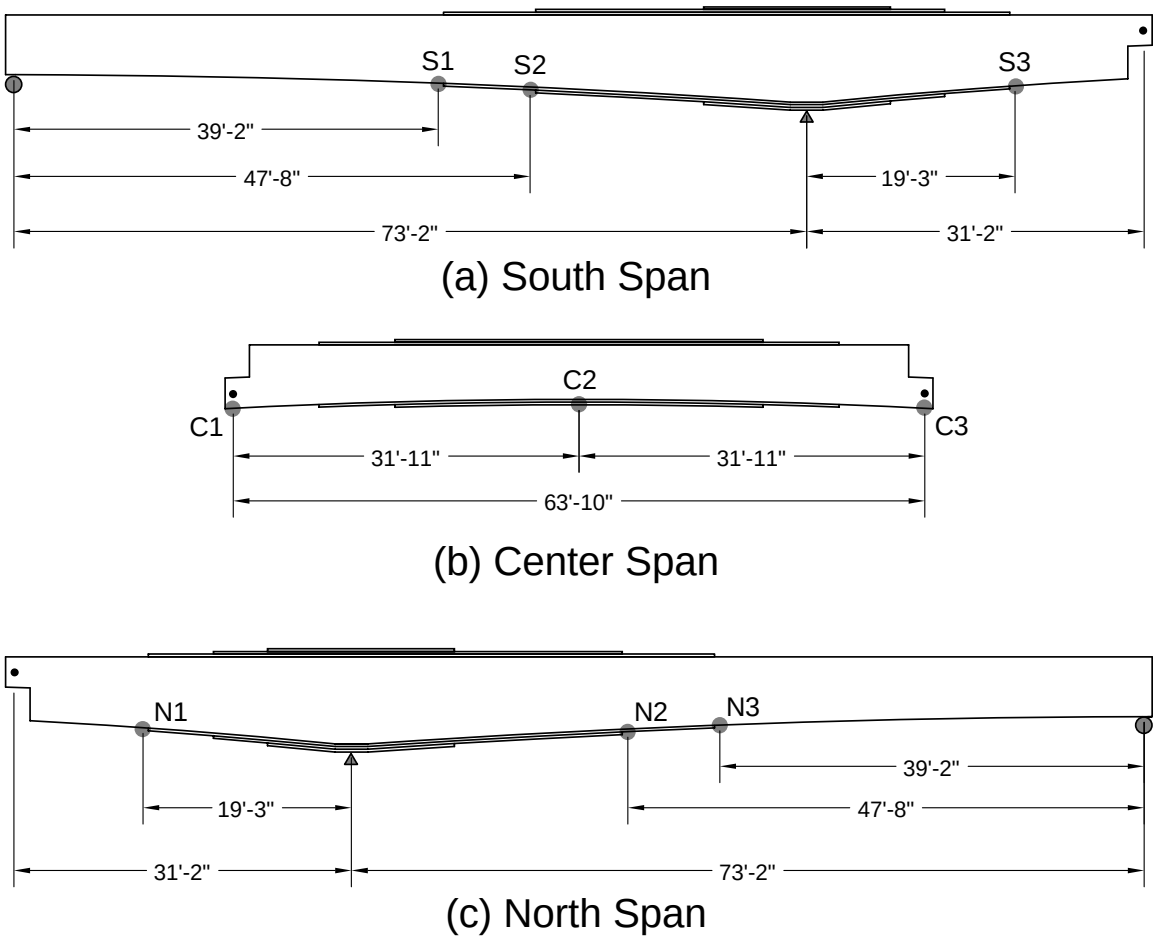

Figure 7.1 Proposed Instrument Locations for Medina River Bridge

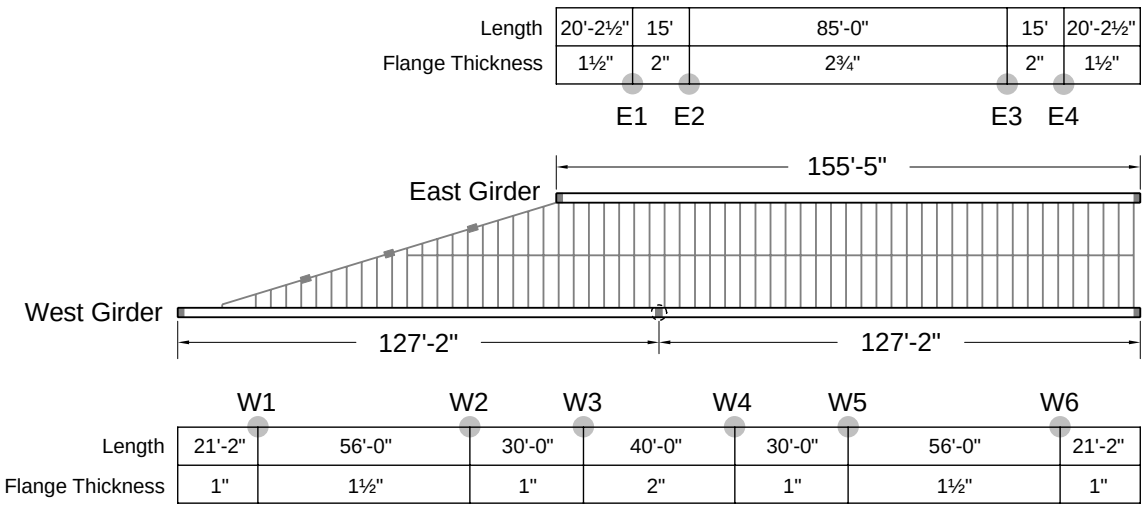

Figure 7.2 Proposed Instrument Locations for 12th Street Exit Ramp

7.2 INSTRUMENTATION

As discussed in Chapters 4 and 5, several of the miniature data acquisition systems did not function as intended when deployed in the field. Therefore, it is recommended that more rigorous testing of each unit be conducted before each bridge is instrumented. As discussed in section 4.3.1, testing the unit under thermal cycles is sufficient to identify data acquisition systems that are not functioning properly – such as unit 1005. Acquiring data in the rainflow only mode for three days should be sufficient for this purpose.

The research team recommends the use of waterproof strain gages, such as WFLA-6-11 manufactured by Tokyo Sokki Kenkyujo, Inc. and distributed by Texas Measurements, Inc., for future field tests. Because these gages are encapsulated in epoxy, they are more robust and easier to install in the field than traditional foil strain gages. Three-wire gages are recommended for all applications.

If possible, it is recommended that duplicate strain gages be positioned at the locations of highest calculated live-load stresses. Duplicate gages will provide redundancy in the event of improper installation of strain gages or battery failure during the rainflow collection period.

It is also recommended that the strain ranges attributed to thermal cycles be monitored during each field test. A steel bar should be instrumented using the same type of strain gages used to monitor the response of the bridge. The bar should be supported such that live loads on the bridge do not induce stresses.

7.3 COLLECTION OF RAINFLOW DATA

A rainflow collection period of three to four weeks is considered to be sufficient to evaluate the fatigue life of a fracture critical bridge. As discussed in Chapter 5, weekly patterns are expected in the traffic data and the collection period should be long enough to capture these trends.

During installation of the strain gages and data acquisition units, raw and rainflow data should be collected from each unit before the start of the rainflow collection period. It is important to capture at least one truck crossing the bridge using each gage to ensure that the gages have been installed properly. If the traffic volume crossing the bridge is low, it may be necessary to use a TxDOT vehicle for this purpose. Note that the raw data are not sufficient to select the bin sizes for the data acquisition systems.

The bin size for each data acquisition unit should be sufficient to capture approximately 1.5 times the maximum stress range calculated for the HS-20 design vehicle. Therefore, this key parameter should be determined before collecting data in the field. Calculated stress ranges and recommended bin sizes for each of the proposed instrument locations are given in Table 7.1. It is recommended to use the same bin size for strain gages at the same location on the east and west girders of the Medina River Bridge, and the minimum recommended bin size is 10 $\mu\varepsilon$.

Table 7.1 Recommended Bin Sizes for Proposed Instrument Locations

Bridge	Location	Relative Priority*	Calculated Response to HS-20 Design Vehicle		Recommended Bin Size ($\mu\varepsilon$)
			Stress Range (ksi)	Strain Range ($\mu\varepsilon$)	
Medina River Bridge+	S1	H	17.4	580	25
	S2	M	11.4	380	20
	S3	M	5.9	200	10
	C1	M	0.0	0	10
	C2	M	5.3	180	10
	C3	M	0.0	0	10
	N1	M	5.9	200	10
	N2	M	11.4	380	20
	N3	H	17.4	580	25
12th Street Exit Ramp	W1	M	3.4	110	10
	W2	H	7.0	230	10
	W3	M	5.2	170	10
	W4	M	4.3	140	10
	W5	H	6.1	200	10
	W6	H	4.7	160	10
	E1	M	1.7	60	10
	E2	M	2.4	80	10
	E3	H	3.3	110	10
	E4	M	2.7	90	10

* H = High priority, M = Medium priority
+ Two strain gages at each location: one on east girder and one on west girder

Interpretation of the measured rainflow data is easier if all the units are programmed using the same noise threshold. A noise threshold of 5 $\mu\varepsilon$ is considered to be adequate for most applications. Selecting an acquisition period of 23 hr, 59 min and a time between acquisition periods of 1 min is recommended.

Because the initial structural model of the bridge may not capture all the key aspects of the actual response of the bridge, it is recommended that rainflow data be collected for 12 to 24 hours before beginning the 3 to 4-week rainflow collection period. The data collected during this short period should be sufficient to ensure that the selected bin size is appropriate for each gage. If the maximum recorded strain range exceeds the 24th bin, the bin size should be increased.

7.4 EVALUATION OF RAINFLOW DATA

After downloading the rainflow data from each miniature data acquisition system at the conclusion of the collection period, careful evaluation of the data is required. As a first step, corrections should be made for the large-amplitude thermal cycles, as discussed in Section 4.3.1.

As discussed in Chapters 4 and 5, it is not possible to distinguish the unreliable data from the reliable data using only the final strain histograms. Evaluation of the number of cycles recorded during each 24-hr acquisition period proved to be an easy means of identifying inconsistencies in the data. Sudden increases in the number of strain cycles were observed immediately before a battery failed, and data from these acquisition periods should be discarded.

After ensuring the reliability of the rainflow data, the maximum and effective stress ranges should be calculated for each strain gage using the procedures discussed in Section 2.3. The corresponding fatigue life of the bridge can then be calculated for the expected level of annual traffic growth, as discussed in Section 2.4.

CHAPTER 8: SUMMARY AND CONCLUSIONS

The recent collapse of the I-35W bridge across the Mississippi River in Minneapolis highlighted the consequences of failure of structural members in a fracture critical bridge. This report describes a method for collecting quantitative data under normal service loads that can be used to estimate the remaining fatigue life of a steel bridge. It should be noted that careful evaluation of the bridge is required to select the instrument locations. Because the data used to evaluate the fatigue life are localized, if the most highly-stressed regions of the bridge are not instrumented, the estimated fatigue life will not be an accurate reflection of the service life of the bridge.

The primary advantage of the proposed method is that the most vulnerable fracture critical bridges can be identified quantitatively based on actual traffic patterns. If necessary, the planning and construction of a replacement bridge can be completed before the end of the useful service life of the existing bridge.

8.1 SUMMARY

The research team instrumented two fracture critical bridges as part of this project: the Medina River Bridge on northbound I-35, south of San Antonio, and the exit ramp from southbound I-35 to 12th Street in downtown Austin. Both bridges have two longitudinal girders, but otherwise the structural systems are very different.

The Medina River Bridge was constructed in 1935. The built-up longitudinal girders are statically determinant and all connections are riveted. An average of 4,000 trucks travel northbound on this section of I-35 each day. The 12th Street Exit Ramp was constructed in 1971. The longitudinal box girders are welded and the transverse floor beams connect to the girders near the bottom flange. As a result, no direct connection exists between the concrete bridge deck and the longitudinal girders. The north abutment of the bridge is skewed more than 60°, but the south abutment is perpendicular to the longitudinal girders. Truck traffic across this bridge is very low.

Each bridge was instrumented with several strain gages and rainflow data were collected using battery-powered, single-channel, miniature, data acquisition systems. The response of each bridge was monitored during two collection periods. The data acquisition systems were not as robust in the field as anticipated from the earlier laboratory tests. Several of the units failed to collect rainflow data and others malfunctioned during the collection periods. However, relatively simple procedures were developed to distinguish the reliable data from the unreliable data.

The measured rainflow response included strain cycles from three sources: electrical noise, temperature changes, and live load. A noise threshold is specified when collecting data to minimize the number of cycles due to electrical noise that are counted and procedures were developed to identify large-amplitude strain cycles caused by thermal changes. Although it is not possible to remove all cycles attributed to electrical noise and temperature changes from the measured rainflow response, the calculated fatigue life of the bridges was not sensitive to these low-amplitude cycles.

Weigh-in-motion data were available from Station 516, which is seven miles south of the Medina River Bridge on I-35. Analyses of the bridge using the measured trucks loads were successful in reproducing the ranges of live-load strains measured by the data acquisition systems, but the total number of loading cycles was underestimated and the number of large-amplitude cycles was overestimated. Therefore, the fatigue lives calculated using only the weigh-in-motion data were significantly shorter than those calculated using the measured rainflow response. The results of this investigation demonstrate that it is not possible to reproduce the measured strain histograms from the measured traffic data. If the service life of a bridge is likely to be limited by fatigue, measuring the rainflow response directly is the only reliable means of collecting the data needed to calculate the remaining fatigue life.

The measured rainflow response indicated that that the effective stress ranges induced in the 12th Street Exit Ramp by vehicular traffic were much lower than those induced in the Medina River Bridge and that the Medina River Bridge is more vulnerable to fatigue damage than the 12th Street Exit Ramp. While this conclusion is expected given the ages of the bridges and the level of truck traffic, without the measured rainflow data, the differences in fatigue life would be impossible to quantify.

8.2 CONCLUSIONS

The remaining fatigue life of the Medina River Bridge is likely to be less than 10 years, while the service life of the 12th Street Exit Ramp is not likely to be limited by fatigue. Federal requirements necessitate a thorough inspection of all fracture critical bridges at least every two years. No distinction is made based on the level of traffic or the remaining service life. By measuring the rainflow response of fracture critical bridges directly, the Texas Department of Transportation will be able to identify the most vulnerable bridges using quantitative data and establish priorities for inspection and replacement of bridges that are approaching the end of their service life. The information obtained using the recommended methodologies will assist the Department in ensuring the safety of bridges throughout the State of Texas.

APPENDIX A: OPERATION OF MICROSAFE DATA ACQUISITION UNITS

Each MicroSAFE unit is a miniature data acquisition system that measures and records strain data. As discussed in Chapter 2, the user may collect raw strain data or rainflow data. The user communicates with the MicroSAFE units using a Graphical User Interface (GUI), which allows for convenient unit programming, viewing of data, and data retrieval. The GUI can be installed on any computer and wiring is completed using a standard serial or USB port.

Key aspects of operation of the MicroSAFE units are summarized in this appendix. Additional information is available in the MicroSAFE User's Guide (Holman, 2003).

A.1 SYSTEM DESCRIPTION

Each individual MicroSAFE unit consists of three components: the MicroSAFE processor, a battery pack, and a communications cable. The processor records the strain history, converts the analog signal from the strain gage to a digital signal, and processes the data using the rainflow counting algorithm. The processor is connected to the battery pack.

The battery pack has two significant functions: it provides power to the MicroSAFE processor and the communications cable between the PC and the processor is connected to the battery pack. The four-pin cable between the battery and the processor provides two pins for communication and two pins for power to the processor. The battery has an expected life of 45 days when recording rainflow data.

The communications cable is a three-pin connector which connects the battery pack to the serial port of a computer. A converter can also be used to convert the cable from a serial port to a USB. The three pins are used for one ground pin and two communication pins (Holman, 2003).

A.2 GRAPHICAL USER INTERFACE

The Graphical User Interface (GUI) is the software used on the PC to communicate with the MicroSAFE units. The MicroSAFE system has four operational modes: Idle, Active Acquisition, Waiting, and Auto-Zeroing. The system is in Idle mode before it has been programmed to collect data, after the data collection period has ended, or after the collection period has been cancelled. The Active-Acquisition mode refers to the time when the unit is acquiring strain data. Between acquisition periods, the unit enters the Waiting mode. There are two types of Waiting modes, Waiting for First Period and Waiting between Periods. Waiting for First Period occurs when the unit has been programmed but the collection period has not begun. If data have been collected during one period, and the unit is waiting to

begin collecting data during the next period, the mode will be Waiting between Periods. The last possible mode is the Auto-Zero function which occurs eight seconds before the start of each acquisition period and centers the raw strain data about the initial value. As common sense would expect, the value of the zero does not affect the Rainflow Analysis.

The main program window of the GUI has seven buttons, six of which are shown in Figure A.1. The two buttons in the bottom left corner of the window (Comm # and About) are related to communication with the computer. Additional information on these buttons is provided in the MicroSAFE User's Manual (Holman, 2003). The other five buttons are discussed in more detail below.

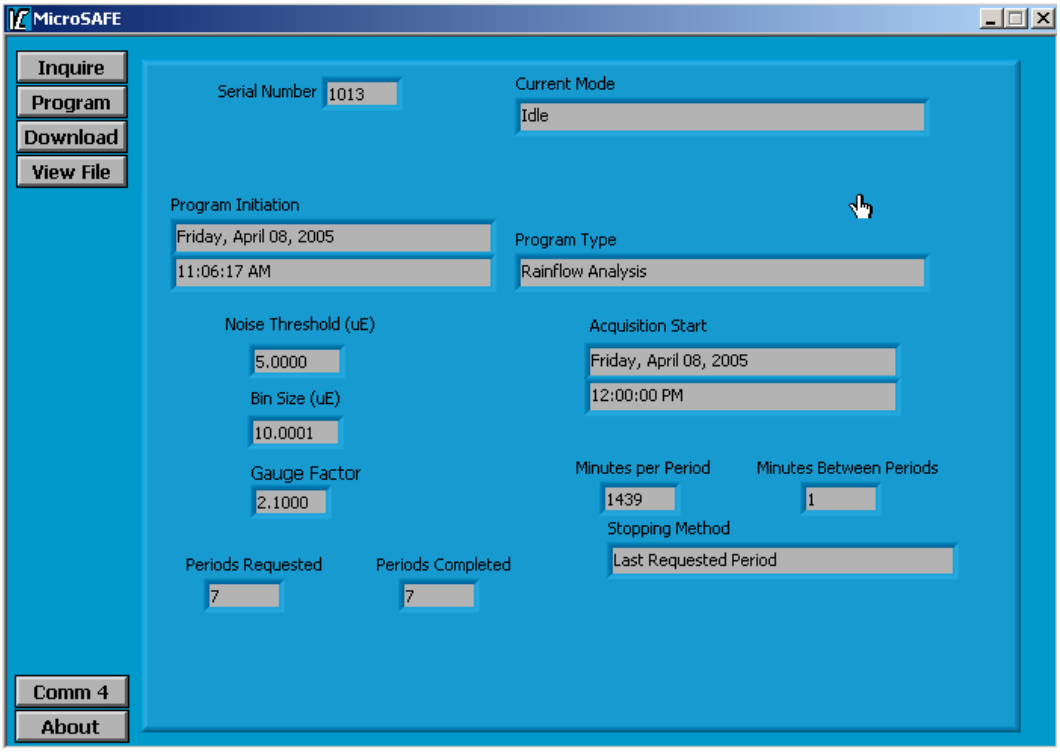

Figure A.1: Main Program Window of GUI

The top left button, Inquire, serves the simple, but useful, function of refreshing the display fields in this window. The Program button allows the user to set up the next data acquisition periods. The Download button copies the data from the MicroSAFE unit to the PC. This option is only available when the unit is in Idle mode or after the first period in a multiple-period acquisition has completed. The View File button allows the user to view a histogram of the Rainflow data files in the MicroSAFE window. The Cancel Acquisition button is only available after the unit has been programmed for Rainflow

Analysis Only or Record Raw Data Only, and can be used to terminate data acquisition during an acquisition period.

During Active Acquisition, the main program window provides feedback about the status of the unit. These fields include a displaying of the unit's serial number, the current mode of the unit, and the number of minutes until completion of the period. Other fields display information about how the unit was programmed including when the unit was last programmed, the type of acquisition being performed (Rainflow Only, Rainflow and Raw, or Raw Only), and the noise threshold selected. The noise threshold is a user-selected value that separates noise from data. Rainflow cycles below this threshold are not counted in the first bin, but are counted separately.

A.3 PROGRAMMING THE MICROSAFE UNITS

Programming of the MicroSAFE units depends on the information that is known about the structure to be instrumented. During programming, the user must specify the number and length of acquisition periods, the bin size, and the noise threshold. The next few paragraphs will discuss the program parameters that can be changed in program setup window (Figure A.2).

The top pull-down menu allows the user to select of the type of data acquired. The three possible options are Rainflow Analysis Only, Rainflow Analysis with Raw Data, and Record Raw Data Only.

When collecting rainflow data, the user must specify three parameters: the gage factor, the bin size, and the noise threshold. Gage factors depend on the type of strain gage, and are specified by the manufacturers. Guidelines for selecting the bin size and noise threshold are presented in Chapter 7. A total of 32 bins are available for rainflow analysis. The noise threshold must always be less than the bin size.

When collecting rainflow data only, the user must also specify the number of data collection periods (Acquisition Periods in Figure A.3). The number of acquisition periods may range from 1 to 512. When collecting raw data only or combined raw and rainflow data, only one period can be defined, and the user is not given the option of specifying the number of acquisition periods (Figure A.2).

The Time Per Acquisition Period establishes the time that data are collected during each acquisition period. Permissible values depend on the acquisition mode and the processor memory. For raw data collection, permissible times vary from 1 to 33 min. For combined rainflow and raw data collection, permissible times vary from 1 to 59 min. When only rainflow data are being collected, permissible times vary from 1 min to 23 hr 59 min. The Time Between Acquisition Periods box applies only to Rainflow Analysis Only, and it must be at least one minute.

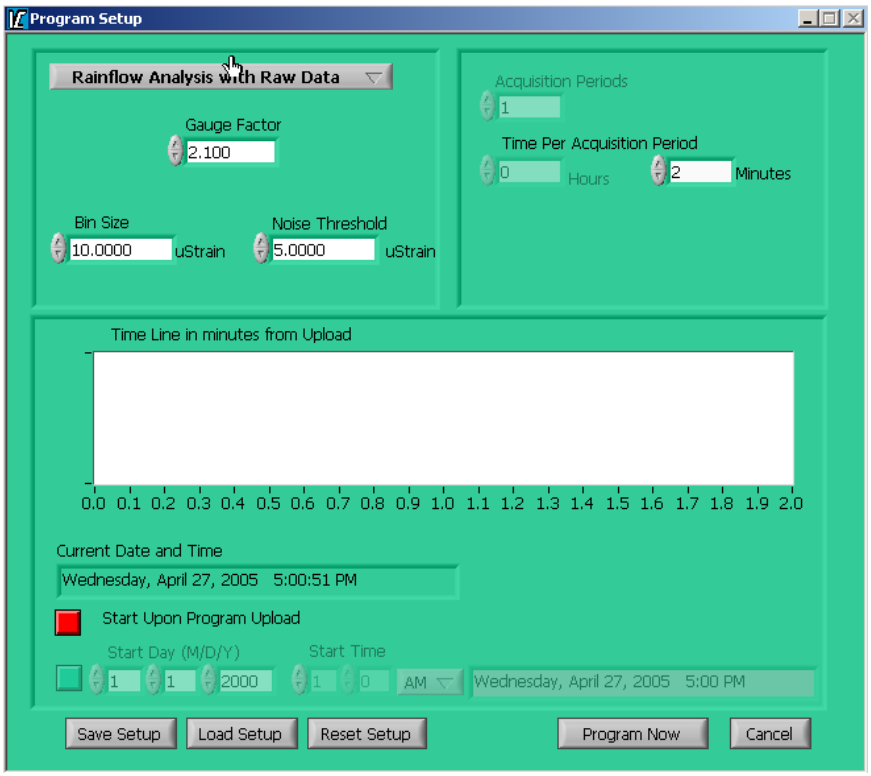

Figure A.2: Program Setup Window for Acquisition of Raw and Rainflow Data

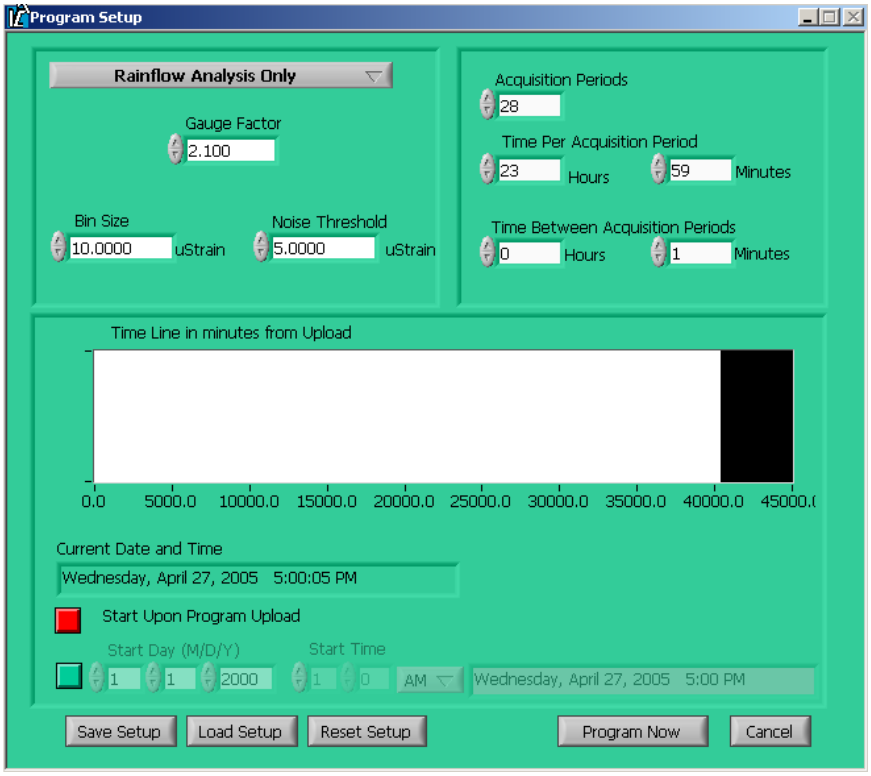

Figure A.3: Program Setup Window for Acquisition of Rainflow Data Only

When the units were installed in the field, the most common settings for Rainflow Analysis Only were for an acquisition period of 23 hr and 59 min and a time between periods of 1 min. With this configuration, each acquisition period is 24 hr, and the data from each 24-hr period are stored in separate files.

The Start Preference option gives a choice between program startup times. The program can be started upon upload, or at a user-specified time. Although starting upon program upload is useful for testing the units and in applications with a single strain gage, multiple units were used simultaneously in this project and it was convenient for each unit to have the same acquisition period. For this reason, choosing the same start time for all units is recommended. In situations where the rainflow data are compared with other types of data – such as weigh-in-motion – it is recommended to set all acquisition period lengths and times to correspond to the lengths and times of the other data.

A.4 DOWNLOADING AND VIEWING MICROSAFE DATA

Downloading and viewing of MicroSAFE data are essential in the process of using the MicroSAFE devices. Downloading can be done in either the Idle mode or in the Active Acquisition mode if at least one period has been completed. If the Download button is available, pressing it and selecting the desired location on the hard drive will remove the data from the MicroSAFE device and place the data in the location specified.

The data can be viewed using the GUI by now pressing the View File button. The raw data from a sample period is shown in Figure A.4 and the rainflow data from that same period is shown in Figure A.5. This is a quick way of checking that the data were collected successfully. There are many viewing options within this window, but for evaluation analysis of the raw strain or rainflow data, exporting the information to Microsoft Excel is recommended.

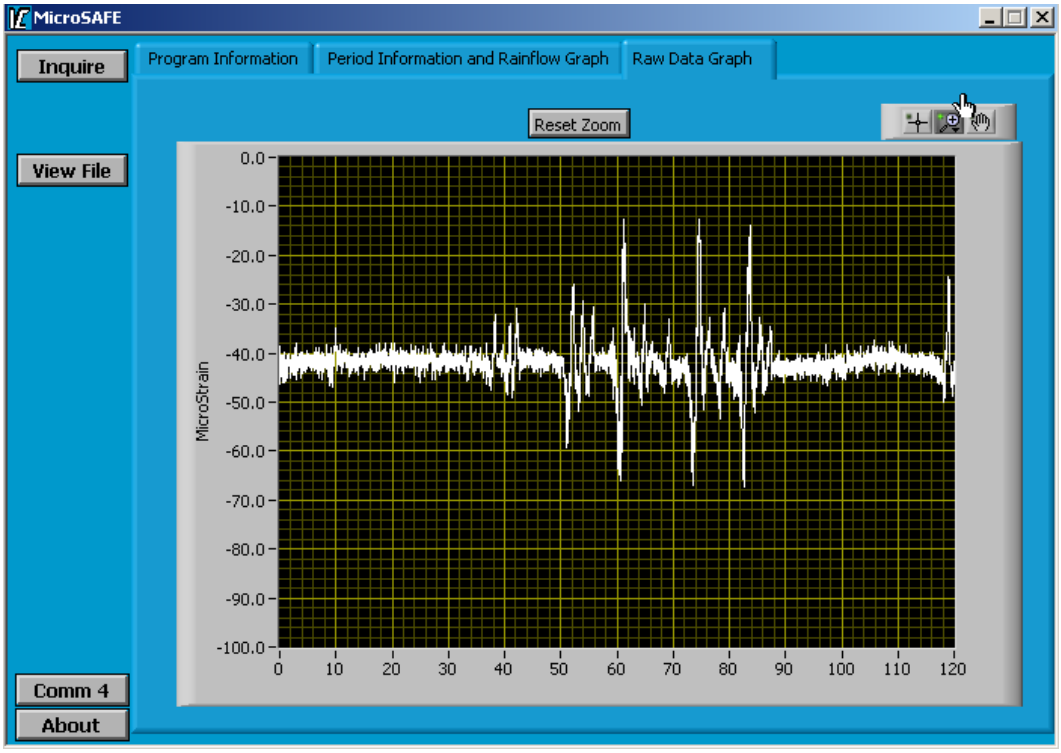

Figure A.4: Viewing a Raw Data File with the MicroSAFE GUI

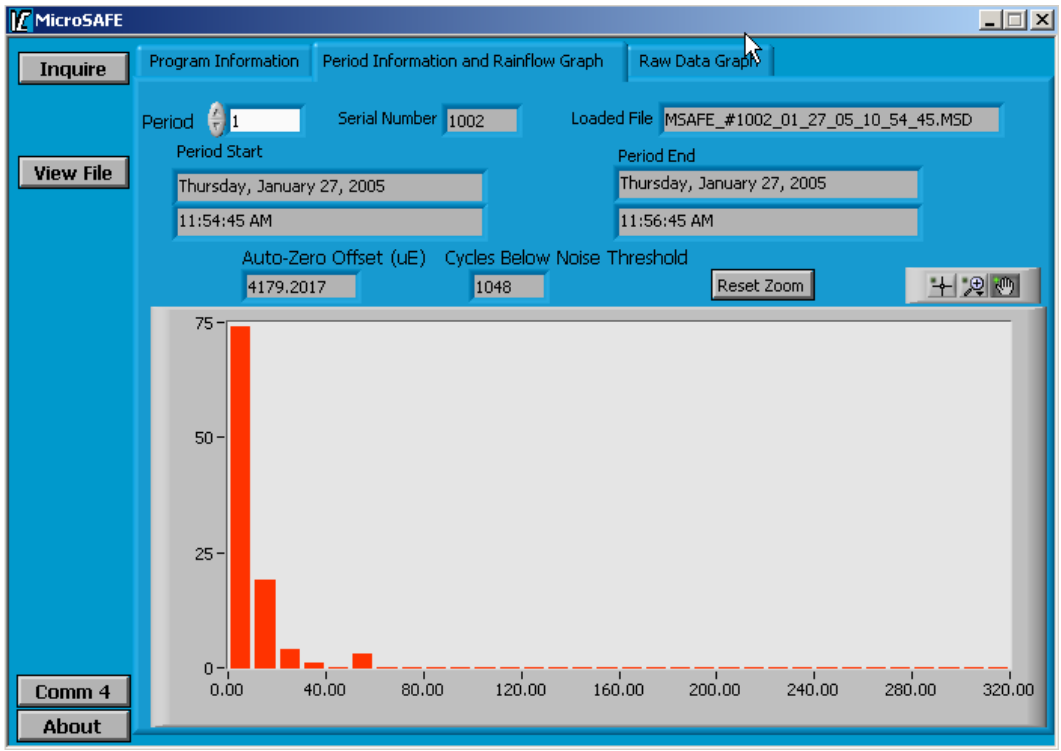

Figure A.5: Viewing a Rainflow Data File with MicroSAFE

APPENDIX B: COMPLETE TRUCK INVENTORY FROM WEIGH-IN-MOTION STATION

A total of 50 days of data from weigh-in-motion Station 516 on I-35 were provided to the research team for evaluation during this project. The data were collected between July 2004 and February 2005. Nearly 200,000 trucks passed the weigh-in-motion station in the northbound direction during this period and 60 different types of trucks were identified. The complete listing of trucks is summarized in Table B.1. The first column in Table B.1 is the designation assigned to the truck configuration by the weigh-in-motion station. This six-digit code is defined in Table B.2.

Table B.1 Truck Inventory from Weigh-in-Motion Station 516

Truck ID	No. of Axles	Total Number Trucks	Truck Designation	Effective Gross Vehicle Weight (kip)	Average Trucks per Day	Average Number of Trucks per Day	Percent of Total
220000	2	65102	T2-1	10.3	1302	1,327	33.3%
090000	2	647	T2-2	7.5	13		
190200	2	603	T2-3	20.4	12		
230000	3	7168	T3-1	30.4	143	252	6.3%
190300	3	2720	T3-2	37.6	54		
200900	3	1623	T3-3	19.7	32		
421000	3	1064	T3-4	19.6	21		
321000	3	116	T3-5	24.5	2		
322000	4	5576	T4-1	24.9	112	160	4.0%
431000	4	1558	T4-2	36.1	31		
331000	4	736	T4-3	32.3	15		
422000	4	97	T4-4	18.0	2		
240000	4	16	T4-5	41.7	0.3		
332000	5	98433	T5-1	56.6	1969	2,216	55.6%
337000	5	8986	T5-2	61.7	180		
521200	5	2934	T5-3	54.5	59		
323000	5	316	T5-4	22.5	6		
522100	5	61	T5-5	54.4	1.2		
423000	5	47	T5-6	59.6	0.9		
441000	5	4	T5-7	40.8	0.1		
341000	5	1	T5-8	17.5	0		
432000	5	1	T5-9	22.5	0		

Table B.1 (cont). Truck Inventory from Weigh-in-Motion Station 516

Truck ID	No. of Axles	Total Number Trucks	Truck Designation	Effective Gross Vehicle Weight (kip)	Average Trucks per Day	Average Number of Trucks per Day	Percent of Total
531200	6	594	T6-1	57.3	12	25	0.6%
333000	6	515	T6-2	60.4	10		
632100	6	167	T6-3	59.9	3		
532100	6	13	T6-4	55.5	0.3		
522200	6	2	T6-5	35.2	0		
622200	6	2	T6-6	38.2	0		
623100	6	2	T6-7	49.5	0		
523100	6	1	T6-8	47.5	0		
533100	7	33	T7-1	68.7	0.7	1	0.0%
532200	7	8	T7-2	60.0	0.2		
343000	7	2	T7-3	90.0	0		
531300	7	1	T7-4	37.5	0		
721220	7	1	T7-5	42.5	0		
721320	8	33	T8-1	45.4	0.7	2	0.1%
523300	8	31	T8-2	39.0	0.6		
543100	8	13	T8-3	99.1	0.2		
541300	8	11	T8-4	74.9	0.2		
522400	8	6	T8-5	70.0	0.1		
444000	8	5	T8-6	95.7	0.1		
532300	8	5	T8-7	38.8	0.1		
722310	8	4	T8-8	40.9	0.1		
533200	8	3	T8-9	34.3	0.1		
723210	8	3	T8-10	38.7	0.1		
722220	8	2	T8-11	40.2	0		
721230	8	1	T8-12	42.5	0		
721410	8	1	T8-13	27.5	0		
731220	8	1	T8-14	47.5	0		
723310	9	14	T9-1	60.7	0.3	1	0.0%
721240	9	12	T9-2	47.5	0.2		
523400	9	4	T9-3	50.4	0.1		
533300	9	4	T9-4	77.7	0.1		
532400	9	3	T9-5	119.3	0.1		
721330	9	3	T9-6	57.1	0.1		
542300	9	2	T9-7	110.6	0		
722230	9	1	T9-8	37.5	0		
722320	9	1	T9-9	47.5	0		
723220	9	1	T9-10	37.5	0		
732310	9	1	T9-11	36.5	0		
Total		**199,315**			**3,986**		

Table B.2 Six-Digit Identification Code Used to Classify Trucks

<table>
<tr><td rowspan="2">Vehicle Type</td><td colspan="6">Character in Six-Digit Identification Code for Vehicles</td></tr>
<tr><td>1st</td><td>2nd</td><td>3rd</td><td>4th</td><td>5th</td><td>6th</td></tr>
<tr><td>Personal passenger vehicles</td><td>0</td><td>9</td><td>0</td><td>See Note A</td><td>0</td><td>0</td></tr>
<tr><td>Buses, motor homes</td><td>1</td><td>9</td><td>0</td><td>See Note B</td><td>0</td><td>0</td></tr>
<tr><td>Single unit trucks or tractors</td><td>2</td><td>See Note C</td><td>0</td><td>See Note A</td><td>0</td><td>0</td></tr>
<tr><td>Tractor and semi trailer</td><td>3</td><td rowspan="5">Total number of axles on power unit</td><td rowspan="5">See Note D</td><td>0</td><td>0</td><td>0</td></tr>
<tr><td>Heavy trucks, dump trucks</td><td>4</td><td>0</td><td>0</td><td>0</td></tr>
<tr><td>Tractor, semi, and full trailer</td><td>5</td><td rowspan="3">See Note D</td><td>0</td><td>0</td></tr>
<tr><td>Truck and two full trailers</td><td>6</td><td>0</td><td>0</td></tr>
<tr><td>Tractor, semi, and two full trailers</td><td>7</td><td>See Note D</td><td>0</td></tr>
</table>

Table B.3 Notes Used in Table B.2

Character	Note A Type of Trailer	Note B Axle Arrangement	Note C Type of Truck	Note D Type of Trailer
0	None	Not determined	Panel/pickup	Single axle
1	Camp	Two axles, four tires	Heavy, two axles, four tires	Two axles
2	Travel or mobile	Two axles, six tires	Two axles, six tires	Three axles
3	Cargo/livestock	Three axles	Three axles	Four axles
4	Boat	Four or more axles	Four axles	Five axles
5	Towed equipment	—	Five axles	Six axles
6	Towed auto	—	Six axles	Two axles, with axles in spread tandem configuration
7	Towed truck	—	Seven axles	Three axles, including a spread tandem
8	Saddle mount	—	Eight or more axles	Four axles, including a spread tandem
9	Not determined	—	—	—

References

American Association of State Highway and Transportation Officials (2004). *LRFD Bridge Design Specifications*, Third Edition with 2005 Interim Revisions. Washington, D.C.

American Society for Testing and Materials (1997). ASTM E 1049, "*Standard Practices for Cycle Counting in Fatigue Analysis*," West Conshohocken, PA.

Bilich, C.T. and Wood, S.L. (2004). "Evaluation of Two Monitoring Systems for Significant Bridges in Texas," Center for Transportation Research, *Research Report 0-4096-1*, University of Texas, Austin, TX.

CSI (2006). *SAP2000*, Integrated Software for Structural Analysis and Design, Berkeley, CA.

Dean, P.K. (2005). "Improving the Evaluation of Fracture Critical Bridges Using Measured Rainflow Response," M.S. Thesis, Department of Civil Engineering, University of Texas, Austin, TX.

Hoadley, P.W., Frank, K.H., and Yura, J.A. (1983). "Estimation of the Fatigue Life of a Test Bridge from Traffic Data," Center for Transportation Research, *Research Report 247-4*, University of Texas, Austin, TX.

Holman, Jr., R.A. (2003) "MicroSAFE User Software and User Manual," Invocon, Inc., Conroe, TX.

Miner, M.A. (1945). "Cumulative Damage in Fatigue," *Journal of Applied Mechanics*, Vol. 12, No. 9.

Neidigh, J.D. and Crawford, J.A. (2004). "Expanding the Texas Weigh-in-Motion Program to Meet AASHTO 2002 Traffic Data Needs," *Proceedings*, North American Travel Monitoring Exposition and Conference, San Diego, CA.

Tilly, G.P. and Page, J. (1980). "A Review of Traffic Loads and Stresses in Steel Bridges," Transport and Road Research Laboratory, *Supplementary Report 596*.